

Metal-Rich SX Phe stars in the *Kepler* Field

James M. Nemeč^{1,2*}, Luis A. Balona³, Simon J. Murphy⁴, Karen Kinemuchi⁵,
and Young-Beom Jeon⁶

¹*Department of Physics & Astronomy, Camosun College, Victoria, British Columbia, V8P 5J2, Canada*

²*International Statistics & Research Corp., Brentwood Bay, British Columbia, V8M 1R3 Canada*

³*South African Astronomical Observatory, PO Box 9, Observatory 7935, Cape Town, South Africa*

⁴*Sydney Institute for Astronomy (SIfA), School of Physics, The University of Sydney, NSW 2006, Australia*

⁵*Apache Point Observatory, Sunspot, New Mexico 88349, USA*

⁶*Korea Astronomy and Space Science Institute, Daejeon, 34055, Korea*

Accepted 2016 November 23. Received 2016 October 29; in original form 2016 August 29

ABSTRACT

A spectroscopic and photometric analysis has been carried out for thirty-two *candidate* SX Phe variable blue straggler stars in the *Kepler*-field (Balona & Nemeč 2012). Radial velocities (RVs), space motions (U, V, W), projected rotation velocities ($v \sin i$), spectral types, and atmospheric characteristics (T_{eff} , $\log g$, $[\text{Fe}/\text{H}]$, ξ_t , ζ_{RT} , etc.) are presented for 30 of the 32 stars. Although several stars are metal-weak with extreme halo orbits, the mean $[\text{Fe}/\text{H}]$ of the sample is near solar, thus the stars are more metal-rich than expected for a typical sample of Pop. II stars, and more like halo metal-rich A-type stars (Perry 1969). Two thirds of the stars are fast rotators with $v \sin i > 50$ km/s, including four stars with $v \sin i > 200$ km/s. Three of the stars have (negative) RVs > 250 km/s, five have retrograde space motions, and 21 have total speeds (relative to the LSR) > 400 km/s. All but one of the 30 stars have positions in a Toomre diagram consistent with the kinematics of *bona fide* halo stars (the exception being a thick-disk star). Observed Rømer time delays, pulsation frequency modulations and light curves suggest that at least one third of the stars are in binary (or triple) systems with orbital periods ranging from 2.3 days to more than four years.

Key words: *Kepler* mission – stars: oscillations – stars: blue stragglers – variable stars: SX Phe stars, RR Lyr stars – stars: binary systems

1 INTRODUCTION

SX Phoenecis stars are the Pop. II counterparts of Pop. I δ Scuti pulsating variable stars (see Breger 1980; Eggen & Iben 1989; Nemeč 1989; Nemeč & Mateo 1990a,b). The best known and nearest examples are the stars SX Phe, DY Peg, BL Cam and KZ Hya. These and other such field SX Phe stars (*i.e.*, those not in star clusters) generally have the kinematics of halo (or thick disk) stars, asymmetric and large-amplitude light curves, and low metallicities (Eggen 1970, 1979; Breger 1975, 1977a,b; McNamara *et al.* 1978, 2007). For many years SX Phe stars were suspected of being Pop. II blue stragglers (BSs), but this was established only when short-period variable stars were found among the BSs in globular clusters (Niss *et al.* 1981; Jørgensen 1982; Jørgensen & Hansen 1984; Jensen & Jørgensen 1985; Nemeč & Harris 1987; DaCosta, Norris & Villumsen 1986; Ne-

mec 1989; Nemeč & Cohen 1989; Mateo *et al.* 1990; Nemeč *et al.* 1994, 1995; Sarajedini 1993; Fusi Pecci *et al.* 1992; McNamara 1997; Gilliland *et al.* 1998; Rodríguez & López-González 2000; Bruntt *et al.* 2001). The leading theory of the formation mechanism for BSs involves mass transfer in a close binary system (Hoyle 1964, McCrea 1964, Eggen & Iben 1989, Leonard 1989). Since many BSs are now known to be eclipsing binaries (Niss *et al.* 1978; Margon & Cannon 1989; Mateo *et al.* 1990; Nemeč & Mateo 1990a,b; Hobbs & Mathieu 1991; Hodder *et al.* 1992; Kallrath *et al.* 1992; Helt *et al.* 1993; Yan & Mateo 1994; Nemeč *et al.* 1995; Kaluzny *et al.* 1996, 2007; Kaluzny 2000; Park & Nemeč 2000; Preston & Sneden 2000; Carney *et al.* 2001, 2005; Cohen & Sarajedini 2012) it follows that SX Phe stars are also likely to have a binary (or triple star) nature.

When the first globular cluster SX Phe stars were discovered they were found to have pulsation amplitudes, A_V , larger than 0.10 mag, and simple light curves consistent with radial pulsation and one or two dominant periods. Their

* E-mail: nemeč@camosun.ca

location in the faint extension of the Cepheid instability strip implies pulsation due to Eddington’s κ -mechanism operating in the HeII partial ionization zone (see Fiorentino *et al.* 2014, 2015). They also were found to obey a well-defined period-luminosity relationship that can be used to estimate distances (see Nemec *et al.* 1994; McNamara 1997, 2011; Petersen & Hog 1998; Sandage & Tammann 2006). Because globular clusters (and Local Group dwarf galaxies) tend to be distant, the SX Phe stars in these systems are quite faint. Moreover, the BSs in globular clusters tend to be centrally concentrated (Nemec & Harris 1987; Nemec & Cohen 1989; Leigh, Sills and Knigge 2011; Ferraro *et al.* 2014) and as a consequence the SX Phe stars are often located in the crowded central regions and therefore are much less amenable to spectroscopic and photometric analysis than those in the field.

Subsequent discoveries revealed that SX Phe stars include lower amplitude pulsators and stars that exhibit more complex radial and non-radial oscillations than previously thought to be the case. Particularly noteworthy was the observation that the A_V amplitude distribution shown in figure 2 of Kaluzny (2000) shows an increase in the number of SX Phe stars down to the detection limit (~ 0.02 - 0.03 mag) of the Warsaw variability surveys, from which it was concluded that “a significant fraction of SX Phe stars residing in the survey clusters were most likely missed.” Over the years many more faint and pulsationally-complex SX Phe stars have been found in 47 Tuc (Gilliland *et al.* 1998), NGC 3201 (Mazur *et al.* 2003), NGC 5466 (Jeon *et al.* 2004), ω Cen (Olech *et al.* 2005) and other clusters. The catalogue compiled by Cohen & Sarajedini (2012) lists ~ 250 SX Phe stars in 46 galactic globular clusters (see their figure 5).

SX Phe stars are now known to be ubiquitous, with many having been identified in our Galaxy (Ramsey *et al.* 2011, Palaversa *et al.* 2013, Preston 2015), in the Magellanic Clouds (Soszynski *et al.* 2002, 2003) and in most Local Group dwarf galaxies (Nemec & Mateo 1990a; Mateo *et al.* 1998; Pych *et al.* 2001; Poretti *et al.* 2008; McNamara 2011; Vivas & Mateo 2013; Ferraro *et al.* 2014; Momany 2014; Fiorentino *et al.* 2014, 2015; Coppola *et al.* 2015; Martínez-Vázquez *et al.* 2016). Despite these numerous discoveries discrimination between SX Phe stars and δ Sct stars can be confusing, and is particularly blurred where multiple and composite stellar populations have overlapping age, metallicity and kinematic distributions.

In 2012 Balona & Nemec (hereafter BN12) identified 34 *candidate* SX Phe stars in the *Kepler* field. The stars were found by cross-referencing a list of 1424 *Kepler*-field δ Sct stars (Balona 2014a) with the UCAC3 proper motion catalogue (Zacharias *et al.* 2010) and selecting those stars with high proper motions, $\mu > 30$ mas/yr, and large tangential velocities, $V_t > 120$ km/s. Several of the candidates are located more than 0.5 kpc above the galactic plane thereby strengthening the conclusion that the sample consists of Pop. II stars. An H-R diagram showing the locations of the 34 candidate SX Phe stars (and 1554 δ Sct stars) relative to stellar evolutionary tracks for masses ranging from 0.8 to 2.0 M_\odot was plotted by BN12, where the luminosities and effective temperatures were taken from the *Kepler* Input Catalog (KIC; Brown *et al.* 2011). Since the physical quantities given in the KIC were derived mainly from photometric relations established for stars cooler than 7000 K, the atmospheric param-

eters given in the KIC were not expected to be particularly reliable. BN12 found that there was little to distinguish the *Kepler* light curves of the candidate SX Phe stars from those of δ Sct stars. Furthermore, whereas many *field* SX Phe stars have one or two dominant pulsation modes and rather high amplitudes, almost all of the *Kepler*-field candidates were found to have relatively low amplitudes and complex Fourier spectra. Thus, BN12 concluded that previous ground-based *field* SX Phe star investigations probably suffer from a selection bias that resulted in the omission of stars with the lowest amplitudes and most complex pulsations.

The goal of the present study was to derive reliable estimates of the physical characteristics of the BN12 SX Phe candidates. Extensive asteroseismic investigations using *Kepler* photometry have already been reported for two of the stars: KIC 11754974, an SX Phe pulsator in a 343-day non-eclipsing binary system (Murphy *et al.* 2013b); and KIC 9244992, an SX Phe star in which both the surface and core exhibit slow, nearly-uniform rotation (Saio *et al.* 2015). Since the SX Phe stars in the *Kepler*-field are unique in having four years of almost-continuous high-precision photometry, estimation of their evolutionary status and atmospheric and physical characteristics based on high-resolution spectra is possible and obviously desirable. Moreover, if the stars are Pop. II BSs then determining whether they are binary or triple systems (with a range of separations, including coalesced binaries) and better characterizing their orbital properties becomes important.

In §2 the results of the spectroscopic analyses are presented, including atmospheric properties, radial velocities, space motions and stellar population classifications (eg., halo, thick disk). In §3 frequency analyses are described for the complete BN12 sample; the results based on all the available long- and short-cadence Q0-Q17 *Kepler* photometry are presented, including the finding that one third of the SX Phe pulsators are in binary systems with orbital periods ranging from a few days to more than four years. A summary of the paper is given in §4.

2 SPECTROSCOPY

High-resolution echelle spectra for 32 of the BN12 candidate SX Phe stars were acquired in 2013 and 2014 with the ESPaDOnS spectrograph mounted on the Canada-France-Hawaii 3.6-m telescope (CFHT). Two stars fainter than 15th magnitude, KIC 5390069 and KIC 7300184, were too faint to be observed. A total of 178 SX Phe star spectra were taken by the CFHT Queue Service Observing team, with the number of spectra taken per star ranging from three to 11, over three to seven independent epochs. Details of the individual spectra are summarized in **Table 1**.

In 2013 ESPaDOnS was used in ‘star+sky’ mode (spectral resolving power $\lambda/\Delta\lambda \sim 66000$) with spectral resolution (gaussian FWHM of instrumental profile) ~ 0.0083 nm at 550 nm, 2.5 pixels per resolution element and velocity resolution 4.5 km/s. In 2014 ‘star-only’ mode was used, which widened the stellar spectra, increased the resolving power to ~ 80000 , reduced the FWHM of the instrumental profile to ~ 0.0070 nm, and improved the velocity resolution to 3.8 km/s. Each spectrum covers the wavelength range 370-1030 nm, spread over 40 orders. Almost all the observations

Table 1. Summary of CFHT and APO spectra. The stars are ordered by KIC number (col.1) and the other columns contain: (2) the spectrum number (CFHT or APO); (3) the UTC mid-exposure date and time, (4) mid-exposure barycentric Julian Day; (5) exposure time (s); (6) signal-to-noise ratio, (7) airmass at the mid-time of the observation; (8) barycentric radial velocity (km/s); and (9) projected equatorial velocity, $v \sin i$ (km/s). For the SB2 system KIC 6780873 the RV and $v \sin i$ entries are for the primary component.

| KIC (1) | Spectrum (2) | UTC date (mid) (3) | BJD (mid) (4) | Exp.(s) (5) | S/N (6) | AM (7) | RV (8) | $v \sin i$ (9) |
|--------------------------------------|-----------------|-----------------------|------------------|----------------|------------|-----------|-----------|-------------------|
| (a) Kepler-field SX Phe stars | | | | | | | | |
| 1162150 | APO (15a) | 2012/10/25, 04:31:53 | 2456225.6893 | 600 | 30 | 1.60 | -11±9 | 195±7 |
| | 1650050 (15b) | 2013/08/26, 08:15:58 | 2456530.8490 | 1800 | 148 | 1.06 | -15±7 | 226±2 |
| | 1650642 (15c) | 2013/08/29, 08:49:18 | 2456533.8720 | 1800 | 155 | 1.10 | -16±6 | 230±2 |
| | APO (15d) | 2014/06/13, 05:59:35 | 2456821.7521 | 1200 | 30 | 1.26 | -13±6 | 194±4 |
| | APO (15e) | 2014/06/13, 06:28:49 | 2456821.7724 | 1200 | 26 | 1.18 | -13±9 | 219±5 |
| | 1733894 (15f) | 2014/08/18, 11:25:36 | 2456887.9809 | 1200 | 106 | 1.43 | -17±5 | 228±2 |
| 3456605 | 1650650 (24a) | 2013/08/29, 11:48:46 | 2456533.9968 | 1350 | 51 | 1.79 | -7.5±0.5 | 13.6±0.8 |
| | 1653557 (24b) | 2013/09/14, 08:02:23 | 2456549.8388 | 1350 | 52 | 1.11 | -6.4±0.5 | 10.0±1.0 |
| | 1741394 (24c) | 2014/09/17, 06:19:24 | 2456917.7672 | 1200 | 52 | 1.06 | -8.4±0.5 | 16.2±0.8 |
| 4168579 | 1650649 (23a) | 2013/08/29, 11:24:43 | 2456533.9801 | 1200 | 38 | 1.63 | 33±6 | 207±6 |
| | 1653555 (23b) | 2013/09/14, 07:17:38 | 2456549.8077 | 1200 | 37 | 1.07 | 23±9 | 201±5 |
| | 1670335 (23c) | 2013/11/19, 04:25:45 | 2456615.6832 | 1200 | 45 | 1.21 | 19±4 | 196±4 |
| | 1670336 (23d) | 2013/11/19, 04:46:26 | 2456615.6976 | 1200 | 39 | 1.26 | 20±4 | 208±9 |
| | 1670337 (23e) | 2013/11/19, 05:07:07 | 2456615.7119 | 1200 | 39 | 1.34 | 24±3 | 197±7 |
| | 1733877 (23f) | 2014/08/18, 06:01:35 | 2456887.7560 | 1200 | 40 | 1.24 | 24±8 | 178±6 |
| 4243461 | 1649174 (4a) | 2013/08/22, 07:18:51 | 2456526.8091 | 1200 | 38 | 1.06 | 58.2±1.3 | 53.0±2.8 |
| | 1649175 (4b) | 2013/08/22, 07:39:32 | 2456526.8235 | 1200 | 35 | 1.06 | 57.8±0.3 | 50.0±2.2 |
| | 1649176 (4c) | 2013/08/22, 08:00:13 | 2456526.8378 | 1200 | 35 | 1.07 | 59.0±1.9 | 50.1±3.3 |
| | 1650640 (4d) | 2013/08/29, 07:59:07 | 2456533.8368 | 1200 | 37 | 1.09 | 58.8±1.2 | 56.7±2.2 |
| | 1654451 (4e) | 2013/09/17, 05:02:14 | 2456552.7129 | 1200 | 46 | 1.08 | 58.6±0.8 | 52.2±2.4 |
| | 1733876 (4f) | 2014/08/18, 05:39:33 | 2456887.7403 | 1200 | 36 | 1.20 | 61.8±0.9 | 55.3±2.0 |
| | 1740694 (4g) | 2014/09/14, 05:46:20 | 2456914.7437 | 1200 | 40 | 1.06 | 62.4±1.4 | 53.3±3.7 |
| | 1753084 (4h) | 2014/10/31, 05:09:04 | 2456961.7143 | 1200 | 36 | 1.21 | 62.9±1.7 | 52.8±1.6 |
| 4662336 | 1650048 (14a) | 2013/08/26, 07:27:05 | 2456530.8151 | 1200 | 48 | 1.07 | -11.4±0.2 | 81.5±1.6 |
| | 1650049 (14b) | 2013/08/26, 07:47:46 | 2456530.8295 | 1200 | 52 | 1.06 | -11.1±0.4 | 84.1±1.5 |
| | 1650647 (14c) | 2013/08/29, 10:41:23 | 2456533.9499 | 1200 | 60 | 1.39 | -10.1±0.6 | 82.4±1.6 |
| | 1741395 (14d) | 2014/09/17, 06:41:53 | 2456917.7827 | 1200 | 52 | 1.07 | -16.9±1.7 | 84.1±1.3 |
| 4756040 | 1650485 (20a) | 2013/08/28, 09:45:15 | 2456532.9110 | 1200 | 46 | 1.19 | 3.3±0.7 | 43.0±1.0 |
| | 1650486 (20b) | 2013/08/28, 10:05:55 | 2456532.9254 | 1200 | 46 | 1.25 | 8.3±0.5 | 34.0±1.1 |
| | 1653556 (20c) | 2013/09/14, 07:39:01 | 2456549.8226 | 1200 | 46 | 1.10 | 4.7±1.0 | 43.4±1.1 |
| | 1741396 (20d) | 2014/09/17, 07:04:15 | 2456917.7983 | 1200 | 46 | 1.08 | 3.2±1.0 | 44.2±0.6 |
| 5036493 | APO (26a) | 2012/10/25, 09:56:58 | 2456225.6652 | 600 | 17 | 1.28 | -1.8±1.8 | 24.9±2.5 |
| | 1653322 (26b) | 2013/09/13, 05:09:41 | 2456548.7192 | 1200 | 80 | 1.16 | -3.4±1.0 | 20.6±0.5 |
| | 1655649 (26c) | 2013/09/22, 07:29:17 | 2456557.8156 | 1200 | 80 | 1.11 | -3.5±0.7 | 18.4±0.6 |
| | 1741397 (26d) | 2014/09/17, 07:27:08 | 2456917.8144 | 1200 | 64 | 1.09 | -5.8±0.4 | 16.1±0.7 |
| 5705575 | 1650644 (22a) | 2013/08/29, 09:37:19 | 2456533.9053 | 1200 | 39 | 1.21 | -31.7±2.4 | 88.6±1.7 |
| | 1653554 (22b) | 2013/09/14, 06:56:00 | 2456549.7926 | 1200 | 37 | 1.08 | -33.7±1.0 | 92.6±1.8 |
| | 1656478 (22c) | 2013/09/26, 04:57:03 | 2456561.7092 | 1200 | 49 | 1.09 | -35.0±2.1 | 89.3±1.7 |
| | 1670338 (22d) | 2013/11/19, 05:28:43 | 2456615.7269 | 1200 | 37 | 1.49 | -30.4±1.4 | 83.3±2.2 |
| | 1670339 (22e) | 2013/11/19, 05:49:24 | 2456615.7412 | 1200 | 37 | 1.61 | -31.9±0.9 | 85.4±2.1 |
| | 1670340 (22f) | 2013/11/19, 06:10:04 | 2456615.7556 | 1200 | 34 | 1.76 | -31.8±2.0 | 95.8±4.4 |
| | 1733896 (22g) | 2014/08/18, 12:09:53 | 2456888.0116 | 1200 | 34 | 1.71 | -42.6±2.2 | 88.5±2.6 |
| | 1740703 (22h) | 2014/09/14, 08:52:26 | 2456914.8734 | 1200 | 36 | 1.26 | -47.3±2.8 | 87.4±2.0 |
| | 1755698 (22i) | 2014/11/10, 06:54:20 | 2456971.7871 | 1200 | 23 | 1.83 | -40.0±5.7 | 84.6±2.8 |
| 6130500 | 1649381 (9a) | 2013/08/23, 07:07:09 | 2456527.8013 | 1200 | 42 | 1.10 | -18.8±1.0 | 42.9±1.7 |
| | 1649382 (9b) | 2013/08/23, 07:27:51 | 2456527.8157 | 1200 | 34 | 1.09 | -19.3±0.8 | 48.6±0.9 |
| | 1649383 (9c) | 2013/08/23, 07:48:33 | 2456527.8301 | 1200 | 35 | 1.08 | -17.1±1.4 | 52.1±1.0 |
| | 1650648 (9d) | 2013/08/29, 11:02:48 | 2456533.9648 | 1200 | 35 | 1.51 | -18.1±1.3 | 51.2±1.4 |
| | 1654724 (9e) | 2013/09/18, 06:31:00 | 2456553.7751 | 1200 | 29 | 1.08 | -19.0±1.3 | 49.2±1.1 |
| | 1733878 (9f) | 2014/08/18, 06:23:21 | 2456887.7710 | 1200 | 36 | 1.20 | -16.0±1.1 | 47.2±2.2 |
| 6227118 | 1653323 (27a) | 2013/09/13, 05:31:29 | 2456548.7343 | 1200 | 60 | 1.13 | 6.4±3.2 | 135.9±1.9 |
| | 1655648 (27b) | 2013/09/22, 07:06:51 | 2456557.8000 | 1200 | 71 | 1.10 | 2.1±1.8 | 133.0±2.3 |
| | 1740707 (27c) | 2014/09/14, 10:05:51 | 2456914.9248 | 1200 | 54 | 1.46 | 7.5±4.4 | 129.4±2.2 |
| | 1755701 (27d) | 2014/11/10, 07:48:04 | 2456971.8248 | 1200 | 29 | 2.18 | 8.5±2.0 | 132.5±3.4 |

Table 1 – *continued*

| KIC (1) | Spectrum (2) | UTC date (mid) (3) | BJD (mid) (4) | Exp.(s) (5) | S/N (6) | AM (7) | RV (8) | $v \sin i$ (9) |
|------------|-----------------|-----------------------|------------------|----------------|------------|-----------|-------------|-------------------|
| 6445601 | 1648978 (2a) | 2013/08/21, 11:11:41 | 2456525.9711 | 1200 | 41 | 1.42 | -7.7±1.6 | 71.3±2.4 |
| | 1648979 (2b) | 2013/08/21, 11:32:17 | 2456525.9855 | 1200 | 42 | 1.52 | -8.4±3.2 | 72.6±1.8 |
| | 1648980 (2c) | 2013/08/21, 11:53:04 | 2456525.9999 | 1200 | 41 | 1.65 | -4.0±0.5 | 70.1±1.7 |
| | 1650645 (2d) | 2013/08/29, 09:58:49 | 2456533.9203 | 1200 | 39 | 1.27 | -4.8±0.9 | 70.4±3.2 |
| | 1654452 (2e) | 2013/09/17, 05:23:57 | 2456552.7285 | 1200 | 44 | 1.10 | -4.2±1.3 | 72.2±2.1 |
| | 1740705 (2f) | 2014/09/14, 09:37:09 | 2456914.9045 | 1200 | 38 | 1.42 | -5.7±1.8 | 70.8±1.7 |
| 6520969 | 1650643 (21a) | 2013/08/29, 09:15:49 | 2456533.8904 | 1200 | 49 | 1.18 | -299.8±1.2 | <4.2±1.6 |
| | 1653553 (21b) | 2013/09/14, 06:34:45 | 2456549.7778 | 1200 | 41 | 1.08 | -299.7±0.8 | <6.9±1.2 |
| | 1740704 (21c) | 2014/09/14, 09:14:52 | 2456914.8890 | 1200 | 38 | 1.35 | -299.4±0.5 | <5.4±1.4 |
| 6780873 | 1649178 (5a) | 2013/08/22, 08:27:28 | 2456526.8571 | 1200 | 36 | 1.09 | 8.9±0.3 | [11] |
| | 1649179 (5b) | 2013/08/22, 08:48:09 | 2456526.8714 | 1200 | 34 | 1.10 | 8.4±0.3 | [11] |
| | 1649180 (5c) | 2013/08/22, 09:08:51 | 2456526.8858 | 1200 | 45 | 1.12 | 10.2±0.4 | [11] |
| | 1650646 (5d) | 2013/08/29, 10:19:56 | 2456533.9349 | 1200 | 39 | 1.34 | -26.81±0.13 | 11±1 |
| | 1654453 (5e) | 2013/09/17, 05:45:33 | 2456552.7435 | 1200 | 36 | 1.09 | -24.13±0.15 | 12±1 |
| | 1740695 (5f) | 2014/09/14, 06:08:57 | 2456914.7600 | 1200 | 40 | 1.09 | 43.08±0.14 | 11±1 |
| | 1741393 (5g) | 2014/09/17, 05:56:60 | 2456917.7515 | 1200 | 40 | 1.09 | -22.56±0.14 | 11±1 |
| | 1753085 (5h) | 2014/10/31, 05:32:15 | 2456961.7311 | 1200 | 35 | 1.22 | 12.99±0.20 | 15±3 |
| | 1755692 (5i) | 2014/11/10, 04:31:38 | 2456971.6881 | 1200 | 25 | 1.17 | -3.79±0.18 | 11±1 |
| 7020707 | 1650474 (16a) | 2013/08/28, 05:51:16 | 2456532.7481 | 1200 | 42 | 1.14 | 5.7±1.4 | 101±3 |
| | 1650475 (16b) | 2013/08/28, 06:11:58 | 2456532.7625 | 1200 | 43 | 1.12 | 4.4±3.8 | 109±3 |
| | 1653552 (16c) | 2013/09/14, 06:12:57 | 2456549.7624 | 1200 | 44 | 1.09 | 0.6±1.0 | 104±3 |
| | 1733891 (16d) | 2014/08/18, 10:18:20 | 2456887.9339 | 1200 | 40 | 1.26 | 2.5±2.9 | 106±3 |
| 7174372 | 1649377 (8a) | 2013/08/23, 05:57:44 | 2456527.7524 | 1200 | 39 | 1.13 | -17.9±2.3 | 39±4 |
| | 1649378 (8b) | 2013/08/23, 06:18:25 | 2456527.7668 | 1200 | 51 | 1.11 | -18.9±2.5 | 42±3 |
| | 1649379 (8c) | 2013/08/23, 06:39:06 | 2456527.7812 | 1200 | 39 | 1.09 | -20.6±1.8 | 43±1 |
| | 1650637 (8d) | 2013/08/29, 06:48:41 | 2456533.7876 | 1200 | 39 | 1.09 | -22.1±2.4 | 39±4 |
| | 1654454 (8e) | 2013/09/17, 06:07:30 | 2456552.7580 | 1200 | 35 | 1.10 | -20.0±2.9 | 42±3 |
| | 1733884 (8f) | 2014/08/18, 07:59:33 | 2456887.8372 | 1200 | 39 | 1.09 | -18.2±1.5 | 38±1 |
| | 1740698 (8g) | 2014/09/14, 07:15:49 | 2456914.8056 | 1200 | 39 | 1.15 | -20.6±1.6 | 46±1 |
| | 1753086 (8h) | 2014/10/31, 05:55:39 | 2456961.7466 | 1200 | 36 | 1.46 | -17.4±1.7 | 40±1 |
| | 1755694 (8i) | 2014/11/10, 05:18:57 | 2456971.7203 | 1200 | 25 | 1.47 | -17.2±2.4 | 40±2 |
| 7301640 | 1649384 (10a) | 2013/08/23, 08:10:45 | 2456527.8456 | 1200 | 36 | 1.09 | -10±6 | 124±4 |
| | 1649385 (10b) | 2013/08/23, 08:31:27 | 2456527.8600 | 1200 | 37 | 1.09 | -11±5 | 121±3 |
| | 1649386 (10c) | 2013/08/23, 08:52:09 | 2456527.8744 | 1200 | 35 | 1.10 | -8±5 | 128±4 |
| | 1653559 (10d) | 2013/09/14, 08:46:24 | 2456549.8695 | 1200 | 36 | 1.21 | -10±6 | 111±7 |
| | 1733885 (10e) | 2014/08/18, 08:21:40 | 2456887.8533 | 1200 | 35 | 1.09 | -17±4 | 122±4 |
| 7621759 | 1649181 (6a) | 2013/08/22, 09:31:44 | 2456526.9018 | 1200 | 33 | 1.14 | 17.8±3.0 | 77.6±2.0 |
| | 1649182 (6b) | 2013/08/22, 09:52:26 | 2456526.9169 | 1200 | 35 | 1.17 | 17.3±3.5 | 79.9±2.4 |
| | 1649183 (6c) | 2013/08/22, 10:13:07 | 2456526.9305 | 1200 | 33 | 1.21 | 18.1±4.4 | 83.2±3.4 |
| | 1653558 (6d) | 2013/09/14, 08:25:14 | 2456549.8548 | 1200 | 33 | 1.18 | 14.5±3.3 | 75.9±2.2 |
| | 1733881 (6e) | 2014/08/18, 06:54:30 | 2456887.7927 | 1200 | 35 | 1.16 | 17.3±2.4 | 76.9±1.4 |
| 7765585 | 1653324 (28a) | 2013/09/13, 05:53:11 | 2456548.7492 | 1200 | 38 | 1.11 | 6.7±2.7 | 125±6 |
| | 1655645 (28b) | 2013/09/22, 05:40:49 | 2456557.7401 | 1200 | 45 | 1.10 | 6.9±1.6 | 125±6 |
| | 1669659 (28c) | 2013/11/16, 05:27:58 | 2456612.7270 | 1200 | 30 | 1.37 | -14.3±2.6 | 124±13 |
| | 1733882 (28d) | 2014/08/18, 07:15:60 | 2456887.8076 | 1200 | 34 | 1.14 | -3.1±4.1 | 123±5 |
| | 1740696 (28e) | 2014/09/14, 06:31:20 | 2456914.7757 | 1200 | 36 | 1.09 | 4.1±4.0 | 122±3 |
| | 1755699 (28f) | 2014/11/10, 07:17:38 | 2456971.8036 | 1200 | 20 | 1.91 | -1.5±2.0 | 121±3 |
| 7819024 | 1650482 (19a) | 2013/08/28, 08:42:28 | 2456532.8672 | 1200 | 35 | 1.14 | -57.0±2.1 | 95.1±5.3 |
| | 1650483 (19b) | 2013/08/28, 09:03:10 | 2456532.8815 | 1200 | 37 | 1.17 | -66.0±3.5 | 100.0±2.9 |
| | 1650484 (19c) | 2013/08/28, 09:23:51 | 2456532.8959 | 1200 | 36 | 1.20 | -62.2±2.2 | 97.8±1.8 |
| | 1654189 (19d) | 2013/09/16, 05:53:05 | 2456551.7487 | 1200 | 56 | 1.10 | -63.5±2.1 | 90.9±1.8 |
| | 1733895 (19e) | 2014/08/18, 11:47:25 | 2456887.9959 | 1200 | 31 | 1.60 | -58.8±2.9 | 91.2±4.5 |
| | 1740702 (19f) | 2014/09/14, 08:28:38 | 2456914.8568 | 1200 | 34 | 1.23 | -55.7±2.9 | 97.5±2.9 |
| | 1753090 (19g) | 2014/10/31, 06:56:43 | 2456961.7896 | 1200 | 37 | 1.60 | -48.4±2.4 | 97.9±2.7 |
| | 1755697 (19h) | 2014/11/10, 06:29:30 | 2456971.7699 | 1200 | 22 | 1.68 | -62.8±2.0 | 92.2±2.3 |
| 8004558 | 1648976 (1a) | 2013/08/21, 10:28:14 | 2456525.9403 | 1200 | 51 | 1.47 | -260±4 | 80±5 |
| | 1648977 (1b) | 2013/08/21, 10:48:56 | 2456525.9546 | 1200 | 42 | 1.58 | -261±4 | 84±4 |
| | 1650636 (1c) | 2013/08/29, 06:27:30 | 2456533.7728 | 1200 | 52 | 1.10 | -254±5 | 82±9 |
| | 1733883 (1d) | 2014/08/18, 07:38:02 | 2456887.8222 | 1200 | 42 | 1.10 | -254±5 | 76±5 |
| | 1740697 (1e) | 2014/09/14, 06:53:45 | 2456914.7902 | 1200 | 43 | 1.14 | -251±4 | 95±8 |
| | 1753087 (1f) | 2014/10/31, 06:20:11 | 2456961.7636 | 1200 | 40 | 1.64 | -251±4 | 92±7 |
| | 1755693 (1g) | 2014/11/10, 04:55:24 | 2456971.7039 | 1200 | 26 | 1.40 | -242±4 | 94±7 |

Table 1 – *continued*

| KIC (1) | Spectrum (2) | UTC date (mid) (3) | BJD (mid) (4) | Exp.(s) (5) | S/N (6) | AM (7) | RV (8) | $v \sin i$ (9) |
|---------------|----------------------|-----------------------|------------------|----------------|------------|-----------|------------|-------------------|
| 8110941 | 1653325 (29a) | 2013/09/13, 06:15:24 | 2456548.7647 | 1200 | 44 | 1.10 | 4.3±0.2 | <7.8±0.6 |
| | 1655646 (29b) | 2013/09/22, 06:03:09 | 2456557.7557 | 1200 | 48 | 1.10 | 4.4±0.4 | <7.2±0.5 |
| | 1669658 (29c) | 2013/11/16, 05:05:27 | 2456612.7114 | 1200 | 34 | 1.29 | 4.4±0.5 | <7.6±0.5 |
| | 1741400 (29d) | 2014/09/17, 08:34:35 | 2456917.8611 | 1200 | 39 | 1.22 | 4.3±0.2 | <7.1±2.1 |
| 8196006 | 1653326 (30a) | 2013/09/13, 06:37:34 | 2456548.7803 | 1200 | 41 | 1.10 | -4.6±1.6 | 90.5±1.6 |
| | 1655848 (30b) | 2013/09/23, 09:54:21 | 2456558.9164 | 1200 | 46 | 1.54 | -2.4±1.9 | 96.4±2.3 |
| | 1670136 (30c) | 2013/11/18, 04:51:24 | 2456614.7017 | 1200 | 36 | 1.23 | -2.2±1.8 | 93.3±2.6 |
| | 1741401 (30d) | 2014/09/17, 08:57:55 | 2456917.8776 | 1200 | 38 | 1.24 | -6.1±3.0 | 92.8±2.3 |
| 8330910 | 1648981 (3a) | 2013/08/21, 12:15:07 | 2456526.0154 | 1200 | 44 | 1.59 | 20±7 | 220±6 |
| | 1648982 (3b) | 2013/08/21, 12:35:50 | 2456526.0298 | 1200 | 43 | 1.73 | 22±15 | 222±6 |
| | 1654192 (3c) | 2013/09/16, 06:58:02 | 2456551.7944 | 1200 | 51 | 1.10 | 24±9 | 231±6 |
| | 1741402 (3d) | 2014/09/17, 09:20:29 | 2456917.8933 | 1200 | 43 | 1.29 | 19±9 | 224±5 |
| 9244992 | 1649185 (7a) | 2013/08/22, 10:45:22 | 2456526.9530 | 1200 | 32 | 1.27 | -15.8±0.4 | <7.4±0.6 |
| | 1649186 (7b) | 2013/08/22, 11:06:03 | 2456526.9674 | 1200 | 33 | 1.32 | -15.9±0.5 | <7.2±0.4 |
| | 1649187 (7c) | 2013/08/22, 11:26:44 | 2456526.9818 | 1200 | 32 | 1.40 | -15.9±0.3 | <5.8±0.5 |
| | 1654191 (7d) | 2013/09/16, 06:36:30 | 2456551.7794 | 1200 | 36 | 1.11 | -16.8±0.6 | <5.8±0.5 |
| | 1733887 (7e) | 2014/08/18, 08:50:09 | 2456887.8731 | 1200 | 34 | 1.11 | -15.4±0.4 | <7.1±0.5 |
| 9267042 | 1649575 (12a) | 2013/08/24, 08:39:11 | 2456528.8647 | 1200 | 42 | 1.16 | -8±4 | 109.8±3.4 |
| | 1649576 (12b) | 2013/08/24, 08:59:53 | 2456528.8790 | 1200 | 37 | 1.19 | -11±5 | 115.4±9.8 |
| | 1649577 (12c) | 2013/08/24, 09:20:35 | 2456528.8934 | 1200 | 37 | 1.23 | -9±3 | 115.2±2.9 |
| | 1650639 (12d) | 2013/08/29, 07:37:38 | 2456533.8217 | 1200 | 47 | 1.12 | -16±4 | 120.7±3.0 |
| | 1654455 (12e) | 2013/09/17, 06:30:10 | 2456552.7740 | 1200 | 37 | 1.13 | -8±3 | 124.2±4.1 |
| | 1733889 (12f) | 2014/08/18, 09:34:01 | 2456887.9029 | 1200 | 39 | 1.21 | -14±5 | 118.9±4.2 |
| | 1740699 (12g) | 2014/09/14, 07:38:17 | 2456914.8215 | 1200 | 39 | 1.19 | -16±7 | 120.4±4.4 |
| | 1754691 (12h) | 2014/11/07, 04:36:12 | 2456968.6912 | 1200 | 22 | 1.26 | -10.5±0.9 | 94.8±3.9 |
| | 1754692 (12i) | 2014/11/07, 04:57:36 | 2456968.7061 | 1200 | 21 | 1.31 | -12.2±0.7 | 97.3±2.1 |
| | 1754693 (12j) | 2014/11/07, 05:19:03 | 2456968.7210 | 1200 | 19 | 1.39 | -11.3±0.3 | 103.4±0.9 |
| | 1755695 (12k) | 2014/11/10, 05:42:19 | 2456971.7369 | 1200 | 24 | 1.55 | -11.8±1.3 | 113.0±3.9 |
| 9535881 | 1650651 [25a] | 2013/08/29, 12:11:48 | 2456534.0127 | 1200 | 41 | 2.01 | 7.1±0.7 | 59.4±1.2 |
| | 1654190 [25b] | 2013/09/16, 06:15:04 | 2456551.7642 | 1200 | 45 | 1.12 | 6.7±0.5 | 51.7±1.2 |
| | 1741398 [25c] | 2014/09/17, 07:49:37 | 2456917.8298 | 1200 | 45 | 1.17 | 6.9±1.3 | 53.1±0.7 |
| | 1753092 [25d] | 2014/10/31, 07:27:07 | 2456961.8111 | 1200 | 27 | 1.68 | 2.9±1.4 | 59.1±1.6 |
| 9966976 | 1653327 (31a) | 2013/09/13, 06:59:20 | 2456548.7952 | 1200 | 47 | 1.12 | -2±5 | 122.6±1.5 |
| | 1655845 (31b) | 2013/09/23, 08:43:48 | 2456558.8673 | 1200 | 53 | 1.32 | -1±5 | 125.6±2.4 |
| | 1670137 (31c) | 2013/11/18, 05:12:58 | 2456614.7167 | 1200 | 38 | 1.35 | -1±6 | 122.3±2.2 |
| | 1741399 (31d) | 2014/09/17, 08:12:28 | 2456917.8458 | 1200 | 42 | 1.19 | 3±6 | 123.7±2.2 |
| 10989032 | 1653560 (32a) | 2013/09/14, 09:08:06 | 2456549.8845 | 1200 | 34 | 1.31 | -44±2 | 44.4±1.6 |
| | 1655844 (32b) | 2013/09/23, 08:21:29 | 2456558.8517 | 1200 | 43 | 1.28 | -43±3 | 47.4±1.6 |
| | 1670135 (32c) | 2013/11/18, 04:29:40 | 2456614.6866 | 1200 | 34 | 1.25 | -32±2 | 47.6±1.9 |
| | 1740691 (32d) | 2014/09/14, 05:11:51 | 2456914.7205 | 1200 | 36 | 1.22 | -14±2 | 41.8±0.9 |
| | 1740708 (32e) | 2014/09/14, 10:28:24 | 2456914.9403 | 1200 | 31 | 1.63 | -8±2 | 46.0±1.4 |
| | 1741390 (32f) | 2014/09/17, 05:24:18 | 2456917.7290 | 1200 | 35 | 1.18 | -15±2 | 45.2±1.4 |
| | 1741405 (32g) | 2014/09/17, 09:51:03 | 2456917.9142 | 1200 | 33 | 1.50 | -22±2 | 47.4±1.4 |
| 1755702 (32h) | 2014/11/10, 08:10:06 | 2456971.8404 | 1200 | 18 | 2.50 | -37±3 | 47.9±2.0 | |
| 11649497 | 1649572 (11a) | 2013/08/24, 07:34:50 | 2456528.8198 | 1200 | 39 | 1.16 | -21.7±0.3 | <5.6±0.3 |
| | 1649573 (11b) | 2013/08/24, 07:55:31 | 2456528.8342 | 1200 | 39 | 1.17 | -21.1±0.3 | <5.9±0.4 |
| | 1649574 (11c) | 2013/08/24, 08:16:13 | 2456528.8486 | 1200 | 42 | 1.18 | -21.4±0.3 | <5.3±0.6 |
| | 1650638 (11d) | 2013/08/29, 07:16:26 | 2456533.8069 | 1200 | 39 | 1.16 | -21.2±0.3 | <4.7±0.4 |
| | 1654456 (11e) | 2013/09/17, 06:52:03 | 2456552.7891 | 1200 | 38 | 1.19 | -21.3±0.3 | <5.8±0.3 |
| | 1733888 (11f) | 2014/08/18, 09:12:12 | 2456887.8876 | 1200 | 40 | 1.22 | -21.9±0.2 | <6.1±0.3 |
| 11754974 | APO (13a) | 2012/10/28, 05:53:24 | 2456228.7455 | 900 | 19 | 2.44 | -301±4 | 27.4±2.2 |
| | APO (13b) | 2012/10/28, 06:10:57 | 2456228.7576 | 900 | 22 | 2.71 | -299±4 | 25.0±2.5 |
| | 1649578 (13c) | 2013/08/24, 09:43:25 | 2456528.9093 | 1200 | 60 | 1.31 | -300.2±1.0 | 25.7±2.1 |
| | 1649579 (13d) | 2013/08/24, 10:04:06 | 2456528.9236 | 1200 | 66 | 1.37 | -306.8±2.0 | 36.6±1.4 |
| | 1650641 (13e) | 2013/08/29, 08:21:22 | 2456533.8521 | 1200 | 62 | 1.20 | -313.2±2.2 | 25.7±2.5 |
| | 1733890 (13f) | 2014/08/18, 09:55:49 | 2456887.9180 | 1200 | 57 | 1.28 | -302.1±0.8 | 25.5±1.5 |
| | 1740700 (13g) | 2014/09/14, 08:00:31 | 2456914.8370 | 1200 | 59 | 1.26 | -301.3±0.9 | 25.6±1.6 |
| | 1755696 (13h) | 2014/11/10, 06:05:49 | 2456971.7536 | 1200 | 35 | 1.66 | -302.3±1.7 | 31.3±1.7 |

Table 1 – *continued*

| KIC/HD (1) | Spectrum (2) | UTC date (mid) (3) | BJD (mid) (4) | Exp.(s) (5) | S/N (6) | AM (7) | RV (8) | $v \sin i$ (9) |
|---|-----------------|-----------------------|------------------|----------------|------------|-----------|--------------------|-------------------|
| 12643589 | 1650476 [17a] | 2013/08/28, 06:33:57 | 2456532.7776 | 1200 | 48 | 1.19 | -61.3 ± 0.3 | 29.2 ± 0.5 |
| | 1650477 [17b] | 2013/08/28, 06:54:38 | 2456532.7920 | 1200 | 38 | 1.18 | -61.6 ± 0.5 | 28.8 ± 0.4 |
| | 1650478 [17c] | 2013/08/28, 07:15:20 | 2456532.8063 | 1200 | 38 | 1.18 | -61.7 ± 0.4 | 28.5 ± 0.5 |
| | 1654187 [17d] | 2013/09/16, 05:10:20 | 2456551.7188 | 1200 | 37 | 1.20 | -61.2 ± 0.4 | 28.5 ± 0.5 |
| | 1733892 [17e] | 2014/08/18, 10:40:16 | 2456887.9489 | 1200 | 35 | 1.41 | -59.5 ± 0.7 | 28.5 ± 0.7 |
| 12688835 | 1650479 (18a) | 2013/08/28, 07:38:01 | 2456532.8221 | 1200 | 35 | 1.18 | -26 ± 10 | 217 ± 15 |
| | 1650480 (18b) | 2013/08/28, 07:58:43 | 2456532.8365 | 1200 | 35 | 1.19 | -20 ± 10 | 239 ± 15 |
| | 1650481 (18c) | 2013/08/28, 08:19:25 | 2456532.8508 | 1200 | 35 | 1.21 | -28 ± 12 | 238 ± 15 |
| | 1654188 (18d) | 2013/09/16, 05:31:20 | 2456551.7334 | 1200 | 37 | 1.19 | -25 ± 10 | 234 ± 15 |
| | 1733893 (18e) | 2014/08/18, 11:02:28 | 2456887.9643 | 1200 | 31 | 1.48 | -51 ± 10 | 221 ± 5 |
| (b) IAU Radial Velocity Standard Stars | | | | | | | | |
| HD 144579 | 1733875 (a) | 2014/08/18, 05:26:16 | 2456887.2267 | 30 | 182 | 1.08 | -59.17 ± 0.41 | 3.65 ± 0.13 |
| | 1733879 (b) | 2014/08/18, 06:36:44 | 2456887.2757 | 30 | 165 | 1.17 | -58.98 ± 0.41 | 3.66 ± 0.11 |
| | 1740690 (c) | 2014/09/14, 04:56:45 | 2456914.2062 | 30 | 186 | 1.19 | -58.97 ± 0.41 | 3.66 ± 0.34 |
| | 1741391 (d) | 2014/09/17, 05:38:18 | 2456917.2351 | 30 | 177 | 1.35 | -59.05 ± 0.42 | 3.76 ± 0.24 |
| HD 154417 | 1733874 (a) | 2014/08/18, 05:19:15 | 2456887.2218 | 30 | 213 | 1.06 | -16.61 ± 0.13 | 5.14 ± 0.17 |
| | 1733880 (b) | 2014/08/18, 06:39:14 | 2456887.2775 | 30 | 217 | 1.09 | -16.50 ± 0.13 | 4.85 ± 0.14 |
| | 1740692 (c) | 2014/09/14, 05:27:38 | 2456914.2277 | 30 | 230 | 1.15 | -16.69 ± 0.13 | 4.33 ± 0.16 |
| | 1741392 (d) | 2014/09/17, 05:42:09 | 2456917.2378 | 30 | 224 | 1.22 | -16.44 ± 0.18 | 4.37 ± 0.14 |
| HD 171391 | 1733886 (a) | 2014/08/18, 08:36:14 | 2456887.3586 | 30 | 349 | 1.26 | 7.69 ± 0.20 | 3.67 ± 0.28 |
| | 1740693 (b) | 2014/09/14, 05:31:31 | 2456914.2304 | 30 | 391 | 1.16 | 7.75 ± 0.19 | 3.63 ± 0.19 |
| | 1741389 (c) | 2014/09/17, 05:09:09 | 2456917.2148 | 30 | 384 | 1.16 | 7.72 ± 0.19 | 3.97 ± 0.38 |
| | 1753083 (d) | 2014/10/31, 04:54:05 | 2456961.2044 | 30 | 380 | 1.52 | 7.78 ± 0.19 | 3.58 ± 0.16 |
| | 1754690 (e) | 2014/11/07, 04:19:19 | 2456968.1803 | 30 | 111 | 1.48 | 7.96 ± 0.19 | 4.04 ± 0.50 |
| HD 182572 | 1740701 (a) | 2014/09/14, 08:14:35 | 2456914.3436 | 30 | 282 | 1.15 | -100.13 ± 0.34 | 2.96 ± 0.12 |
| | 1741403 (b) | 2014/09/17, 09:34:00 | 2456917.3988 | 30 | 349 | 1.59 | -100.07 ± 0.33 | 2.81 ± 0.15 |
| | 1753088 (c) | 2014/10/31, 06:36:40 | 2456961.2756 | 30 | 327 | 1.56 | -99.66 ± 0.32 | 2.87 ± 0.12 |
| | 1755691 (d) | 2014/11/10, 04:16:12 | 2456971.1781 | 30 | 180 | 1.12 | -99.53 ± 0.33 | 2.95 ± 0.12 |
| HD 187691 | 1740706 (a) | 2014/09/14, 09:51:18 | 2456914.4108 | 30 | 288 | 1.46 | 0.22 ± 0.12 | 3.45 ± 0.14 |
| | 1741404 (b) | 2014/09/17, 09:36:41 | 2456917.4006 | 30 | 324 | 1.44 | 0.22 ± 0.12 | 4.03 ± 0.15 |
| | 1753091 (c) | 2014/10/31, 07:11:56 | 2456961.3001 | 30 | 323 | 1.65 | 0.21 ± 0.12 | 3.94 ± 0.14 |
| | 1754694 (d) | 2014/11/07, 05:33:51 | 2456968.2320 | 30 | 143 | 1.24 | 0.36 ± 0.12 | 2.76 ± 0.14 |
| | 1754695 (e) | 2014/11/07, 05:35:02 | 2456968.2328 | 30 | 126 | 1.24 | 0.34 ± 0.12 | 3.47 ± 0.17 |
| | 1754696 (f) | 2014/11/07, 05:36:12 | 2456968.2337 | 30 | 143 | 1.25 | 0.38 ± 0.12 | 3.31 ± 0.19 |
| | 1755700 (g) | 2014/11/10, 07:32:58 | 2456971.3147 | 30 | 129 | 2.55 | 0.37 ± 0.12 | 4.08 ± 0.18 |

were made under photometric conditions. Starting in 2014 several IAU faint radial velocity standard stars, selected from the list given by Udry *et al.* (1999), were observed each night in addition to the program stars (Table 1). All raw spectra were preprocessed using the ‘Libre-Esprit’/‘Upena’ CFHT pipeline (see Donati *et al.* 1997). The reductions included barycentric velocity corrections, small radial velocity corrections based on the telluric lines, and rectification of the spectra. The Versatile Wavelength Analysis (VWA) ‘rainbow’ program (Bruntt *et al.* 2010a,b) was used to merge the overlapping echelle orders and to improve, where necessary, the normalization of the continuum level. Sample spectra for the 32 observed stars are shown in **Figure 1**.

High-resolution spectra also were taken at the Apache Point Observatory (APO) with the ARCES echelle spectrograph on the Astrophysical Research Consortium (ARC) 3.5-m telescope. Some of the spectra were of well-known field SX Phe stars taken for comparison purposes, including three RV standard stars selected again from the Udry *et al.* list. The resolution of the APO spectra, $R \sim 31500$ (or 2.5 pixels), is lower than that for the CFHT spectra,

and the wavelength coverage was from 320 to 1000 nm, dispersed over 107 orders. The default slit (size $1.6'' \times 3.2''$) was used for all the observations, and the readout noise typically was less than $7 e^-/\text{pixel}$ with a gain of $3.8 e^-/\text{ADU}$. All the spectra were preprocessed with IRAF. Because of their lower resolution and lower signal-to-noise ratios the APO spectra were used mainly for additional radial velocity and rotation velocity information. Details of the APO observations of the *Kepler*-field SX Phe stars also are given in Table 1.

While acquiring the APO spectra, KIC 1162150 (*15) and KIC 6227118 (*27) were seen in the 3.5-m telescope finder fields to be optical doubles with very close, relatively-bright neighbours. Finding charts made from the DSS digital sky survey are shown in **Figure 2** for these and two other stars. KIC 1162150 is seen to be located among a clump of relatively bright stars, and the image of KIC 6227118 is quite asymmetric. It is possible that photometric observations (and possibly our spectroscopy) for these two stars are contaminated by light from the neighbour stars.

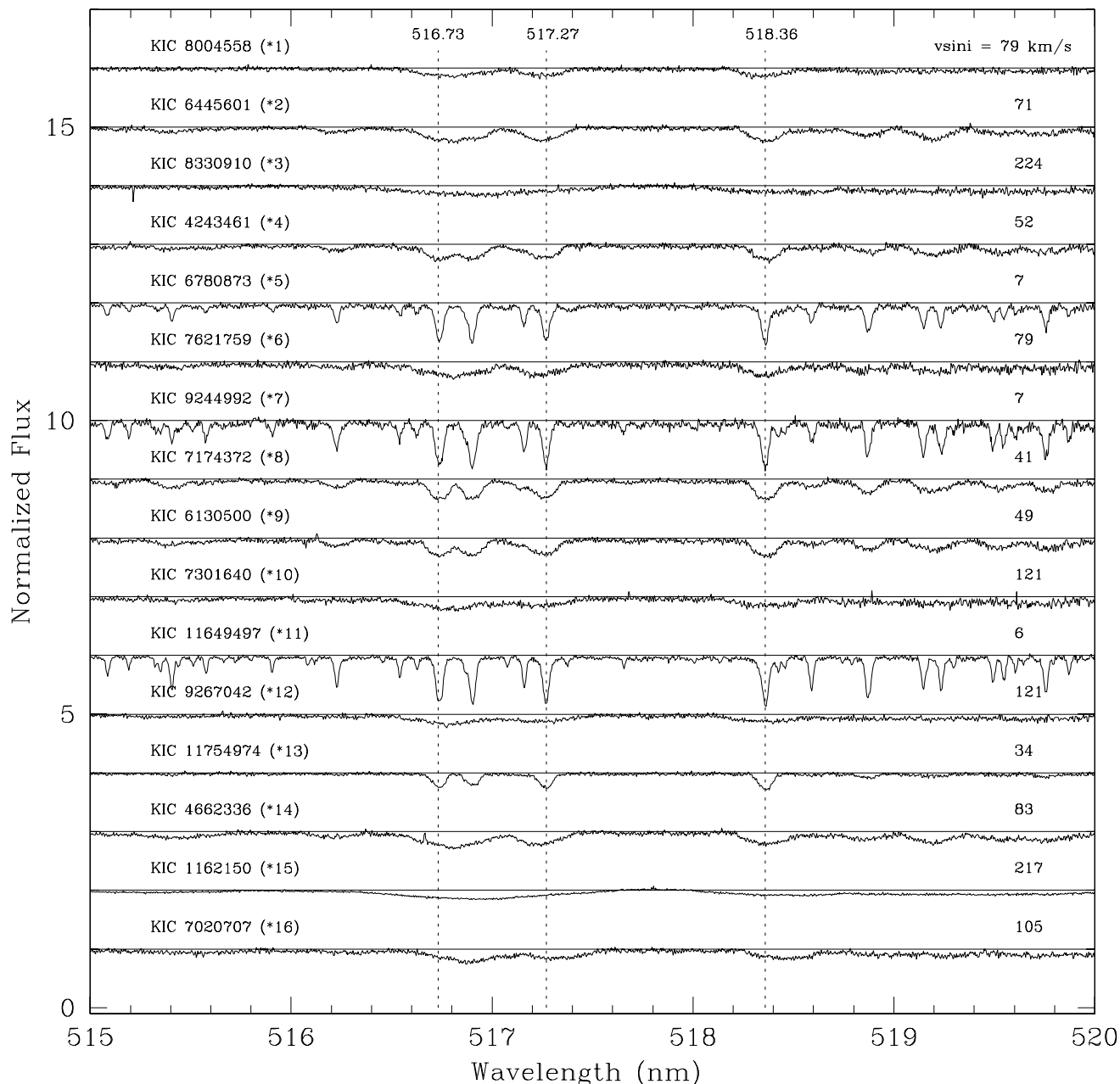


Figure 1. ESPaDOnS (CFHT) spectra for the wavelength region 515 to 520 nm, illustrating the wide range of line broadenings. Each spectrum is identified by the KIC number (and in parentheses the CFHT star number). The dashed vertical lines identify the Mg triplet lines, and on the right hand side of the diagram the average $v \sin i$ (km/s) values are given. The ordering is by CFHT star number.

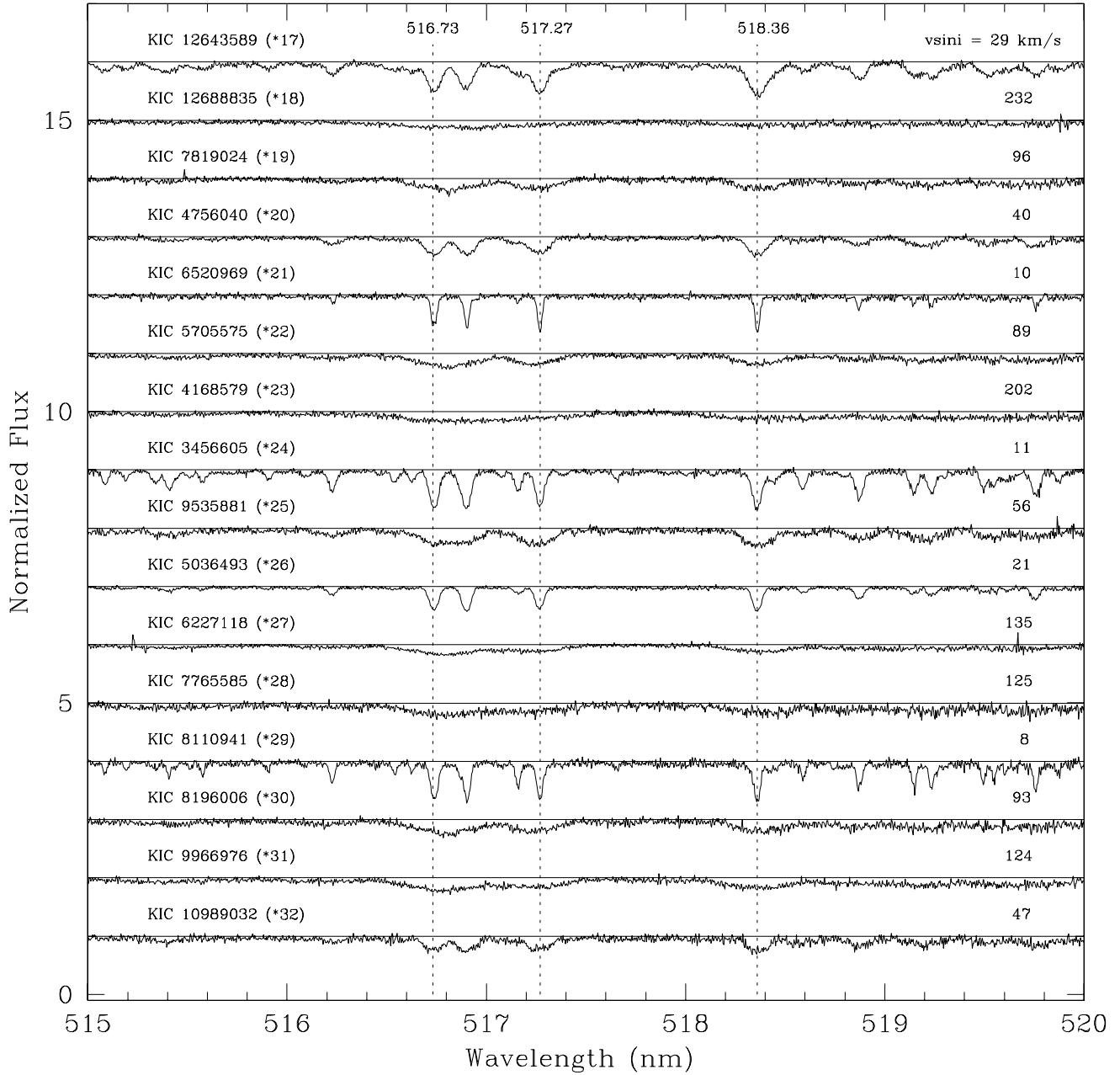
2.1 Radial Velocities

Barycentric radial velocities (RVs) were measured for each spectrum using the cross correlation methods implemented in the routines ‘fxcor’ and ‘xcsao’ in IRAF (Tonry & Davis 1979; Kurtz & Mink 1998) and the ‘rcros’ program of Díaz *et al.* (2011), and by fitting synthetic spectra. Since only minor differences were found using the different methods we chose to adopt the ‘fxcor’ values, where the cross correlation function (CCF) was based on appropriate template synthetic

spectra. The resultant RVs for the individual spectra are presented in Table 1, and mean RVs are given in Table 2.

The RV zero-points were checked using the IAU standard star observations. When the mean RVs for the five standards observed with ESPaDOnS were compared with those given by Udry *et al.* (1999) the mean difference (ours minus the Udry *et al.* value) was 0.38 ± 0.06 km/s. This mean is comparable with the ± 0.3 km/s uncertainty in the Udry *et al.* RV values. Our velocities also show good agreement with those from other studies: for HD 171391 Massarotti *et al.*

Figure 1 – continued



(2008) found $RV=7.59\pm0.05$ km/s, compared with our mean value (five spectra) of 7.78 ± 0.05 km/s; and for HD 182572 Nidever *et al.* (2002) measured $RV=-100.29$ km/s, compared with our -99.84 ± 0.15 km/s (four spectra). Comparisons for the three IAU RV standard stars observed at APO likewise showed excellent agreement between our RVs and the standard values: mean difference between our estimates and the Udry *et al.* values amounted to -0.4 ± 0.4 km/s.

2.1.1 Stars with High Radial Velocities

Three of the stars have large negative RVs: KIC 6520969 (*21) with $RV=-299.5\pm0.1$ km/s; KIC 8004558 (*1) with $RV=-254.1\pm1.5$ km/s; and KIC 11754974 (*13) with $RV=-307\pm4$ km/s. Two of the stars (KIC 8004558 and 11754974) were already of interest because of their resemblance to field SX Phe stars (see Table 3 of BN12). Since all three stars have retrograde motions and low metallicities (see below, Figs. 6 and 13) there is little doubt that they are *bona fide* SX Phe stars. Their metal abundances are comparable to those of the SX Phe BSs found in metal-rich globular

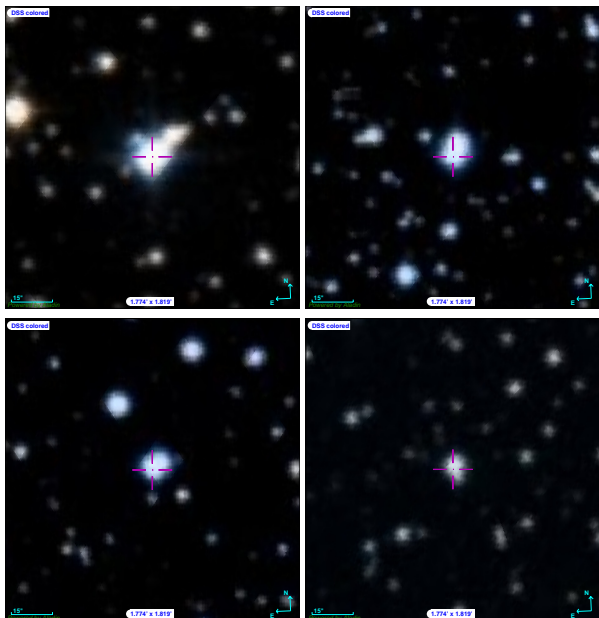


Figure 2. Finding charts for four stars that appear non-circular due to close neighbours: KIC 1162150 (*15, upper left), KIC 5036493 (*26, upper right), KIC 6227118 (*27, lower left) and KIC 7621759 (*6, lower right). All are colour DSS images from the Aladin Sky Atlas, 1.774×1.819 arcmin across, with North to the top and East to the left. For KIC 5036493 the brighter bluer star to the South is the SX Phe candidate.

clusters, for example, 47 Tuc (Gilliland *et al.* 1998; Bruntt *et al.* 2001) and M71 (Hodder *et al.* 1992; McCormac *et al.* 2013). The 47 Tuc stars observed with HST also resemble the *Kepler* stars in exhibiting multiperiodic variations and of having similarly low amplitudes (~ 5 -50 mmag).

KIC 11754974 is known to reside in a 343 d binary system (Murphy *et al.* 2013b), and, based on an analysis of the complete set of *Kepler* Q0-Q17 photometry, we show below that KIC 8004558 also is a photometric time-delay binary (orbital period ~ 262 d). In both cases the variable star is thought to be the more massive primary ($\mathcal{M} \sim 1.5 \mathcal{M}_{\odot}$) and the secondary has a mass $\sim 0.5 \mathcal{M}_{\odot}$. No photometric or spectroscopic evidence could be found to suggest that KIC 6520969 (*21) is a binary system.

2.1.2 Radial Velocity Variations

There are several reasons why one might expect some of the program stars to show RV variations: (1) all of the stars exhibit light variations due to radial and non-radial pulsations (usually multiperiodic); (2) at least ten of the pulsators are in binary systems (see §3.3 below); and (3) the two misclassified stars, KIC 9535881 and KIC 12643589, are known to be close eclipsing binaries¹.

Since the spectroscopic part of this study was intended only as a first-look survey the sampling design is far from optimal for analyzing temporal variations in the spectra,

and only a relatively small number of spectra were taken for each star (typically 5 and at most 11). Moreover, owing to the wide range of line widths of the sample stars the uncertainties of the individual RV measurements range from $\sim \pm 10$ km/s for the four rapidly rotating stars to only a few tenths of a km/sec for the narrow-lined metal-rich (and standard) stars that have high signal-to-noise ratio (S/N) spectra. Furthermore, the spacing of the observations is not ideal for identifying RV variations, in particular: (1) the ~ 300 day gaps between the 2012, 2013 and 2014 observations are a potential cause of aliasing difficulties; (2) many of the stars were observed only once in 2014; and (3) the spacing may be inappropriate for detecting certain orbital and pulsation periods (*i.e.* cycle-count and Nyquist aliasing). Finally, the IAU RV standards observed at CFHT were observed only in 2014, and thus year-to-year offsets in the RVs are possible (although this seems unlikely given the constancy of the RVs for several program stars).

Despite these potential problems, time-series graphs show some evidence of RV variability for approximately half of the 30 candidate stars with spectra. Stars were ranked by RV range, where $\Delta RV = RV(\max) - RV(\min)$. In the absence of variability, and assuming a normal distribution of RVs, $\Delta RV / \sqrt{n} \sim \sigma_{RV}$, where σ_{RV} is the standard deviation of the RVs and n is the number of measured RVs for a given star. For the non-variable standard stars a typical value for $\Delta RV / \sqrt{n}$ is ~ 0.1 , which is comparable to the uncertainties given in Table 1.

KIC 6780873 (*5) has narrow spectral lines and the largest RV range, $\Delta RV = 69.9 \pm 0.3$ km/s. **Figure 3** shows that five of its nine spectra exhibit line doubling, identified by two distinct peaks in the cross-correlation function; thus it is clearly a double-lined spectroscopic binary (SB2). In Table 1 only the RVs for the primary star (assumed to be the SX Phe star) are given; these were calculated using the stronger and wider of the two CCF peaks (*i.e.*, the peak with the larger area and larger height above the baseline). The observed RVs of the SX Phe star vary from -26.81 ± 0.13 km/s to $+43.08 \pm 0.14$ km/s. The RVs for both components, noted in Fig. 3 and plotted in **Figure 4**, are consistent with KIC 6780873 being a close binary with a 9.161 ± 0.001 d orbital period (see §3.3). The widths of the CCFs suggest that $v \sin i$ for the primary is larger than that of the secondary, 11 ± 2 km/s versus 5 ± 2 km/s. The observation of spectral lines due to the secondary suggests that the less luminous companion star is a low-mass main-sequence star and not a companion or white dwarf.

The other SX Phe candidates with large ΔRV values are: KIC 12688835 (*18), 10989032 (*32), 7765585 (*28), 7819024 (*19), 8004558 (*1), 5705575 (*22), 11754974 (*13) and 9267042 (*12). All except KIC 12688835 and KIC 7765585 are binary systems (see §3.3). The large ΔRV of KIC 12688835 (*18) is based on four 2013 spectra with $RV \sim -25$ km/s and a single 2014 spectrum with $RV = -51 \pm 10$ km/s; owing to the large uncertainties which result from broad spectral lines this evidence for its RV variability must be considered tentative. Likewise, the evidence for the RV variation of KIC 7765585 (*28) hinges primarily on one of the RVs being significantly different from the rest. The measured $\Delta RV = 14 \pm 6$ km/s for KIC 11754974 (*13), the 344-d non-eclipsing binary studied by Murphy *et al.* (2013b), is consistent with the photometric K_1 value of 8.2 ± 0.2 km/s

¹ Squared parentheses around the CFHT star numbers for KIC 9535881 [*25] and KIC 12643589 [*17] have been used throughout this paper to distinguish these two stars from the 32 *bona fide* candidate SX Phe pulsators.

(see §3.3); the significant RV differences seen for the three August 2013 spectra, if real, hint at additional variability.

Two other time-delay binaries exhibit small RV ranges consistent with their photometrically predicted small K_1 values (see Table 9): KIC 4243461 (*4) was found to have $\Delta RV = 5.1 \pm 2.0$ km/s, which is to be compared with the predicted $K_1 = 5.3 \pm 0.2$ km/s; and KIC 9966976 (*31) has $\Delta RV = 5 \pm 5$ km/s (the large uncertainty being due to its large $v \sin i$) compared with the predicted $K_1 = 0.64 \pm 0.04$ km/s. A third time-delay binary, KIC 7300184, which was not observed spectroscopically, also is predicted (based on $K_1 = 0.02 \pm 0.02$ km/s) to have a small RV range.

Finally, several of the above-mentioned stars show broadened CCFs and structure that is (or may be) due to RV variation in a binary system (see §3.3), but might also be caused by rotation, large amounts of macroturbulence, noise, etc. The CCFs for four such stars are shown in **Figure 5**. As noted earlier KIC 8004558 (*1) is a high-velocity 262 d binary system; if the CCFs for its eight spectra are fitted with a Gaussian the RVs appear to shift from -260 ± 4 to -242 ± 4 km/s, consistent with binary motion. KIC 10989032 (*32) exhibits the second largest ΔRV (37.5 ± 1.2 km/s), and the *Kepler* Q0-Q17 light curve shows it to be a close semi-detached binary system with an orbital period of 2.3 d. If it is a single-line spectroscopic binary and its broadening is due to stellar rotation then $v \sin i \sim 45 \pm 2$ km/s (see §2.3). The star is listed in the Villanova Eclipsing Binary (EB) Catalog² where its P_{orb} is given as 2.305097 days. The RV curve derived from the eight available spectra appears to be sinusoidal and thus suggests that the orbits have been circularized (see §3 below).

Higher SNR spectroscopic observations and more sophisticated analysis methods (such as the ‘broadening functions’ advocated by Rucinski 1999) might help to better assess the RV variations of the program stars.

2.2 Distances and Space Motions

Membership in the galactic halo stellar population is one of the defining features of an SX Phe star. Height above the galactic plane and space motions are often used to discriminate between Pop. II and Pop. I stars, where stars with vertical height greater than ~ 500 pc and total speed greater than ~ 200 km/s almost certainly are Pop. II stars.

Galactic coords (l , b), $E(B-V)$ reddenings, distances, d (pc), and vertical heights above the galactic plane, z (pc), for the program stars are given in **Table 2**. The KIC distances are derived from the Sloan photometry which gives estimates of T_{eff} and $\log g$. The radii in the KIC follow from the gravities and model masses, and the T_{eff} and radius information gives the luminosity, L . From L and the observed apparent magnitude Brown *et al.* (2011) calculate the distance, from which the $E(B-V)$ reddening and the A_V extinctions are estimated using the simple exponential fall-off model given by their equations 8-13 (see BN12). The only program star for which the KIC does not give $E(B-V)$, and

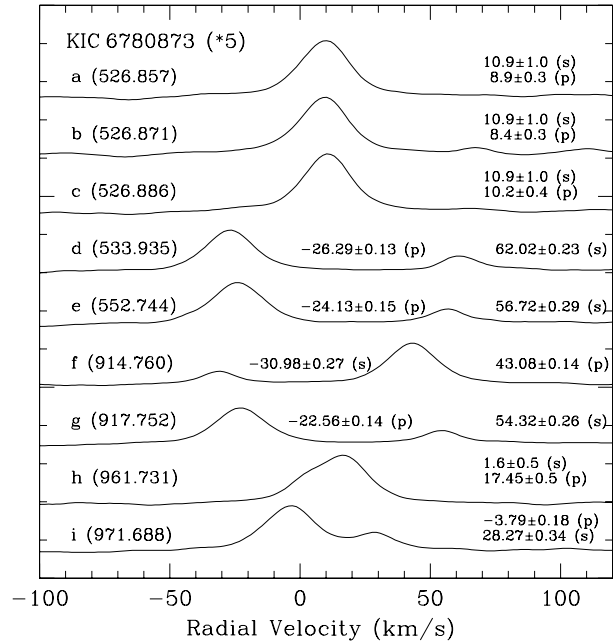


Figure 3. CCFs for the nine spectra of KIC 6780873, a 9.3-day close binary system shown here to be double-lined. Each CCF has been labelled with a letter (a-i) identifying the measured spectrum, and the time of the observations (BJD minus 2456000). Using the peak strengths, each CCF ‘bump’ has been identified as being due to either the primary (p) or secondary (s) star. Also given (right side) are the RVs (km/s) for each component.

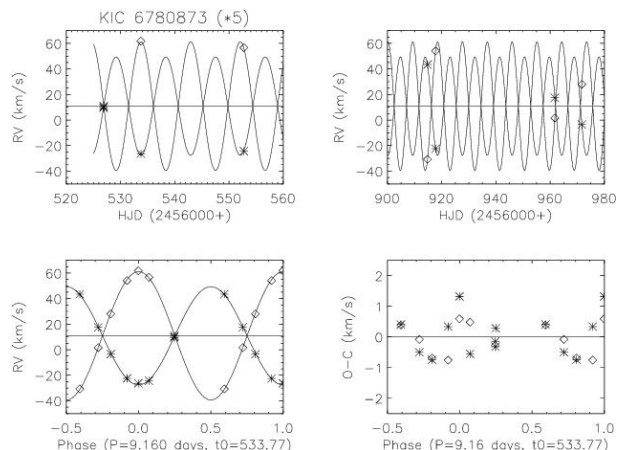


Figure 4. The top two panels show the individual RVs for KIC 6780873 (*5), the 2013 data on the left and the 2014 data on the right, overplotted with model curves assuming eccentricity $e=0$, orbital period $P_{orb}=9.16$ d, HJD time of maximum RV for the secondary = 2456533.77, RV semi-amplitudes for the primary and secondary $K_1 = 38.5$ km/s and $K_2 = 50.3$ km/s, and systemic radial velocity $\gamma = 10.885$ km/s. The bottom left panel shows the observed RVs (asterisks for the primary and open diamonds for the secondary) and the corresponding primary and secondary phased RV curves. The bottom right panel shows the O-C residuals, where the averages for the primary and secondary are 0.009 km/s and -0.011 km/s, respectively, and corresponding standard deviations of the residuals about the means, 0.65 and 0.60 km/s.

² The Villanova Eclipsing Binary catalog (Prša *et al.* 2011; Slawson *et al.* 2011; Matijevic *et al.* 2012) is available on-line at <http://keplerebs.villanova.edu>.

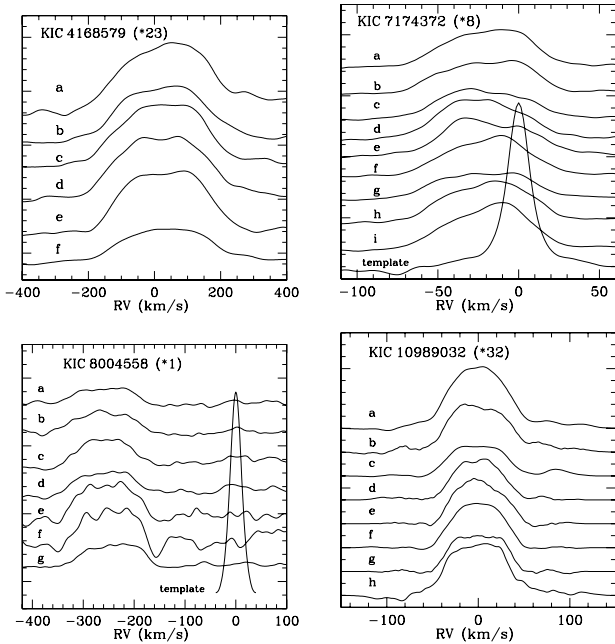


Figure 5. CCFs for four of the BN12 stars, where the ‘letter’ labels on the left identify the individual spectra (see Table 1). For KIC 10989032 (*32, KOI 7397), which is a close binary system with an orbital period of 2.3 d, the CCFs have been Doppler shifted so that the mean RV is zero. KIC 7174372 (*8) and KIC 8004558 (*1) also are probable binary systems (see §3.3). Also shown for KIC 7174372 and KIC 8004558 are the much narrower autocorrelation CCFs for the template synthetic spectra.

consequently distance information, is KIC 11754974, the star studied by Murphy *et al.* (2013b).

Brown *et al.* (2011) warned that where there is a clumpy distribution of interstellar matter “the result is systematic misclassification” in the KIC due to “a scattered and confused relation between T_{eff} and color, and other failings”. For this reason new distance and reddening estimates were derived. These were made using the on-line ‘cumulative reddening *vs.* distance’ tool created for the ‘3D Dust Mapping’ project (see Green *et al.* 2014, 2015) available at <http://argonaut.skymaps.info/query>. This tool requires as input a direction indicator (l, b or RA, DEC) and the distance modulus, $\mu_V (=m_V - M_V)$, and calculates $E(B-V)$ and d (pc), where the interstellar extinction is based on dust maps (see Schlegel *et al.* 1998, Schlafly & Finkbeiner 2011) rather than an exponential model.

For each star μ_V was derived using the apparent visual magnitude m_V given in column 4 of Table 5, and by estimating the absolute visual magnitude, M_V , by assuming for the mass the value $1.5 M_{\odot}$ (*i.e.*, estimated mean for SX Phe stars) and by substituting the spectroscopic estimates of $\log g$ and T_{eff} (given in Table 4, columns 4 and 6) into the following equations:

$$\log(R/R_{\odot}) = 0.5 [\log \mathcal{M} / \mathcal{M}_{\odot} - \log(g/g_{\odot})],$$

$$\log(L/L_{\odot}) = 2 \log(R/R_{\odot}) + 4 \log(T_{\text{eff}}/T_{\text{eff},\odot}),$$

$$M_V = 4.79 - 2.5 \log(L/L_{\odot}).$$

For the Sun we adopted $T_{\text{eff},\odot} = 5772$ K and $\log g_{\odot} = 4.438$, and for the program stars the bolometric corrections, which are small, were ignored. The derived reddenings, distances and vertical heights are given next to the KIC values in Table 2.

The new reddenings are smaller than the KIC values for all but six of the stars, and in general the distances are greater³. The average reddening is 0.12 mag, the average distance is 2.1 kpc, and the average height above the galactic plane is 400 pc. The new reddenings and distances improve upon the KIC values in two ways: (1) T_{eff} and $\log g$ now are based on measurements of high-dispersion spectra, whereas the KIC estimates are based on photometry and have been shown, at least for cooler stars, to be systematically too low by over 200 K (Pinsonneault *et al.* 2012; see below); and (2) the patchy distribution of the interstellar gas and dust, which is evident in the appearance of multiple discrete interstellar lines in several of the CFHT spectra⁴, is now taken into account.

Galactic U, V, W space velocities were estimated by combining the mean RVs given in Table 2 (col. 7), the new distances (col. 5), and the proper motion information summarized in BN12. The velocities are with respect to the Local Standard of Rest (LSR), assuming for the solar motion the values $(U, V, W)_{\odot} = (-8.5 \pm 0.29, 13.38 \pm 0.43, 6.49 \pm 0.26)$ km/s (Coşkunoğlu *et al.* 2011). The calculations were made using the general method given by Johnson & Soderblom (1987), as implemented in the IDL ‘Astrolib’ routine “gal_uvw”, which assumes U positive in the anti-center direction, V positive in the direction of galactic rotation, and W positive in the direction of the North Galactic Pole (*i.e.*, left-handed Galactic system). Also calculated were total space motions, T , equal to $(U^2 + V^2 + W^2)^{1/2}$. The resulting velocities are given in column 8 of Table 2.

The ‘Toomre diagram’ is a graphical summary of U, V, W space motions that is useful for discriminating halo, thick disk and thin disk stars (Sandage & Fouts 1987, Venn *et al.* 2004). Of course, population discrimination based solely on kinematic information is subject to error because the underlying velocity distributions for the different stellar populations overlap by various amounts (Nemec & Linnell Nemec 1991, 1993), a problem that is compounded when

³ Increasing (decreasing) the assumed mass by 0.25 M_{\odot} has little impact on μ_V and d (pc): the μ_V is larger (smaller) by ~ 0.17 mag, and the distance is larger (smaller) by ~ 150 pc; the effect of such a change on $E(B-V)$ depends on the distance and gradient in the $E(B-V)$ *vs.* μ_V graph, but is usually small.

⁴ The distinction between stellar and interstellar Na I D lines is clear for almost all the stars. This is especially true for the three stars with large RVs where the interstellar Na I D lines are shifted ~ 0.5 nm to the right of the stellar lines. For several of the stars two or three individual sets of interstellar lines are seen, each presumably arising from a separate interstellar cloud. For several of the stars the interstellar Na I lines are saturated, an extreme example being KIC 9244992 (*7), which has one of the largest E_{B-V} reddenings. A large range in line strengths was observed for the interstellar neutral potassium (KI) line at 769.8 nm. Surprisingly, KIC 3456605 with $E_{B-V} = 0.14$ has a particularly strong and broad interstellar KI line. Detailed quantitative analysis of the interstellar lines, such as that performed by Poznanski *et al.* (2012), might be useful for investigating these and other spectral features but is beyond the scope of the present paper.

Table 2. Locations and kinematics for the 34 SX Phe candidates. The columns contain: (1-2) KIC and CFHT star numbers; (3) galactic latitude and longitude (degrees); (4-5) $E(B-V)$ reddening (mag) and distance d (pc), from the KIC and based on dust maps; (6) height above the galactic plane z (pc), KIC values and assuming the new distances; (7) mean radial velocity \pm standard error (with number of measured spectra given in parentheses) - for binary systems the systemic RVs are given and underlined; (8) space motions, U , V , W , and total speed, T , all relative to the Local Standard of Rest.

| KIC no. (1) | CFHT no. (2) | Galactic Coords. l (J2000) b (3) | $E(B-V)$ KIC, new (4) | d (pc) KIC, new (5) | z (pc) KIC, new (6) | $\langle RV \rangle$ (km/s) (7) | (U, V, W, T) (km/s) (8) |
|----------------|-----------------|--|-----------------------------|-----------------------------|-----------------------------|--|---------------------------------|
| 1162150 | 15 | 69.5124, 9.7968 | 0.160, 0.07 | 729, 1060 | 124, 180 | -14.8 ± 0.9 (6) | 99, -5, 234, 254 |
| 3456605 | 24 | 72.2362, 8.1478 | 0.203, 0.14 | 956, 1690 | 135, 240 | -7.4 ± 0.6 (3) | -335, -70, -186, 389 |
| 4168579 | 23 | 72.6974, 8.8075 | 0.257, 0.17 | 1644, 3620 | 252, 550 | 22.9 ± 1.7 (6) | -345, 70, -841, 912 |
| 4243461 | 4 | 69.8106, 14.9474 | 0.153, 0.11 | 983, 1580 | 254, 410 | <u>57.2 ± 1.8</u> (8) | -331, -169, 456, 588 |
| 4662336 | 14 | 73.0933, 9.2758 | 0.204, 0.12 | 1059, 1760 | 171, 280 | -11.3 ± 0.4 (4) | -455, -93, -233, 520 |
| 4756040 | 20 | 73.2980, 8.9596 | 0.206, 0.11 | 1048, 1780 | 163, 280 | 5.9 ± 1.4 (4) | -149, 35, -343, 376 |
| 5036493 | 26 | 74.8907, 6.7575 | 0.223, 0.27 | 996, 1890 | 117, 220 | -4.9 ± 0.7 (4) | -355, -62, -187, 406 |
| 5390069 | - | 75.5152, 6.5051 | 0.174, 0.19 | 693, 4200 | 78, 480 | - | - |
| 5705575 | 22 | 73.4695, 11.2094 | 0.209, 0.09 | 1412, 2220 | 275, 430 | <u>-38.1 ± 1.0</u> (9) | -364, 125, -1214, 1274 |
| 6130500 | 9 | 74.6166, 9.9930 | 0.212, 0.12 | 1235, 2170 | 214, 380 | -18.3 ± 0.5 (6) | 147, 145, -586, 622 |
| 6227118 | 27 | 76.0714, 7.6323 | 0.364, 0.12 | 4172, 850 | 539, 110 | 5.3 ± 1.7 (4) | -68, 22, -125, 144 |
| 6445601 | 2 | 74.5439, 10.9821 | 0.185, 0.08 | 1026, 2260 | 195, 430 | -4.5 ± 0.5 (6) | -416, -191, 439, 634 |
| 6520969 | 21 | 74.1754, 11.9396 | 0.212, 0.08 | 1718, 2850 | 355, 590 | -299.5 ± 0.1 (3) | 112, -395, 571, 703 |
| 6780873 | 5 | 74.9284, 11.0447 | 0.153, 0.06 | 729, 2090 | 140, 400 | <u>10.1 ± 0.3</u> (9) | -603, -128, -27, 617 |
| 7020707 | 16 | 73.5340, 14.8428 | 0.166, 0.04 | 1236, 1970 | 317, 510 | 2.4 ± 1.3 (4) | -297, -122, 196, 376 |
| 7174372 | 8 | 71.9764, 18.9932 | 0.136, 0.05 | 1135, 2970 | 369, 970 | <u>-19.2 ± 0.6</u> (9) | -1120, -404, 102, 1195 |
| 7300184 | - | 76.8302, 8.7823 | 0.181, 0.27 | 832, 4240 | 127, 650 | - | - |
| 7301640 | 10 | 77.0021, 8.5969 | 0.212, 0.26 | 1068, 2110 | 160, 320 | -12.0 ± 1.8 (5) | 95, 93, -431, 451 |
| 7621759 | 6 | 76.8876, 9.5983 | 0.207, 0.19 | 1120, 2550 | 187, 430 | 17.0 ± 0.6 (5) | 543, 128, 189, 588 |
| 7765585 | 28 | 77.0330, 9.6755 | 0.115, 0.18 | 455, 1820 | 76, 310 | 1.1 ± 3.3 (6) | 707, 158, 128, 736 |
| 7819024 | 19 | 75.4361, 13.1002 | 0.184, 0.05 | 1310, 1950 | 297, 440 | <u>-63.7 ± 4.4</u> (8) | -298, -61, -259, 399 |
| 8004558 | 1 | 72.7607, 20.3549 | 0.135, 0.05 | 1519, 1430 | 528, 500 | <u>-254.1 ± 1.5</u> (7) | -198, -290, -92, 363 |
| 8110941 | 29 | 77.6587, 9.6836 | 0.184, 0.15 | 910, 1760 | 153, 300 | 4.4 ± 0.3 (4) | -52, -62, 414, 422 |
| 8196006 | 30 | 79.3018, 7.0045 | 0.198, 0.32 | 850, 1820 | 104, 220 | -3.5 ± 0.8 (4) | -133, 26, -311, 339 |
| 8330910 | 3 | 79.6884, 6.8192 | 0.228, 0.31 | 1036, 1770 | 123, 210 | 20.9 ± 1.1 (4) | 572, 142, -9, 590 |
| 9244992 | 7 | 80.6380, 7.8965 | 0.288, 0.22 | 1858, 1470 | 255, 200 | -15.9 ± 0.2 (5) | -37, 40, -334, 338 |
| 9267042 | 12 | 75.8193, 17.8478 | 0.156, 0.05 | 2170, 1580 | 665, 480 | <u>-11.5 ± 1.0</u> (11) | 506, -124, 774, 933 |
| 9535881 | [25] | 79.4210, 11.1577 | 0.168, 0.07 | 864, 1940 | 167, 380 | <u>5.0 ± 0.1</u> (4) | 247, 55, 71, 263 |
| 9966976 | 31 | 80.7107, 10.1734 | 0.221, 0.09 | 1396, 1400 | 247, 250 | <u>-0.1 ± 1.1</u> (4) | 362, 62, 68, 374 |
| 10989032 | 32 | 82.0254, 11.1154 | 0.230, 0.10 | 1931, 2710 | 372, 520 | <u>-25.0 ± 0.3</u> (8) | -997, -236, 436, 1113 |
| 11649497 | 11 | 79.6609, 19.5242 | 0.138, 0.04 | 1374, 1950 | 459, 650 | -21.5 ± 0.2 (6) | -246, 48, -273, 371 |
| 11754974 | 13 | 80.5370, 17.8823 | - , 0.04 | - , 1250 | - , 380 | <u>-307 ± 4</u> (8) | -379, -393, 76, 552 |
| 12643589 | [17] | 82.5739, 17.7885 | 0.111, 0.05 | 592, 1200 | 181, 370 | <u>-60.9 ± 0.1</u> (5) | 568, 144, -365, 691 |
| 12688835 | 18 | 82.7967, 17.5845 | 0.159, 0.03 | 2445, 1890 | 739, 570 | -31.2 ± 7.6 (5) | 318, 14, 34, 321 |

the complexity of the distributions is increased by possible galaxy mergers and local streaming events (see, for example, Bensby *et al.* 2007; Carollo *et al.* 2007, 2010). The Toomre diagram also ignores chemical composition and age differences (see Carollo *et al.* 2016). Despite these limitations the diagram has proven to be useful for identifying Pop. II stars (see, for example, Schuster *et al.* 2012, and Ramírez *et al.* 2013).

A Toomre diagram for the candidate SX Phe stars is plotted in **Figure 6**. The (red) dashed vertical line at -220 km/s separates the stars with prograde motions from those with retrograde motions, and the (blue) dashed curve divides the halo population stars from the thick disk stars which have total space velocities $80 < T < 180$ km/s. Also plotted in Fig. 6 are points for 24 of the *Kepler*-field RR Lyrae stars, where the U, V, W velocities were calculated using the proper motions and distances given in BN12 and the mean velocities from Nemec *et al.* (2013). The metal-poor RR Lyrae stars

(*i.e.*, those with $[\text{Fe}/\text{H}] < -1.0$ dex) are shown as open circles, and the four ‘metal-rich’ RR Lyrae stars (V782 Cyg, V784 Cyg, V2470 Cyg and KIC 11125706) are plotted as open triangles.

Based on the new distances and velocities we conclude that: (1) half of the stars have z -heights greater than 400 pc; (2) in the Toomre diagram all the stars (except possibly KIC 6227118 which is located just inside the thick-disk boundary) have total space motions $T > 180$ km/s, including 16 stars with T greater than 500 km/s; (3) five of the stars orbit the Galaxy in a retrograde direction⁵; and (4) the space motions of the SX Phe stars, in particular the

⁵ Other well-known field SX Phe stars on retrograde orbits include SX Phe itself, BL Cam (=GD 428), and KZ Hya (see Table 1 of Nemec & Mateo 1990b). Given the extreme retrograde motion of the SDSS halo blue straggler J1300+0422 (Tillich *et al.* 2010) it would be of interest to see if it too is pulsationally unstable.

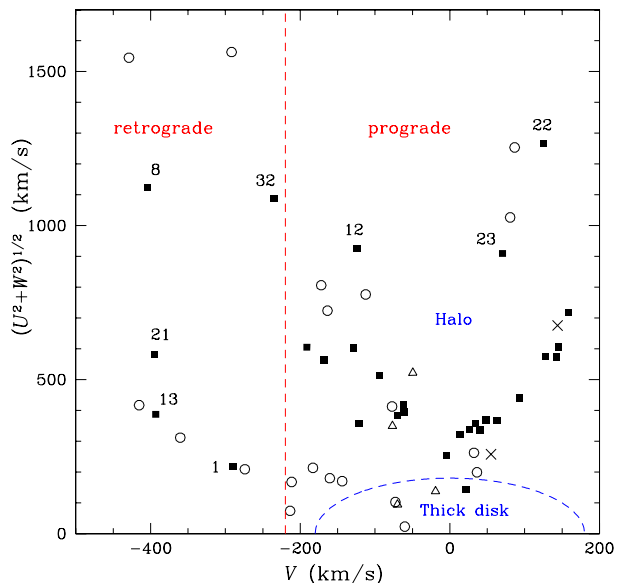


Figure 6. Toomre diagram for the candidate SX Phe stars in the *Kepler* field (solid squares). For comparison purposes 24 of the *Kepler*-field RR Lyrae stars are also plotted (open circles for metal-poor, open triangles for metal-rich). The vertical line at $V = -220$ km/s separates stars undergoing retrograde and prograde motion (asymmetric drift), and the curved line at total space velocity $T=180$ km/s separates the thick disk and halo stars. The labels for the most extreme SX Phe stars are the CFHT star numbers. The two close binaries that were misclassified as candidate SX Phe stars, KIC 9535881 [*25] and KIC 12643589 [*17], are plotted as crosses.

fraction on retrograde orbits, are not substantially different from those of the *Kepler*-field RR Lyrae stars. Each of these findings supports the argument that most, if not all, of the SX Phe candidate stars belong kinematically to the galactic halo stellar population, a conclusion that remains unchanged regardless of whether the z -heights and space motions are based on the new spectroscopic values or on the information in the KIC. Finally, if the galactic halo consists of “two broadly overlapping structural components” as advocated by Carollo *et al.* (2007, 2016) then the stars with retrograde orbits may be members of the outer-halo component.

2.3 Spectral Types

SX Phe (and δ Sct) stars usually have spectral types in the range A3 to F2, corresponding to surface temperatures ranging from ~ 8600 to ~ 6900 K. They also define the blue and red edges of the instability strip at absolute magnitudes $\langle M_V \rangle \sim 1.5$ to 3.5 (*i.e.*, L/L_\odot from ~ 15 to 3). The SX Phe stars found among BSs in globular clusters tend to have, on average, lower luminosities and masses than Pop. I δ Sct stars.

Spectral types and luminosity classes for the program stars were determined using the rectified CFHT spectra and are given in **Table 3** (cols. 5-8). Separate classifications were made based on the appearance of the hydrogen lines, the Ca II K-line, and the overall metallic-line spectrum, using the following criteria: **(H)** the hydrogen Balmer lines have their maximum strength at A2 with the cores and the wings

of the lines decreasing in strength as the temperatures decrease; **(K)** the Ca II K line at 393.3 nm increases in strength towards later spectral types, starting from a line depth comparable to that of the Mg II 448.1 nm line near A0, to a depth that surpasses that of H ϵ at F0; and **(M)** the line strengths of neutral metals steadily increase towards later spectral types⁶.

For the early-A stars, the luminosity class was established using the hydrogen lines, which are luminosity sensitive and permit discrimination within the main-sequence band. For the early-F stars, the metal lines, which are sensitive to both temperature and luminosity, were used – the primary luminosity indicator being the Fe/Ti $\lambda 4172-9$ blend. The most uncertain luminosity classes are those for the late-A stars where the hydrogen and metal-line criteria do not quite overlap (see Gray & Garrison 1989). Inspection of Table 3 reveals that most of the stars are of luminosity class V and thus are on or near the upper main sequence. Of particular interest is the main sequence character of KIC 6227118 (*27), whose distance, $\log g$ and $\log L/L_\odot$ in the KIC, were found to be outliers by BN12 (see their Table 1), and the high-luminosity character of KIC 9244992 (*7), which is consistent with its apparently advanced evolutionary state (see fig. 2 of BN12, and Saio *et al.* 2015).

For single main sequence stars application of any one of the above indicators usually gives the same spectral type; however, such agreement is not necessarily expected for A-F stars, especially those having chemical peculiarities, such as the Am stars (at least half of which are spectroscopic binaries), or for SX Phe stars, whose blue straggler nature and possibility of coalescence or mass transfer in binary systems complicates matters. The greatest disparities in spectral type were found for KIC 8004558 and KIC 11754974, both of which are binary systems (see §3.3).

Assignment of spectral type can also be problematic for spectra that have broad metal lines (see Fig. 2). Since rotation broadens spectral lines, rapid rotators (at least those with i significantly greater than 0°) have lines that are wider and correspondingly shallower than those for slow rotators. Placing too much emphasis on line depth rather than width may lead to an erroneous classification. To mitigate this problem, and improve upon the metal-line spectral types, the spectra of the rapid rotators were compared with the spectra of rapidly rotating standard stars selected from the high $v \sin i$ standard star lists provided by Gray & Garrison (1989) and Gray & Corbally (1994, 2009).

Owing to instrumental artefacts, arising perhaps as remnants of the merging of the orders in the echelle spectra, certain lines were less useful than others for classification purposes. For instance, the H δ line was often unnatural in shape. For this reason, the assigned hydrogen line type was always determined from H γ , and occasionally checked against H δ . Often it was difficult to find the continuum near

⁶ The G-band at 430 nm, which is a useful temperature indicator for mid-to-late F-type stars, was also used to assess the spectral type of KIC 12643589 [*17], one of the two misclassified SX Phe stars and the star with the latest spectral type. Its G-band spectral type is F6 V, which is to be compared with the F5 V type from H γ , and F5/F6 from the metal lines. All the spectral indicators are consistent with a relatively cool temperature, ~ 6500 K.

Table 3. Spectral types, luminosity classes, mean projected rotational velocities, $\langle v \sin i \rangle$ (km/s), and mean radial-tangential macroturbulent velocities, $\langle \zeta_{\text{RT}} \rangle$ (km/s), for the *Kepler*-field candidate SX Phe stars. The columns contain: (1) KIC number; (2) CFHT number; (3-4) Right Ascension and Declination (J2000); (5-7) spectral type based on the K-line, the Hydrogen lines, and the metal lines; (8) luminosity class; (9) weighted average of the $v \sin i$ values given in Table 1, with the number of spectra measured given in parentheses; (10) the mean $v \sin i$ values derived using the goodness-of-fit method; and (11) the average ζ_{RT} derived using the goodness-of-fit method. In the last two columns the uncertainty is the standard deviation of the mean, and in (11) the number of lines that were measured is given in parentheses.

| KIC no. (1) | CFHT no. (2) | RA (J2000) DEC | | Spectral Type | | | Lum. Class (8) | $\langle v \sin i \rangle$ | | $\langle \zeta_{\text{RT}} \rangle$ GOF (11) |
|-------------------|--------------------|------------------|-------------------|---------------|-----------|-------------|----------------------|----------------------------|-------------|--|
| | | h : m : s (3) | ° : ' : '' (4) | K (5) | H (6) | M (7) | | FT (9) | GOF (10) | |
| 1162150 | 15 | 19:25:16.66 | +37:17:22.84 | - | F1 | A7 | V | 225 ± 5 (6) | ... | ... |
| 3456605 | 24 | 19:38:34.22 | +38:30:45.46 | F0 | F0 | F0 | II/IIIa | 13.7 ± 1.7 (3) | 11 ± 3 | 16 ± 3 (20) |
| 4168579 | 23 | 19:36:41.30 | +39:13:34.36 | A8 | F1 | A9 | V | 197 ± 4 (6) | ... | ... |
| 4243461 | 4 | 19:01:45.58 | +39:19:09.88 | A9 | A9 | A9 | V | 53.2 ± 0.8 (8) | 53 ± 3 | 29 ± 6 (08) |
| 4662336 | 14 | 19:35:29.34 | +39:47:26.20 | A9 | A9 | A9 | III | 83.2 ± 0.6 (4) | ... | ... |
| 4756040 | 20 | 19:37:26.19 | +39:49:17.59 | A7 | F1 | F0 | V | 42.3 ± 2.1 (4) | 48 ± 2 | 18 ± 4 (05) |
| 5036493 | 26 | 19:51:29.03 | +40:07:58.53 | A3 | A7 | A3 | V | 19.0 ± 1.1 (4) | 18 ± 1 | 15 ± 1 (27) |
| 5705575 | 22 | 19:27:19.60 | +40:59:57.71 | A5 | A9 | A6 | V | 88.2 ± 1.1 (9) | ... | ... |
| 6130500 | 9 | 19:35:48.64 | +41:27:13.79 | - | - | F0 | IV: | 49.3 ± 1.1 (6) | 48 ± 1 | 25 ± 2 (20) |
| 6227118 | 27 | 19:50:33.67 | +41:35:04.07 | A6 | A8 | A5 | V | 133 ± 2 (4) | ... | ... |
| 6445601 | 2 | 19:30:55.42 | +41:50:28.11 | F2 | F2 | F2 | V | 71.3 ± 0.4 (6) | 70 ± 2 | 25 ± 4 (20) |
| 6520969 | 21 | 19:25:27.08 | +41:56:30.11 | A3 | A7 | A3 | V | <5.8 ± 0.8 (3) | <8 ± 1 | 15 ± 2 (35) |
| 6780873 | 5 | 19:31:32.23 | +42:12:22.83 | F1 | F1 | F1 | IV | <8 ± 1 (3) | <8 ± 1 | 16 ± 1 (13) |
| 7020707 | 16 | 19:09:46.88 | +42:35:07.20 | - | F1 | F0 | V | 105 ± 2 (4) | ... | ... |
| 7174372 | 8 | 18:45:48.25 | +42:43:36.90 | A9 | A9 | A9 | III | 41.6 ± 1.0 (9) | 41 ± 1 | 26 ± 2 (21) |
| 7301640 | 10 | 19:48:28.67 | +42:51:41.00 | A9 | A9 | A9 | V | 123 ± 2 (5) | ... | ... |
| 7621759 | 6 | 19:43:22.63 | +43:14:43.47 | F1 | F1 | F1 | IV/V | 77.7 ± 1.0 (5) | ... | ... |
| 7765585 | 28 | 19:43:22.71 | +43:24:29.74 | A9 | A9 | A9 | V | 122 ± 1 (6) | ... | ... |
| 7819024 | 19 | 19:22:38.01 | +43:33:08.38 | A9 | F1 | A9 | V | 95.1 ± 1.3 (8) | ... | ... |
| 8004558 | 1 | 18:40:04.07 | +43:52:18.06 | A2.5 | F0 | A2 | V | 84.2 ± 2.6 (7) | ... | ... |
| 8110941 | 29 | 19:44:57.95 | +43:57:15.65 | F0 | F0 | F0 | III | <7.5 ± 0.2 (4) | <6 ± 1 | 11 ± 1 (19) |
| 8196006 | 30 | 20:02:23.14 | +44:01:32.08 | - | F0 | F2 | V | 92.6 ± 1.3 (4) | ... | ... |
| 8330910 | 3 | 20:04:23.03 | +44:15:22.01 | - | - | - | - | 224 ± 3 (4) | ... | ... |
| 9244992 | 7 | 20:01:57.43 | +45:37:15.59 | F0 | F0 | F0 | II | <6.7 ± 0.3 (5) | <6 ± 1 | 12 ± 3 (13) |
| 9267042 | 12 | 18:58:52.07 | +45:44:57.85 | A7 | A7 | A3 | V | 106 ± 3 (11) | ... | ... |
| 9535881 | [25] | 19:42:14.31 | +46:10:40.94 | F0.5 | F0.5 | F0.5 | V | 54.6 ± 1.7 (4) | 62 ± 2 | 18 ± 5 (09) |
| 9966976 | 31 | 19:50:46.42 | +46:49:28.71 | F0 | F0 | F0 | V | 123 ± 1 (4) | ... | ... |
| 10989032 | 32 | 19:49:34.46 | +48:24:38.88 | A5 | A5 | A5 | V | 45.0 ± 0.9 (8) | 44 ± 1 | 15 ± 2 (26) |
| 11649497 | 11 | 18:56:55.73 | +49:44:33.42 | - | A6 | F0 | III | <5.6 ± 0.2 (6) | <5 ± 1 | 12 ± 2 (07) |
| 11754974 | 13 | 19:08:15.95 | +49:57:15.56 | A3 | F1 | A2 | V | 28.8 ± 1.7 (8) | 31 ± 1 | 13 ± 2 (21) |
| 12643589 | [17] | 19:13:17.13 | +51:43:35.59 | - | F5 | F5.5 | V | 28.7 ± 0.1 (5) | 32 ± 2 | 18 ± 2 (06) |
| 12688835 | 18 | 19:15:01.07 | +51:50:55.34 | A3 | A7 | A3 | V | 230 ± 5 (5) | ... | ... |

the Ca II K-line, in which case a Ca II K-line type is not provided in Table 3. In general the least weight was placed on the K-line when it was used in the classifications.

2.4 Rotational and Macroturbulent Velocities

The spectra exhibit a wide range of line widths, with two thirds of the stars having broad lines (see Fig. 2). Stellar rotation is usually the dominant broadening mechanism; however macroturbulence and pulsations may also be contributing factors. For stars with narrow lines (which tend to be the slowest rotators but may, like Procyon, be fast rotators seen pole-on) the line profile shapes are determined mainly by instrumental and natural broadening, photospheric thermal motions, Coulomb interactions of neighbouring particles, and microturbulence.

2.4.1 Projected equatorial rotation velocities

The projected equatorial rotation velocity, $v \sin i$, was measured for each spectrum using the Fourier transform (FT) method pioneered by Carroll (1928, 1933) and further developed by Gray (1973, 1975, 1978), Smith & Gray (1976) and others (Dravins 1982; Reiners & Schmitt 2002; Reiners & Royer 2004; Simón-Díaz & Herrero 2007, 2014)⁷. Since most of the available spectra have signal-to-noise ratios <100 no attempt was made to measure differential rotations or to investigate line bisectors. The $v \sin i$ values given in Table 1

⁷ The v in $v \sin i$ is the equatorial velocity, and the inclination angle, i , is the angle between the observer's line-of-sight and the direction of the rotation axis. This i is not to be confused with the orbital inclination angle used in §3 to describe the binary systems, where i is the angle between the line-of-sight and the line perpendicular to the orbital plane.

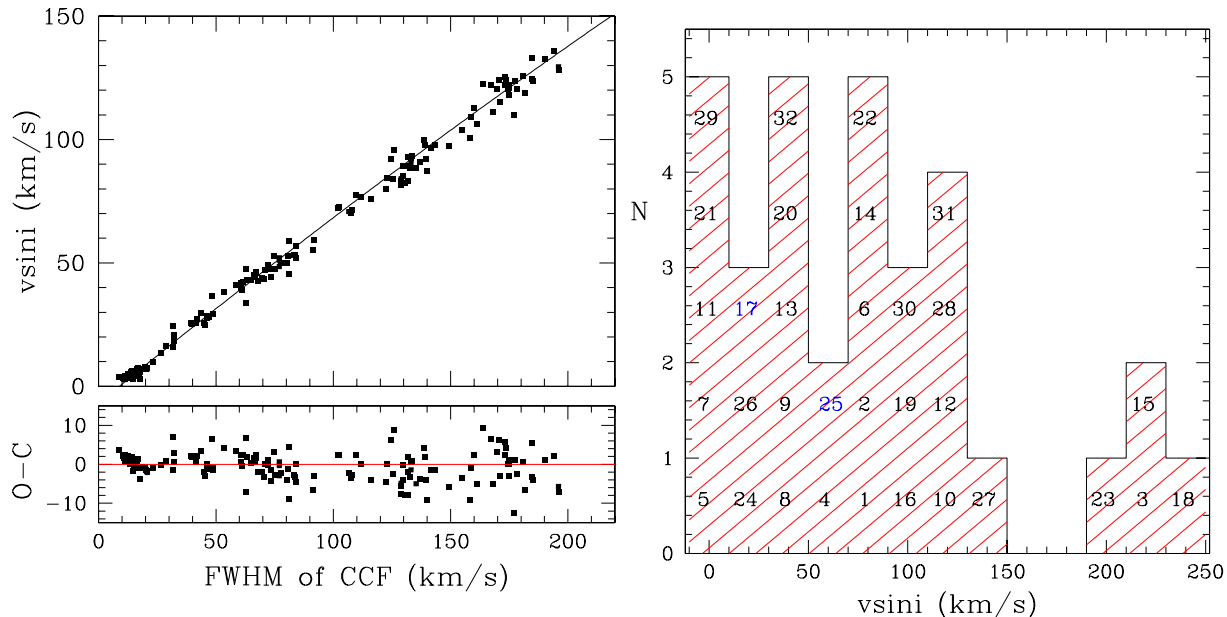


Figure 7. Left: The upper panel shows the correlation between the $v \sin i$ values derived using the Díaz *et al.* (2011) Fourier transform method, and the gaussian FWHM of the CCF (object-template). The lower panel shows the residuals from the quadratic fit, the rms scatter about zero amounting to ~ 6 km/s. Right: Histogram of the derived mean $v \sin i$ values for the *Kepler*-field candidate SX Phe stars. The labels are the CFHT star numbers (see Table 1) and are coloured blue for the two close binaries misclassified as candidate SX Phe stars: KIC 9535881 [*25] and KIC 12643589 [*17].

(col.9) were derived using the ‘rcros’ program of Díaz *et al.* (2011). This algorithm calculates the cross-correlation function (CCF) between an object spectrum and a template spectrum, where user-specified wavelength intervals (e.g., 200-400Å) replace individual lines. The $v \sin i$ values follow from the location of the first zero in the FT of the CCF central maximum (assuming a linear limb darkening law with $\epsilon = 0.6$, and taking account of wavelength dependence). For our spectra, the method has several advantages over measuring individual line profiles, the greatest being that in the FTs the first zeros were usually well defined with sidelobe signatures significantly higher than the background noise level. Using simulations Díaz *et al.* concluded that “for the usual values of S/N and instrumental broadening, the variation in the first zero position caused by additional broadening and noise is below 1%.” Selection of the template spectra depended on the amount of line broadening. For the spectra with broad lines both narrow- and broad-lined templates appropriate for A- and early-F spectral types were used, including synthetic spectra with $v \sin i$ values equal to 10, 50 and 100 km/s. For the stars with narrow-lined spectra (including the RV standards) the adopted template spectrum consisted of either a synthetic solar spectrum, an A-star spectrum, or the spectrum of one of the very narrow-lined program or standard stars.

The derived $v \sin i$ values correlate well with the measured Gaussian full-width at half-maximum (FWHM) values of the CCFs (see left panel of **Figure 7**). Because the four fastest rotators have CCFs that deviate from a Gaussian distribution they have been excluded from the graph; no corrections were made for the ~ 4 km/s instrumental broadening. The quadratic least-squares fit is given by $y = -2.859 \times 10^{-4}x^2 + 0.781x - 6.888$, where x is the FWHM of the CCF, and y is the value of $v \sin i$. The residuals have

an rms scatter of approximately 6 km/s. The uncertainties in the $v \sin i$ values depend on the width of the CCF central maximum, the height of the CCF peak, and the noise in the CCF. The largest random errors occur for the fastest rotators with the broadest lines. For the narrow-lined spectra the rotational broadening is comparable in magnitude to the instrumental and other broadenings mentioned above and hence the $v \sin i$ values are upper limits.

Weighted-average $v \sin i$ values based on the FT method applied to all the spectra are given in column 9 of **Table 3**, and a histogram of the $\langle v \sin i \rangle$ values is plotted in the right panel of **Figure 7**. Although the number of stars is relatively small, the distribution appears approximately uniform between 0 and 150 km/s, with the four fastest rotators having $\langle v \sin i \rangle$ values greater than 195 km/s. The four slowest rotators have $\langle v \sin i \rangle$ values smaller than 8 km/s, and about two-thirds of the stars have $v \sin i$ values larger than 50 km/s. Since main-sequence A-type stars generally have $v \sin i$ values ranging from the resolution limit of the instrumentation to nearly as high as the rotational break-up limit ~ 350 km/s, and because F-type stars tend to rotate much more slowly (see Fig. 18.21 of Gray 2005, Fig. 1 of Royer *et al.* 2007, and Fig. 11 of Bruntt *et al.* 2010b), the observed range of line broadenings meets expectations for a sample of A- and early-F type stars.

2.4.2 Macroturbulent velocities

The existence of granulation cells larger than the mean free path of a photon (*i.e.*, macroturbulence; see Gray 2005, Chapter 17) is often invoked to explain line broadening in excess of that attributed to rotation. It has been suggested that gravity waves, possibly originating with non-radial os-

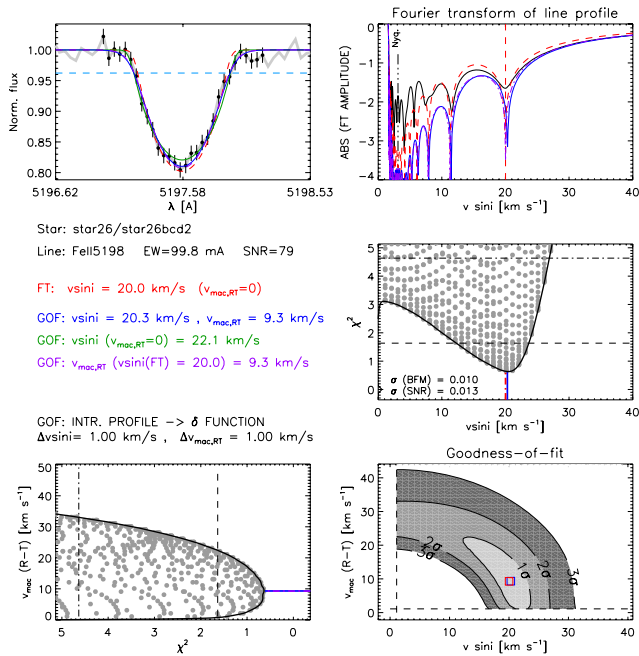


Figure 8. Example output from the ‘IACOB-broad tool’, which was used to estimate radial-tangential macroturbulent velocity, ζ_{RT} , and the projected rotation velocity, $v \sin i$. Here, the strong Fe II line at 5197.58\AA was measured in the coadded spectrum of KIC 5036493 (*26). The resulting FT and GOF $v \sin i$ values for this line are in excellent agreement with the $\langle v \sin i \rangle$ value derived using ‘rcros’, 19.0 ± 1.1 km/s. The resulting ζ_{RT} of 9 ± 8 km/s (the uncertainty follows from the contour plot in the bottom right panel) is smaller than, but consistent with, the mean value of $\langle \zeta_{RT} \rangle = 15 \pm 1$ km/s derived from measurements of this line and 26 other lines in the same spectrum.

cillations (Lucy 1976; de Jager 1990; Cantiello *et al.* 2009; Simón-Díaz *et al.* 2010; Aerts *et al.* 2009, 2014; Balona 2011; Schiodde *et al.* 2013; Grassitelli *et al.* 2015), may cause or contribute to macroturbulent broadening. In many cases the amount of line broadening due to macroturbulence may be as much or more than that caused by rotation (e.g., Markova *et al.* 2014).

The radial-tangential macroturbulent velocity dispersion, ζ_{RT} (Gray 1973, 1975, 1978), was estimated for sixteen BN12 stars using the ‘IACOB-broad’ tool of Simón-Díaz & Herrero (2014). Artificial line profiles were fitted to unblended high-SNR lines in the observed spectra by varying $v \sin i$ and ζ_{RT} , where the combined Fourier transform (FT) and goodness-of-fit (GOF) methodology was used to infer the optimum (minimum χ^2) values of $v \sin i$ and ζ_{RT} for each line. These values were then averaged over lines to give the final estimates for each star, which are given in the last two columns of Table 3.

An application of the IACOB-broad tool is illustrated in **Figure 8**. The upper-left panel shows observed and fitted profiles for the 5197.58\AA Fe II line in the spectrum of KIC 5036493 (*26). The upper-right panel shows the Fourier transform of the observed line profile, where the first dip corresponds to the $v \sin i$ value if $\zeta_{RT} = 0$; the middle-right and lower-left panels show χ^2 plots; and the middle-left panel summarizes the FT and GOF estimates. Here,

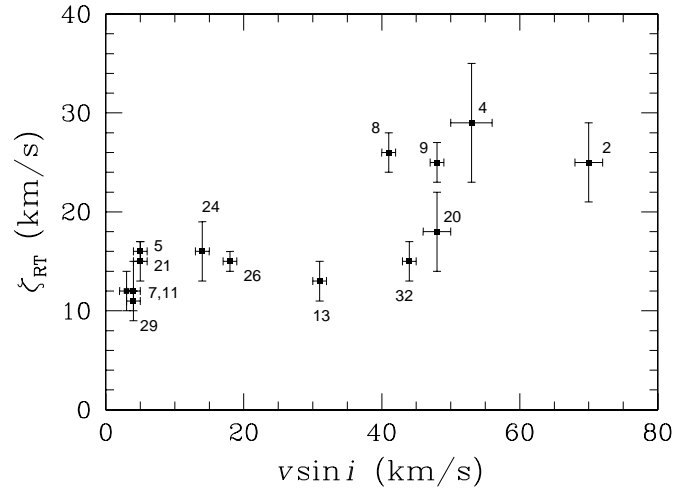


Figure 9. Macroturbulent velocity dispersion, ζ_{RT} , versus projected equatorial velocity, $v \sin i$, for 14 SX Phe stars. The labels are the CFHT star numbers.

and for most of the other stars, the FT and GOF values are consistent. Plots similar to the bottom-right contour graph, where the ‘banana-shaped’ contours reflect the relation $v_{\text{tot}}^2 = [(v \sin i)^2 + \zeta_{RT}^2]^{1/2}$ introduced by Saar & Osten (1997), have been presented by Ryans *et al.* (2002), Dall *et al.* (2010), and Bruntt *et al.* (2010a). Since the GOF $v \sin i$ values agree extremely well with those derived using the ‘rcros’ FT method (see §2.4.1) the latter were adopted, and only the ζ_{RT} retained.

Figure 9 shows that the derived macroturbulent velocity dispersions fall in the range 10–30 km/s, with an apparent trend of increasing ζ_{RT} with increasing $v \sin i$. Without knowing the inclination angle it is hard to know whether there is correlation between the equatorial velocity and ζ_{RT} .

For main sequence stars the ‘granulation boundary’ that marks the onset of convection (Böhm-Vitense 1958; Böhm-Vitense & Canterna 1974; Gray & Nagel 1989; Paxton *et al.* 2011, 2013, 2015) occurs near spectral type F0, corresponding to $B-V \sim 0.3$ and $T_{\text{eff}} \sim 7000$ K. This boundary appears to be coincident with the red edge of the Cepheid instability strip (Böhm-Vitense & Nelson 1976). Since the stars considered here are mainly mid-to-late A-type pulsators with $(B-V)_0 < 0.30$ mag (see Table 4) they tend to lie on the hot side of the granulation boundary in the instability strip. Such stars might be expected to have reversed-C shaped line bisectors (Gray & Toner 1986; Gray 2009) and possibly significant atmospheric velocity fields (Landstreet 1999; Landstreet *et al.* 2009). In addition, many may have chemical abundance anomalies (Preston 1974; Adelman 2004) that are undoubtedly related to magnetic fields (Donati & Landstreet 2009) and diffusion (Michaud *et al.* 1976).

The hotter and more luminous OB-stars (for which microturbulence is assumed to be negligible) tend to have very large ζ_{RT} values, possibly as high as ~ 150 km/s, which appear to increase with increasing T_{eff} and $v \sin i$ (see Ryans *et al.* 2002; Simón-Díaz & Herrero 2014; Markova *et al.* 2014). On the cool side of the granulation boundary the F, G and K-type stars (see Gray 1988) tend to show an increase in ζ_{RT} with increasing temperature (and luminosity). For the Sun $\zeta_{RT} \sim 3.5$ km/s, and for F5 V stars values reach

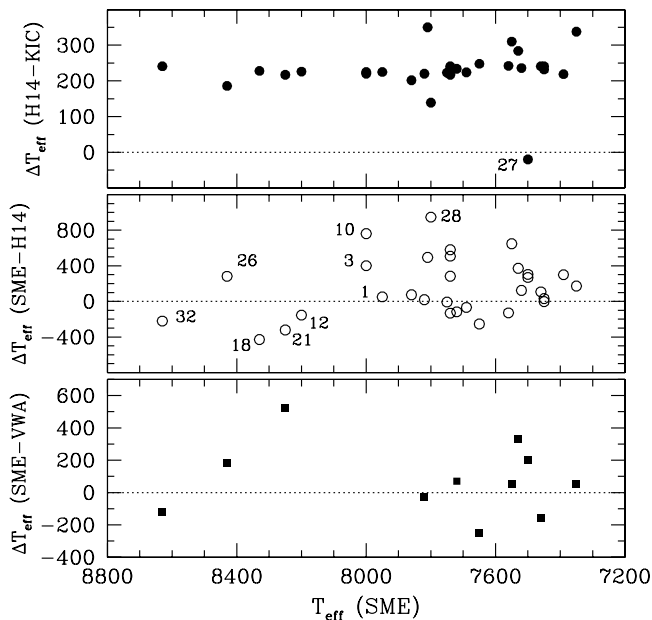


Figure 10. (Top) Comparing the KIC and H14 photometric effective temperatures for the SX Phe candidates reveals a systematic difference of ~ 240 K, in agreement with, and extending to hotter temperatures, the conclusion reached earlier by Pinsonneault *et al.* (2012). KIC 6227118 (*27) is an obvious outlier. (Middle) Comparison of the SME spectroscopic T_{eff} and the H14 photometric T_{eff} values – nine stars have been labelled with the CFHT star number; (Bottom) Comparing the spectroscopically derived effective temperatures.

~ 6 km/s (see Fig. 17.10 of Gray 2005; Bruntt *et al.* 2010b; Doyle *et al.* 2014). Fig. 3 of Valenti & Fischer (2005) shows that for stars with $T_{\text{eff}} = 6200$ K the upper limit of ζ_{RT} is ~ 9 -10 km/s. Such cool stars tend to be slow rotators (see above), have C-shaped line bisectors (Gray & Nagel 1989; Gray 1989, 2009), and show chromospheric emission in UV spectra (Böhm-Vitense & Dettmann 1980; Gray & Toner 1986). Simple interpolation suggests that our program stars might be expected to have intermediate ζ_{RT} values, which is, in fact, borne out by the observation that the average $\langle \zeta_{\text{RT}} \rangle = 18 \pm 2$ km/s for the measured stars.

Recent precise $v \sin i$ and ζ_{RT} measurements made by Gray (2014) for five narrow-lined A0-A2 main sequence stars show them to have much lower ζ_{RT} values than the hot but slightly cooler stars studied here. It is perhaps significant that our sample stars are all pulsating while the stars studied by Gray are outside the instability strip and do not appear to pulsate. This observation lends support to the notion that the relatively high macroturbulent velocity dispersions of the SX Phe stars are due to (or at least related to) non-radial pulsations.

2.5 Other Atmospheric Characteristics

In addition to $v \sin i$ and ζ_{RT} velocities, several other atmospheric characteristics were derived from the spectra. These include: effective temperature, T_{eff} ; surface gravity, $\log g$; microturbulent velocity, ξ_t , and metal abundance, [Fe/H]. Since the *Kepler* SX Phe sample consists of stars exhibiting a

wide range of line widths and metallicities, stars with radial speeds as high as 300 km s^{-1} , close and wide binary systems, etc., and spectra with a wide range of SNRs, it was necessary to employ several different methods for the spectral data analyses. In general synthetic spectra were fitted to observed spectra, where χ^2 minimization techniques were used to optimize atmospheric parameters. In all cases 1D plane-parallel atmospheres in LTE were assumed. Specifically, the ATLAS9 model atmospheres of Kurucz (see Castelli & Kurucz 2004) were used for the radiative transfer calculations. Basic spectral line information (excitation potentials, $\log g f$ values) was taken from the VALD3 website (Piskunov *et al.* 1995; Kupka *et al.* 1999), and for the assumed composition mix the Asplund *et al.* (2009) solar abundances were adopted.

All the spectra (both individual and coadded) were measured using the ‘Spectroscopy Made Easy’ (SME) program of Valenti & Piskunov (1996). Initially, wavelength ranges were limited to the same ‘windows’ used by Valenti & Fischer (2005), supplemented by regions around the first three Balmer lines. The results were then refined using simultaneous fitting of the 25 wavelength windows as advocated by Brewer *et al.* (2015 - see their Table 2), where the initial estimates served as starting values. A sample fit for a portion of the KIC 7020707 spectrum can be found in Nemeč *et al.* (2015).

For those narrow-lined stars for which equivalent widths (EWs) of unblended lines could be reliably measured, the curve-of-growth (COG) method, also known as the equivalent width (EW) method, was used to derive a second set of estimated atmospheric characteristics. The analyses were performed using both MOOG (Sneden 1973) and VWA (Bruntt *et al.* 2002). For the MOOG analyses the EWs were measured using ARES (Sousa *et al.* 2007, 2015), while for the VWA analyses they were measured as part of the reductions. To help ensure comparability of the results from VWA and MOOG every attempt was made to measure the same iron lines; usually there was good agreement. VWA diagnostic diagrams were plotted, including derived iron abundances, $A(\text{Fe}) (= \log N_{\text{Fe}}/N_{\text{tot}})$, versus measured EW, and $A(\text{Fe})$ versus lower excitation potential (EP). The T_{eff} values were derived by requiring independence of $A(\text{Fe})$ and EP. The microturbulent velocities ξ_t were derived by requiring independence of $A(\text{Fe})$ and EW. And the $\log g$ were derived by requiring similar mean $A(\text{Fe})$ values for the Fe I and Fe II lines (*i.e.*, ionization equilibrium).

The results of the spectral analyzes are summarized in **Table 4**, where the first row for each star summarizes the parameter estimates derived using SME, and the second row gives, if available, the results of the most reliable VWA/MOOG analyses; also given are the photometric estimates from the KIC and from Huber *et al.* (2014). When individual parameters were assumed, such as for the difficult-to-measure surface gravity, the values that were assumed are given in parentheses; otherwise derived values (with uncertainties) are recorded. Since the T_{eff} and $\log g$ estimates ignore variation over the pulsation cycle the true uncertainties are difficult to estimate and may be larger than the reported values.

Table 4. Atmospheric characteristics for 32 of the 34 candidate SX Phe stars in the *Kepler* field. For all the stars the first row gives the SME estimates, and when VWA/MOOG estimates (based on the EW/COG method) were also made they are given on the 2nd row. Assumed and uncertain values are given in parentheses. The KIC and CFHT star numbers are given in the first two columns. The third to ninth columns give, respectively, the derived surface gravity, effective temperature, microturbulent velocity and metal abundance. For comparison purposes the table also contains the KIC and Huber *et al.* (2014) photometrically-based values.

| KIC no. (1) | CFHT no. (2) | log g (cm/s ²) | | T_{eff} (K) | | ξ_t (km/s) This paper (7) | [Fe/H] (dex) | |
|-------------------|--------------------|------------------------------|--------------------------|----------------------|--------------------------|-------------------------------------|-----------------|--------------------------------|
| | | KIC, H14 (3) | This paper (4) | KIC, H14 (5) | This paper (6) | | KIC, H14 (8) | This paper (9) |
| 1162150 | 15 | 3.46, 3.49 | 3.61 ± 0.10 | 6871, 7090 | 7390 ± 50 | (7 ± 2) | -0.01, +0.02 | -0.20 ± 0.30 |
| 3456605 | 24 | 3.94, 3.94 | 3.99 ± 0.05 4.2 ± 0.2 | 7112, 7353 | 7460 ± 90 7630 ± 50 | 3.8 ± 0.1 2.8 ± 0.2 | -0.18, -0.18 | +0.50 ± 0.10 +0.58 ± 0.11 |
| 4168579 | 23 | 3.79, 3.84 | 3.57 ± 0.08 | 7534, 7757 | 7750 ± 90 | 5.3 ± 2.0 | -0.09, -0.1 | +0.08 ± 0.20 |
| 4243461 | 4 | 4.15, 4.20 | 4.33 ± 0.05 | 6918, 7159 | 7740 ± 50 | 6.8 ± 0.2 | -0.24, -0.22 | +0.11 ± 0.15 |
| 4662336 | 14 | 3.89, 3.88 | 3.95 ± 0.05 | 7211, 7452 | 7450 ± 50 | 5.9 ± 0.1 | -0.13, -0.14 | -0.05 ± 0.15 |
| 4756040 | 20 | 4.09, 4.09 | 4.08 ± 0.05 4.1 ± 0.2 | 7603, 7837 | 7720 ± 50 7650 ± 100 | 4.9 ± 0.3 2.8 ± 0.2 | -0.01, -0.02 | -0.15 ± 0.20 -0.12 ± 0.15 |
| 5036493 | 26 | 3.95, 3.97 | (4.7 ± 0.2) 4.5 ± 0.2 | 7962, 8148 | 8430 ± 100 8250 ± 100 | 2.7 ± 0.2 2.4 ± 0.3 | +0.00, +0.07 | -0.02 ± 0.15 -0.22 ± 0.20 |
| 5705575 | 22 | 3.99, 4.03 | 4.00 ± 0.05 | 7583, 7785 | 7860 ± 50 | (10 ± 2) | -0.16, -0.18 | -0.1 ± 0.2 |
| 6130500 | 9 | 4.14, 4.11 | 4.1 ± 0.2 | 7581, 7801 | 7820 ± 100 | 5.3 ± 1.0 | -0.01, -0.02 | -0.07 ± 0.20 |
| 6227118 | 27 | 1.03, 2.84 | (4.5 ± 0.3) | 7217, 7197 | 7500 ± 200 | 4.2 ± 1.0 | -0.15, -0.5 | (+0.04 ± 0.20) |
| 6445601 | 2 | 4.09, 4.11 | 3.90 ± 0.15 | 7186, 7419 | 7450 ± 60 | 6.0 ± 0.5 | -0.17, -0.16 | +0.3 ± 0.2 |
| 6520969 | 21 | 3.96, 3.78 | (3.80) 4.3 ± 0.2 | 8355, 8572 | 8250 ± 50 7730 ± 100 | 2.7 ± 0.3 2.4 ± 0.2 | -0.13, -0.2 | -0.7 ± 0.2 -0.84 ± 0.16 |
| 6780873 | 5 | 4.35, 4.36 | 4.03 ± 0.08 4.3 ± 0.2 | 6874, 7158 | 7530 ± 50 7200 ± 100 | 3.7 ± 0.4 1.3 ± 0.3 | -1.09, -1.1 | (+0.0 ± 0.3) (+0.16 ± 0.20) |
| 7020707 | 16 | 4.00, 3.95 | 3.93 ± 0.05 | 7447, 7689 | 7560 ± 50 | (10 ± 2) | -0.21, -0.2 | -0.2 ± 0.2 |
| 7174372 | 8 | 4.10, 4.10 | 3.4 ± 0.2 3.7 ± 0.2 | 7228, 7457 | 7740 ± 100 7380 ± 100 | 3.4 ± 0.5 2.1 ± 0.2 | -0.30, -0.3 | -0.2 ± 0.2 +0.11 ± 0.20 |
| 7301640 | 10 | 4.07, 4.13 | 4.2 ± 0.2 | 7014, 7239 | 8000 ± 100 | (14 ± 2) | -0.01, +0.02 | +0.45 ± 0.15 |
| 7621759 | 6 | 4.05, 4.02 | (4.02) | 6966, 7316 | 7800 ± 80 | (11 ± 2) | -0.26, -0.24 | (-0.24) |
| 7765585 | 28 | 4.80, 4.31 | (4.31) | 6714, 6853 | 7800 ± 150 | (9 ± 2) | +0.15, +0.07 | +0.15 ± 0.10 |
| 7819024 | 19 | 4.10, 4.10 | 4.13 ± 0.10 | 7534, 7758 | 7690 ± 50 | 7.0 ± 1.5 | -0.27, -0.32 | +0.00 ± 0.20 |
| 8004558 | 1 | 3.90, 3.89 | 4.3 ± 0.2 | 7674, 7899 | 7950 ± 100 | 5.2 ± 0.4 | -0.45, -0.44 | -0.3 ± 0.2 |
| 8110941 | 29 | 4.13, 4.13 | 4.13 ± 0.05 4.0 ± 0.2 | 6839, 7177 | 7350 ± 150 7300 ± 150 | 2.9 ± 0.5 2.5 ± 0.5 | -0.09, -0.06 | +0.1 ± 0.2 +0.06 ± 0.20 |
| 8196006 | 30 | 4.25, 4.28 | 4.27 ± 0.05 | 7015, 7232 | 7740 ± 65 | (10 ± 2) | -0.44, -0.44 | +0.16 ± 0.20 |
| 8330910 | 3 | 4.06, 4.07 | (4.13) | 7379, 7599 | 8000 ± 60 | (7 ± 2) | -0.20, -0.24 | -0.1 ± 0.3 |
| 9244992 | 7 | 3.51, 3.52 | 3.52 ± 0.15 | 6592, 6902 | 7550 ± 100 | 4.5 ± 0.7 | -0.14, -0.16 | +0.1 ± 0.3 |
| 9267042 | 12 | 3.80, 3.76 | 4.28 ± 0.10 | 8128, 8354 | 8200 ± 80 | (8 ± 2) | -0.11, -0.14 | -0.02 ± 0.20 |
| 9535881 | [25] | 4.18, 4.07 | 3.97 ± 0.05 | 7161, 7397 | 7520 ± 70 | 6.1 ± 0.8 | -0.22, -0.2 | -0.03 ± 0.15 |
| 9966976 | 31 | 3.93, 3.92 | 4.32 ± 0.06 | 7638, 7872 | 7740 ± 50 | (7 ± 2) | +0.05, +0.07 | +0.02 ± 0.10 |
| 10989032 | 32 | 4.07, 4.08 | (4.10) | 8610, 8851 | 8630 ± 100 | (5 ± 2) | -0.01, +0.07 | +0.3 ± 0.3 |
| 11649497 | 11 | 4.02, 4.03 | 3.98 ± 0.05 | 7656, 7904 | 7650 ± 80 | 4.4 ± 0.1 | -0.10, -0.04 | +0.2 ± 0.2 |
| 11754974 | 13 | - , 3.98 | 3.98 ± 0.05 4.0 ± 0.2 | - , 7231 | 7500 ± 50 7300 ± 150 | 2.3 ± 0.2 2.1 ± 0.3 | - , +0.01 | -1.1 ± 0.2 -1.4 ± 0.2 |
| 12643589 | [17] | 4.44, 4.39 | 4.40 ± 0.15 | 6501, 6657 | 7000 ± 50 | 4.3 ± 0.4 | -0.26, -0.34 | +0.14 ± 0.20 |
| 12688835 | 18 | 3.86, 3.81 | 4.3 ± 0.4 | 8531, 8759 | 8330 ± 80 | (7 ± 3) | -0.28, -0.3 | -0.15 ± 0.10 |

2.5.1 Effective Temperatures

In BN12 the primary source of temperature information was the KIC, where the T_{eff} values were derived from Gunn-Thuan (SDSS) *griz* and 2MASS *JHK* photometric magnitudes and colours. Since then several photometric investigations have provided additional information about the temperatures (and other atmospheric characteristics) of the *Kepler*-field program stars: Pinsonneault *et al.* (2012) found that, for stars with T_{eff} in the range 4000-6500 K, the KIC temperature scale needed a correction of about +200 K; Greiss *et al.* (2012) presented the *Kepler* Isaac Newton 2.5-m Telescope Survey (KIS) consisting of stellar photometry through *U, g, r, i* and $H\alpha$ filters for over ~50% of the *Kepler*

field; Everett *et al.* (2012) presented Johnson *U, B, V* photometry for over 4 million sources in the *Kepler* field; and Huber *et al.* (2014, hereafter H14) constructed a catalogue of revised stellar properties for over 196,000 stars in the *Kepler* field. In **Table 5** much of this new photometric data, in particular colour indices relevant for estimating effective temperatures, have been summarized for our program stars.

The spectroscopic (SME, VWA/MOOG) and photometric (KIC, H14) effective temperatures for the program stars are compared in **Figure 10**. The stars are seen to have (SME) temperatures ranging from 7300 K to 8600 K (*i.e.*, $3.863 < \log T_{\text{eff}} < 3.934$ K). The upper temperature matches well the blue edge of the theoretical δ Sct instability strip (*e.g.*, Dupret *et al.* 2004); however, the lower temperature

Table 5. Mean magnitudes and colours for the *Kepler*-field SX Phe candidates. The columns contain: (1-2) KIC and CFHT star numbers; (3) mean *Kepler Kp* magnitude from the KIC; (4-6) mean Johnson *V* magnitudes, *B* – *V* colours and *U* – *B* colours – the top row is from Everett *et al.* (2012), and the lower rows are new photometric observations; (7-8) dereddened *B* – *V* and *U* – *B* colours, assuming both the KIC and new reddenings (given in Table 2); (9) Gunn–Thuan (SDSS) *g* – *r* colour from the KIC catalog and from the Kepler-INT Survey (KIS); (10-12) *r* – *i*, *H* – *K* and *J* – *K* colours given in the KIC.

| KIC no. | CFHT no. | <i>Kp</i> (KIC) | <i>V</i> Everett <i>et al.</i> (2012), new (this paper) | <i>B</i> – <i>V</i> | <i>U</i> – <i>B</i> | (<i>B</i> – <i>V</i>) ₀ KIC, new | (<i>U</i> – <i>B</i>) ₀ KIC, new | <i>g</i> – <i>r</i> KIC, KIS | <i>r</i> – <i>i</i> (KIC) | <i>H</i> – <i>K</i> (KIC) | <i>J</i> – <i>K</i> (KIC) |
|------------|-------------|--------------------|---|---------------------|---------------------|--|--|---------------------------------|------------------------------|------------------------------|------------------------------|
| (1) | (2) | (3) | (4) | (5) | (6) | (7) | (8) | (9) | (10) | (11) | (12) |
| 1162150 | 15 | 11.240 | – | – | – | –, – | –, – | 0.233, 0.352 | 0.012 | 0.032 | 0.292 |
| 3456605 | 24 | 13.108 | 13.181 | 0.452 | 0.154 | 0.25, 0.31 | 0.01, 0.05 | 0.235, 0.422 | 0.015 | 0.058 | 0.208 |
| 4168579 | 23 | 13.612 | 13.720 | 0.373 | 0.021 | 0.12, 0.20 | –0.16, –0.10 | 0.205, 0.347 | 0.032 | 0.028 | 0.172 |
| 4243461 | 4 | 13.786 | 13.856 | 0.360 | 0.070 | 0.21, 0.25 | –0.04, –0.01 | 0.185, 0.361 | –0.009 | 0.019 | 0.170 |
| | | | 13.765 | 0.335 | 0.043 | 0.18, 0.23 | –0.07, –0.04 | | | | |
| 4662336 | 14 | 13.105 | 13.258 | 0.389 | 0.070 | 0.19, 0.27 | –0.08, –0.02 | 0.225, 0.394 | 0.030 | 0.032 | 0.198 |
| 4756040 | 20 | 13.315 | 13.396 | 0.345 | 0.019 | 0.14, 0.24 | –0.13, –0.06 | 0.160, 0.371 | –0.012 | 0.005 | 0.181 |
| 5036493 | 26 | 12.553 | 12.626 | 0.315 | 0.110 | 0.09, 0.05 | –0.05, –0.08 | 0.103, 0.242 | –0.049 | 0.167 | 0.138 |
| 5390069 | – | 15.110 | 15.241 | 0.475 | 0.132 | 0.30, 0.29 | 0.01, 0.00 | 0.310, 0.411 | 0.075 | 0.059 | 0.275 |
| 5705575 | 22 | 13.692 | 13.718 | 0.341 | 0.011 | 0.13, 0.25 | –0.14, –0.05 | 0.162, 0.313 | –0.019 | –0.058 | 0.075 |
| | | | 13.579 | 0.338 | 0.041 | 0.13, 0.25 | –0.11, –0.04 | | | | |
| 6130500 | 9 | 13.869 | 13.880 | 0.331 | 0.054 | 0.12, 0.21 | –0.10, –0.03 | 0.174, 0.321 | –0.010 | 0.017 | 0.128 |
| 6227118 | 27 | 12.932 | 13.013 | 0.366 | 0.066 | 0.00, 0.25 | –0.20, –0.02 | –0.015, 0.306 | –0.016 | 0.090 | 0.177 |
| 6445601 | 2 | 13.595 | 13.679 | 0.383 | 0.050 | 0.20, 0.30 | –0.08, –0.01 | 0.216, 0.411 | 0.028 | 0.036 | 0.215 |
| 6520969 | 21 | 13.422 | 13.486 | 0.187 | –0.061 | –0.03, 0.11 | –0.21, –0.12 | 0.023, 0.222 | –0.066 | 0.026 | 0.126 |
| 6780873 | 5 | 13.746 | 13.827 | 0.386 | 0.049 | 0.23, 0.33 | –0.06, 0.01 | 0.231, 0.434 | 0.069 | 0.041 | 0.214 |
| | | | 13.773 | 0.447 | –0.052 | 0.29, 0.39 | –0.16, –0.13 | | | | |
| 7020707 | 16 | 13.433 | – | – | – | –, – | –, – | 0.141, 0.310 | –0.016 | 0.007 | 0.144 |
| 7174372 | 8 | 13.621 | 13.633 | 0.374 | 0.109 | 0.24, 0.32 | 0.01, 0.07 | 0.162, 0.345 | 0.002 | 0.053 | 0.165 |
| | | | 13.640 | 0.331 | 0.053 | 0.20, 0.28 | –0.04, –0.03 | | | | |
| 7300184 | – | 15.430 | 15.563 | 0.504 | 0.163 | 0.32, 0.23 | 0.03, –0.03 | 0.377, 0.485 | 0.100 | 0.061 | 0.288 |
| 7301640 | 10 | 13.862 | 13.971 | 0.367 | 0.125 | 0.16, 0.11 | –0.03, –0.06 | 0.285, 0.430 | 0.039 | 0.046 | 0.180 |
| 7621759 | 6 | 13.912 | 14.033 | 0.467 | 0.002 | 0.26, 0.28 | –0.15, –0.13 | 0.267, 0.446 | 0.070 | –0.044 | 0.137 |
| 7765585 | 28 | 13.980 | 14.085 | 0.451 | 0.165 | 0.34, 0.27 | 0.08, 0.04 | 0.288, 0.395 | 0.039 | 0.096 | 0.263 |
| | | | 14.010 | 0.424 | 0.095 | 0.31, 0.24 | 0.01, 0.02 | | | | |
| 7819024 | 19 | 13.799 | 13.886 | 0.317 | –0.078 | 0.13, 0.27 | –0.21, –0.11 | 0.140, 0.327 | –0.002 | 0.024 | 0.179 |
| | | | 13.781 | 0.325 | –0.055 | 0.14, 0.28 | –0.19, –0.13 | | | | |
| | | | 13.793 | 0.309 | –0.051 | 0.13, 0.26 | –0.18, –0.13 | | | | |
| 8004558 | 1 | 13.350 | 13.296 | 0.310 | –0.121 | 0.18, 0.26 | –0.22, –0.16 | 0.053, 0.251 | –0.040 | 0.071 | 0.163 |
| | | | 13.390 | 0.255 | –0.123 | 0.12, 0.21 | –0.22, –0.20 | | | | |
| 8110941 | 29 | 13.749 | 13.798 | 0.449 | 0.082 | 0.27, 0.30 | –0.05, –0.03 | 0.286, 0.472 | 0.049 | 0.068 | 0.253 |
| 8196006 | 30 | 13.810 | 13.903 | 0.435 | 0.079 | 0.24, 0.12 | –0.06, –0.15 | 0.265, – | 0.069 | 0.095 | 0.278 |
| 8330910 | 3 | 13.457 | 13.520 | 0.389 | 0.072 | 0.16, 0.08 | –0.09, –0.15 | 0.216, 0.407 | 0.033 | 0.050 | 0.229 |
| 9244992 | 7 | 13.998 | 14.206 | 0.571 | 0.191 | 0.28, 0.35 | –0.02, 0.03 | 0.429, 0.561 | 0.156 | 0.110 | 0.286 |
| 9267042 | 12 | 13.424 | 13.447 | 0.233 | –0.004 | 0.08, 0.18 | –0.12, –0.04 | 0.001, 0.175 | –0.117 | –0.023 | 0.086 |
| | | | 13.409 | 0.202 | 0.006 | 0.05, 0.15 | –0.11, –0.07 | | | | |
| 9535881 | [25] | 13.402 | 13.466 | 0.349 | 0.010 | 0.18, 0.28 | –0.11, –0.04 | 0.204, 0.395 | 0.030 | 0.006 | 0.163 |
| 9966976 | 31 | 13.491 | 13.577 | 0.356 | 0.039 | 0.14, 0.27 | –0.12, –0.03 | 0.173, 0.278 | –0.025 | 0.027 | 0.142 |
| | | | 13.517 | 0.285 | 0.018 | 0.06, 0.20 | –0.14, –0.06 | | | | |
| 10989032 | 32 | 13.866 | 13.933 | 0.240 | 0.056 | 0.01, 0.14 | –0.11, –0.02 | 0.013, 0.199 | –0.106 | –0.034 | –0.002 |
| 11649497 | 11 | 13.432 | 13.454 | 0.252 | 0.089 | 0.11, 0.21 | –0.01, 0.06 | 0.083, 0.270 | –0.059 | –0.035 | 0.105 |
| 11754974 | 13 | 12.678 | 12.605 | 0.255 | –0.158 | –, 0.22 | –, –0.19 | 0.148, 0.234 | –0.046 | –0.010 | 0.128 |
| | | | 12.570 | 0.259 | –0.174 | –, 0.22 | –, –0.25 | | | | |
| 12643589 | [17] | 13.754 | 13.858 | 0.457 | 0.028 | 0.35, 0.41 | –0.05, –0.01 | 0.305, 0.459 | 0.071 | 0.023 | 0.267 |
| | | | 13.831 | 0.493 | –0.028 | 0.38, 0.44 | –0.11, –0.11 | | | | |
| | | | 13.815 | 0.489 | –0.004 | 0.38, 0.44 | –0.08, –0.08 | | | | |
| | | | 13.833 | 0.481 | –0.016 | 0.37, 0.43 | –0.10, –0.10 | | | | |
| 12688835 | 18 | 13.801 | 13.806 | 0.169 | 0.025 | 0.01, 0.14 | –0.09, 0.00 | –0.078, 0.178 | –0.072 | –0.118 | –0.018 |

is a few hundred Kelvins hotter than the theoretical red edge. The top panel reveals a systematic offset of ~ 240 K between the KIC and H14 photometric temperatures, consistent with the Pinsonneault *et al.* upward revision of the KIC temperatures, and extending its range to temperatures ~ 8600 K. The most extreme outlier is the crowded optical

double KIC 6227118 (*27). The middle panel shows that for most of the cooler stars, the SME temperatures are hotter than the H14 temperatures, the average difference being ~ 300 K; the largest discrepancies occur for KIC 7765585 (*28) and KIC 7301640 (*10), both of which are rapid rotators. For the five hottest stars, the H14 temperatures appear

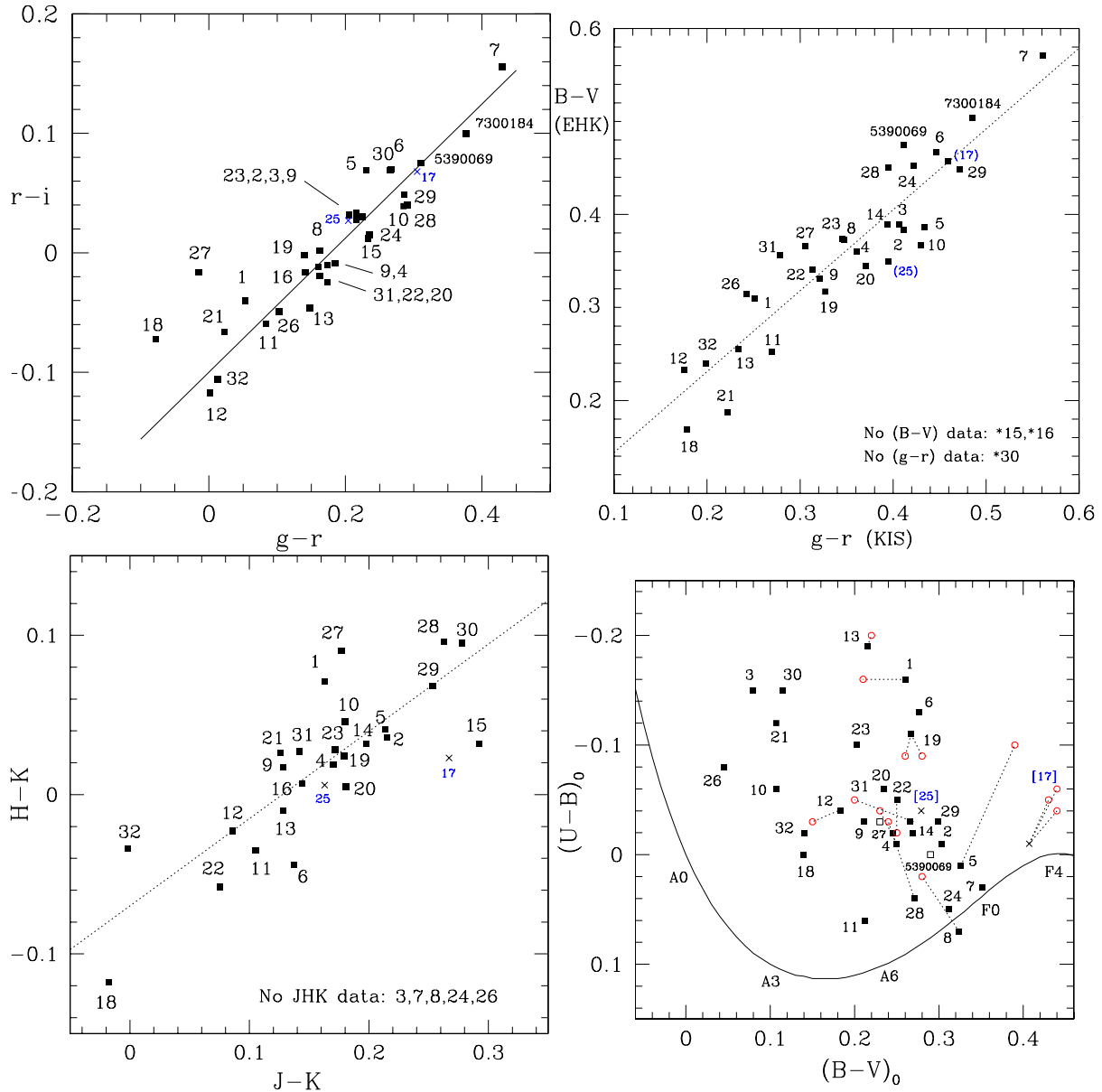


Figure 11. Two-colour diagrams for the candidate SX Phe stars. In each panel the stars have been labelled with the CFHT star numbers, except the two stars too faint to have been observed spectroscopically which have been labelled with their KIC numbers. **(Top left)** Gunn-Thuan griz (SDSS) system two-colour diagram, $r-i$ versus $g-r$ (both from the KIC), for the candidate SX Phe stars. The equation of the line, $r-i = 0.5611(g-r) - 0.0998$, was derived excluding the two outliers, KIC 6227118 (*27) and KIC 12688835 (*18), and excluding the two misclassified non-SX Phe stars, KIC 12643589 (*17) and KIC 9535881 (*25). **(Top right)** Two-colour diagram for the candidate SX Phe stars, comparing the $B-V$ colours from Everett *et al.* (2012) with the $g-r$ colours given in the Greiss *et al.* (2012) *Kepler*-INT survey (KIS). The equation of the line, $B-V = 0.870(g-r) + 0.057$, with $R^2 = 0.85$, was derived after excluding the two misclassified stars, KIC 12643589 (*17) and KIC 9535881 (*25). For KIC 4662336 (*14) the KIC $g-r$ colour, 0.225, transformed to the KIS system using the relation $g-r(\text{KIS}) = 0.817 g-r(\text{KIC}) + 0.199$, *i.e.*, 0.383, rather than the too-red KIS colour, 0.584, was used. **(Bottom left)** Near-infrared (2MASS) two-colour diagram for the candidate SX Phe stars. The equation of the line is: $H-K = 0.5478(J-K) - 0.0698$, with $R^2 = 0.68$. **(Bottom right)** Reddening-corrected $(U-B)_0$ vs $(B-V)_0$ diagram. The adopted E_{B-V} reddenings are the new values given in Table 2, and the E_{U-B} reddenings were calculated using the relation $(U-B)_0 = (U-B) - 0.72 E_{B-V}$. The curve is the standard relation for unreddened main sequence stars; the solid black squares represent the Everett *et al.* (2012) photometry reddening-corrected with the new reddenings; and the red open circles correspond to the new Bohyunsan Observatory *UBV* photometric observations.

to be ~ 200 K hotter than the SME temperatures, *i.e.*, more in line with the original KIC temperatures. In the bottom panel the SME and VWA/MOOG spectroscopic temperatures are compared. Apart from a scatter ~ 200 K there is reasonable agreement. The largest discrepancy, ~ 500 K, is

for KIC 6520969 (*21). We suspect that a large part of the observed difference can be attributed to the different wavelength intervals that were measured.

The T_{eff} 's from asteroseismology, 7100 ± 150 K for KIC 11754974 (Murphy *et al.* 2013b) and 6622 K for

KIC 9244992 (Saio *et al.* 2015), are both somewhat cooler than the spectroscopic values: the KIC 11754974 value is within the measuring errors, but the asteroseismology value for KIC 9244992 is ~ 1000 K cooler than that derived here!

In order of decreasing temperature the five hottest stars ($T_{\text{eff}} > 8100$ K) appear to be: KIC 10989032 (*32), KIC 5036493 (*26), KIC 12688835 (*18), KIC 6520969 (*21) and KIC 9267042 (*12). The hottest of these is a 2.3 d semidetached binary (see §3). All five stars have early-A spectral types (see Table 3) and are correspondingly hot in the H14 study. The five coolest stars (excluding the misclassified binary KIC 12643589) appear to be KIC 6780873 (*5), which is the newly discovered SB2 system discussed above, the two faint stars not observed spectroscopically (KIC 5390069 and KIC 7300184), KIC 3456605 (*24), and KIC 7174372 (*8).

To establish a relative T_{eff} ranking four photometric colour-colour graphs have been plotted in **Figure 11**. The top-left panel compares the $r-i$ and $g-r$ colours, two of the main indices used by the KIC and by H14. The top-right panel is a plot of the Everett *et al.* (2012) $B-V$ colours versus the Kepler-INT $g-r$ colours, and the bottom-left panel shows the near-infrared $H-K$ vs. $J-K$ two-colour diagram. In all three graphs significant linear correlations are seen, which appear to confirm that KIC 10989032 (*32), KIC 12688835 (*18) and KIC 9267042 (*12) are among the hottest stars in the sample (KIC 5036493 was not measured in the near-IR).

The bottom-right panel of Figure 11 is a two-colour plot of $U-B$ vs. $B-V$, where, unlike the other three panels, the broad-band colours have been dereddened using the new reddenings in Table 2 (col. 4). The $(B-V)_0$ ordering should, therefore, be closer to a temperature ranking. The graph includes the well-known $U-B$, $B-V$ two-colour main sequence curve (in this case based on the colours given in Table 1.1 of Böhm-Vitense 1989) with the corresponding spectral types given along the curve. Also plotted for 11 of the program stars are new UBV colours based on photometric observations made in October 2014 with the 1.8-m Bohyunsan Observatory telescope (the magnitudes and colours are given in Table 5). The new colours agree well with the Everett *et al.* (2012) colours, the largest differences occurring, as one might expect, for the SB2 system KIC 6780873 (*5). Note that at a given $(B-V)_0$ colour the program stars have $(U-B)_0$ colours that lie well above the main sequence curve (but well below the blackbody curve which passes through the point $[(B-V)_0, (U-B)_0] = [+0.20, -0.68]$). As seen clearly in Fig. 16 of Preston & Sneden (2000), there is, unfortunately, considerable overlap of curves of constant metal abundance and apparent age; as a consequence, the UV-excess is rendered “an ambiguous indicator of abundance” in this situation.

2.5.2 Surface Gravities

The surface gravities derived from the CFHT spectra are listed in column 4 of Table 4. When there are many overlapping echelle spectral orders $\log g$ is not an easy parameter to measure (Smalley 2004; Catanzarro *et al.* 2011); therefore, and the derived values are not in many cases well constrained. In Table 4 the values measured using SME are in the top row, and VWA (or MOOG) values are in the row below; assumed or uncertain values are enclosed parenthe-

ses. Also listed are the KIC and H14 gravities that were derived by matching observed photometric colours to stellar atmosphere models. All stars, except KIC 6227118 (*27) and KIC 7765585 (*28), have KIC and H14 values that are practically identical (note: the KIC does not give $\log g$ for KIC 11754974, but all other surface gravity derivations, including that by Murphy *et al.* 2013b, suggest a value close to 4.0). It is important to recall that Brown *et al.* (2011) warned against relying on the KIC estimates of $\log g$ for hot main sequence stars, such as those being investigated here.

A comparison of the photometric and spectroscopic $\log g$ values shows that for all but the hottest stars there is reasonably good agreement, the mean difference between the H14 and SME values being 0.05, with a standard deviation of the differences amounting to 0.29. For the hottest stars the spectroscopic $\log g$ values tend to be significantly larger than the photometric values (which has the effect of increasing the derived temperatures and metal abundances). No attempt was made to constrain the spectroscopic $\log g$ values using the photometric values (see Torres *et al.* 2012).

The surface gravity of KIC 6227118 (*27) clearly is a problem. The KIC value, $\log g = 1.03$, is exceptionally small, resulting in an unrealistically high luminosity, $\log L/L_{\odot} \sim 4.0$. The revised gravity given by H14, $\log g = 2.84$, is higher but is still much smaller than expected for an SX Phe (or δ Sct) star. KIC 6227118 is an outlier in the top panel of Fig. 10 – presumably because it is an optical double (see footnote 1) and highly reddened (see Table 2). The gravity derived using SME, $\log g = 4.5 \pm 0.3$, is quite uncertain but is more consistent with the star being close to the main sequence.

Two stars for which the photometric and spectroscopic gravities differ significantly are KIC 5036493 (*26) and KIC 7174372 (*8). For KIC 5036493 the SME and VWA estimates of $\log g$ are both greater than $\log g = 4.3$, the expected value for an A5 zero-age main sequence star, and larger than the H14 photometric value of 3.97. The spectroscopic values for KIC 7174372 suggest that $\log g$ is closer to 3.5 (which is consistent with the A9 III spectral type) than the H14 value of 4.1.

In Fig. 2 of BN12 two other stars appear to have low gravities (and therefore high luminosities since for stars of a given temperature $g \propto L^{-1}$): KIC 1162150 (*15), and KIC 9244992 (*7). Both stars are relatively cool and may represent stars that have evolved away from the main sequence. Although KIC 1162150 has a relatively bright neighbour to its northwest and an even closer faint blue star to its southeast, the spectroscopically and photometrically derived $\log g$ values are in close agreement, and are near $\log g = 3.5$. In contrast, there was a lack of agreement between the spectroscopic and photometric estimates for KIC 9244992, the star studied in detail by Saio *et al.* (2015). The $\log g \sim 4.5$ derived assuming ionization balance differs by 1.0 from the SME and photometric values, which are all close to 3.5. For now, little can be said except that the value, $\log g = 4.0$, derived by Saio *et al.*, lies midway between the SME and VWA spectroscopic estimates.

2.5.3 Microturbulent Velocities

The concept of microturbulence was introduced by Struve & Elvey (1934) as a means of deriving, using the curve-

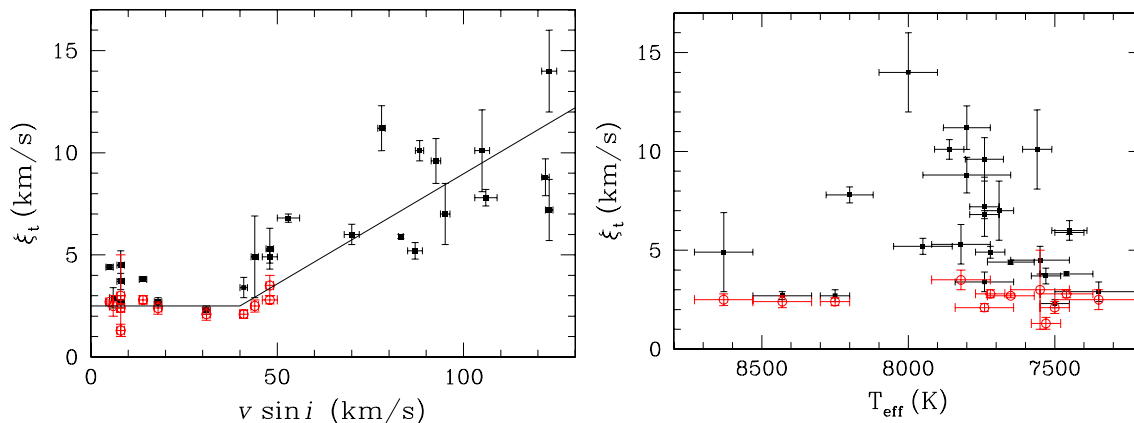


Figure 12. Microturbulent velocity ξ_t vs. projected equatorial velocity $v \sin i$ (left) and vs. SME effective temperature (right). The black filled squares are the SME values, and the red open circles are VWA values. Both graphs exclude the four very rapidly rotating stars (*i.e.*, those with $v \sin i > 190$ km/s), the problematic star KIC 6227118 (*27), and the two misclassified stars.

of-growth method, consistent chemical abundances from weak and strong spectral lines (see Gray 1988, 2005; Böhm-Vitense 1989, Landstreet *et al.* 2009, Aerts *et al.* 2014). Physically, the microturbulent velocity, ξ_t , is related to the mean free path of a photon through small convection cells. In practice ξ_t accounts for excess (Gaussian) line broadening over and above that of thermal broadening.

For each of the program stars ξ_t was estimated using SME. For the 12 stars with the narrowest lines, estimates were also derived using VWA and MOOG (by adjusting ξ_t until the derived abundances were independent of EW). The resulting ξ_t values are given in column 7 of Table 4, where, for each star, the SME value is given in the first row and the VWA/MOOG value is in the second row.

Figure 12 shows that there is a systematic difference between the SME and VWA microturbulent velocities, with the SME values (black filled squares) being ~ 1 -2 km/s larger than the VWA values (red open circles), which are more in line with expectation for A-type stars. The left panel shows that the broad line (more rapidly rotating) stars, for which only SME measurements were made, exhibit a significant trend of increasing ξ_t with increasing $v \sin i$. Whether this trend is real, or a result of the increasing difficulty of measuring ξ_t as line blending increases, is uncertain. The right panel shows that for the slow rotators, *i.e.*, the stars with narrow lines and $v \sin i < 50$ km/s (red open circles), there is no apparent dependence of ξ_t on surface temperature.

How do these results compare with previous ξ_t measurements for similar stars? Gray (1988) discusses variations of microturbulence across the HR diagram and concludes that “there is no strong change in ξ with effective temperature within a given luminosity class”; for main sequence stars the adopted value for ξ_t was 1 km/s. More recently, Gray (2014) concludes from his analysis of five slowly rotating early-A stars that “an upper limit of $\lesssim 2$ km s $^{-1}$ is placed on the microturbulence dispersion”. On the other hand, Landstreet (1998) found ξ_t values as large as 4.5 km/s in his analysis of later A-type stars. More recently, Landstreet *et al.* (2009) concluded (see their Fig. 2) that ξ_t reaches a maximum of ~ 4 km/s near 8000 K, falling as temperatures increase or decrease, with the highest values occurring where chemical

peculiarities (such as are seen in Am stars) are exhibited. Smalley’s (2004, Fig. 4) graph shows a variation of ξ_t with T_{eff} , suggesting ξ_t values ~ 3 km/s for stars with temperatures in the range 7500-8300 K. Thus, while ξ_t values ~ 4 -5 km/s are known for A-type stars from high-dispersion high SNR spectra, values as large as 10-15 km/s (as derived here using SME) are unusually high, suggesting that they may be the result of difficulties in measuring ξ_t for fast rotators with broad and blended lines.

2.5.4 Metal abundances

The spectral synthesis method (as implemented in SME) was used to measure metal abundances for the program stars. For those narrow-lined stars with unblended lines and reliable equivalent widths (EWs), the curve-of-growth method (as implemented in VWA and MOOG) was also used to measure [Fe/H]. Most of the measurements were made of co-added spectra, but when high SNR spectra were available the abundance calculations were repeated using individual spectra, and the results were folded into those from the coadded spectra. Unfortunately our spectra were too noisy at near-UV wavelengths for reliable CaII K-line EWs to be measured and used for [Fe/H] determinations (see Preston & Sneden 2000). The final derived abundances are given in the last column of Table 4.

The most metal-poor star in the BN12 sample is KIC 11754974 (*13), the 343 d time-delay binary (Murphy *et al.* 2013b). The mean abundance estimated from our spectra, [Fe/H] = -1.2 ± 0.3 dex, is lower than (but within the measurement error of) the abundance -0.5 ± 0.5 dex reported by Murphy *et al.* that was based on lower-dispersion spectra. Other low metal abundance stars include the narrow-lined star KIC 6520960 (*21) with [Fe/H] = -0.8 ± 0.2 dex, and KIC 8004558 (*1) with [Fe/H] = -0.3 ± 0.2 dex. All three stars are halo objects with retrograde galactic orbits and exhibit ultraviolet (UV) excesses in the bottom-right panel of Fig. 11 (see also Fig. 1a of Preston *et al.* 1994). The other two stars on retrograde orbits, KIC 7174372 (*8) and KIC 10989032 (*32), are not metal poor and do not show UV excesses.

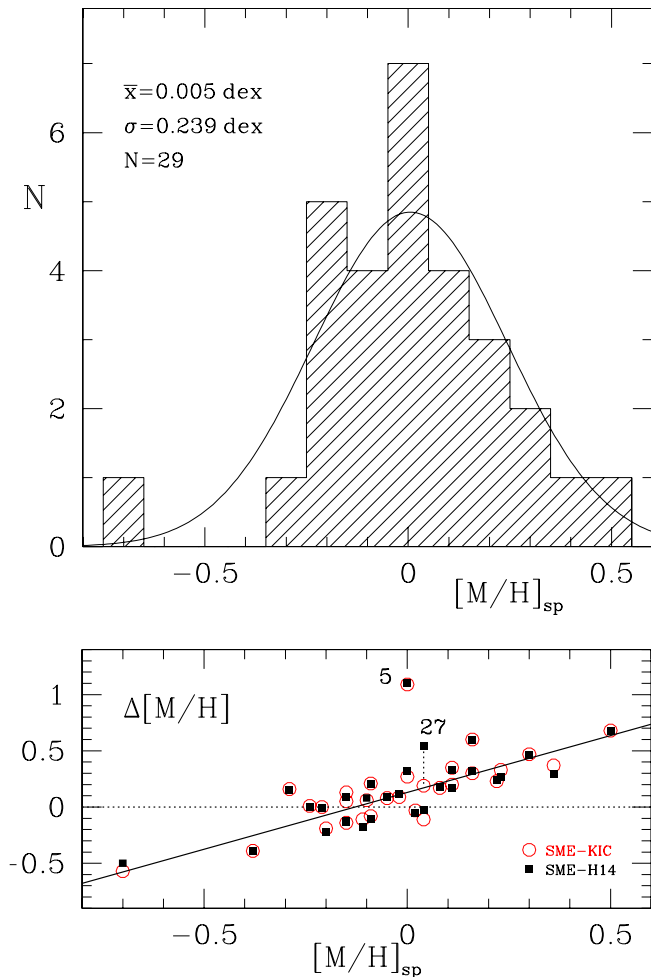


Figure 13. (Top panel) Histogram of spectroscopic metal abundances, $[M/H]_{sp}$, for 29 of the BN12 SX Phe candidates, fitted with a Gaussian of mean 0.005 dex and standard deviation 0.239 dex; note that KIC 11754974 is off-scale at $[M/H]_{sp} = -1.2 \pm 0.3$ dex. (Bottom panel) Comparing the spectroscopic metallicities from SME and the photometry-based KIC (red circles) and H14 (black squares) metallicities: a well-defined linear trend is seen. The equation of the fitted line, after excluding the double-lined spectroscopic binary KIC 6780873 (*5), is $\Delta[M/H] = 0.949 [M/H]_{sp} + 0.127$, with $R^2 = 0.73$.

Discrepancies between the SME and VWA/MOOG abundances are most likely due to difficulties associated with line blending, the fact that our spectra have only moderate SNRs, and the differences between the methods (*e.g.*, SME includes several ‘metals’ in addition to iron in the various wavelength windows, whereas the VWA and MOOG analyses were restricted to iron lines). For those stars with broad lines, that is, with $v \sin i$ between ~ 50 and 230 km/s, accurate measurement of $[Fe/H]$ became increasingly difficult as $v \sin i$ increased. Given the size of the overall uncertainties the small differences between $[M/H]$ and $[Fe/H]$ have been ignored.

The KIC and H14 photometric metal abundances tend to be within ± 0.10 dex of each other. The largest difference (0.35 dex) occurs for KIC 6227118 (*27), the star identified earlier as an outlier with respect to other quantities. Ex-

cluding this star from the calculations, the mean difference between the KIC and H14 $[Fe/H]$ values is 0.00 dex, with a standard deviation for the 31 stars of only 0.04 dex.

A histogram of the spectroscopic metallicities is shown in the upper panel of **Figure 13**, and the spectroscopic and photometric metal abundances are compared in the lower panel. The differences, $\Delta[M/H]$, are in the sense ‘SME minus H14’ (solid black squares) and ‘SME minus KIC’ (open red circles). The observed trend implies that for metal-poor stars the KIC/H14 abundances are more metal-rich than the spectroscopic abundances, and for the metal-rich stars, the KIC/H14 abundances are too metal-poor. For example, the KIC and H14 metallicities for KIC 3456605 (*24) are both -0.18 dex, compared with the SME value of $+0.50 \pm 0.10$ dex; and for KIC 11754974 (*13) the KIC metallicity is $+0.01$ dex compared with the SME value of -1.1 ± 0.2 dex. The largest difference is for KIC 6780873 (*5), the newly-discovered SB2 system discussed above. For it, both the KIC and H14 give -1.1 dex, compared with the SME metallicity 0.0 ± 0.3 dex and the VWA abundance $+0.16 \pm 0.20$ dex; no attempt was made to disentangle the spectral lines and so the uncertainties should be considered to be minimum values.

3 KEPLER PHOTOMETRY

The *Kepler* photometry available at the time of the BN12 analysis comprised long cadence (LC) data from quarters Q0-Q5, and limited short cadence (SC) data for three stars: KIC 1162150 (Q4.3), KIC 9267042 (Q3.3) and KIC 11754974 (Q3.1). Since then three additional years of LC photometry have become available, including two additional full quarters (Q6, Q7) of SC photometry for KIC 11754974; the latter have been analyzed in detail by Murphy *et al.* (2013b) and Balona (2014b). BN12 give pulsation frequencies for the four stars that most closely resemble large-amplitude field SX Phe stars, as well as periodograms for the ten stars located well above the galactic plane.

Periodograms (also referred to as ‘Fourier transforms’) based on the four years of available *Kepler* photometry (Q0-Q17) are presented below for all 34 candidate stars. Included are the two stars too faint to have been observed spectroscopically, and the two close eclipsing binaries misclassified as candidate SX Phe stars. Pulsation frequencies, amplitudes and rotation periods have been derived from the periodograms and subsequently analyzed. A significant result is the discovery of numerous binary systems and the derivation of their orbits.

3.1 Pulsations

Periodograms derived using the *Kepler* LC and SC photometry are shown in **Figures 14** and **15**, respectively. The frequency searches were made using the Lomb-Scargle algorithm (Press & Rybicki 1989). Six of the stars (KIC 4168579, 4662336, 4756040, 9966976, 11649497 and 11754974) were located on *Kepler*’s failed Module 3 and thus every fourth quarter is missing from the LC photometry. The gaps slightly altered the spectral windows but otherwise were not found to cause serious problems.

Another surmountable problem was the discrimination

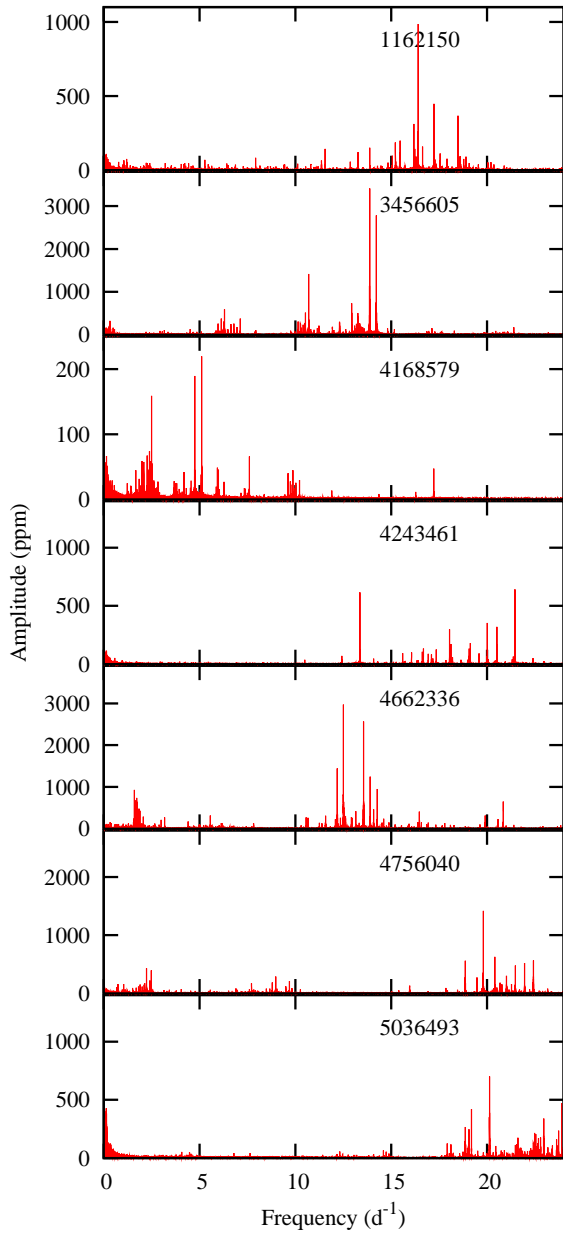
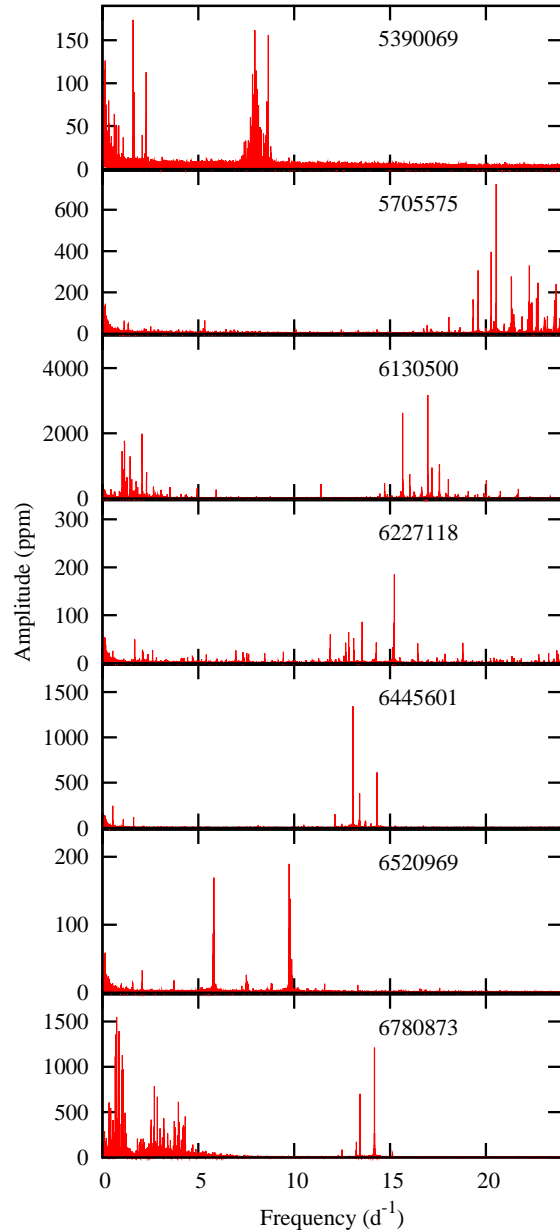


Figure 14. Periodograms for the 34 candidate SX Phe stars. The graphs are ordered by KIC number, and the frequency maximum has been set to 24.46 d^{-1} , the Nyquist frequency of the *Kepler* LC data. The number of brightness measurements that were analyzed usually amounted to ~ 52000 long-cadence points per star, sampled over ~ 1470 days. *Erratum:* in Fig. 3 of BN12 there are two panels with the label ‘11649497’; the lower label is correct, and the upper label should have been ‘10989032’.

between ‘real’ and ‘alias’ peaks in the LC periodograms due to aliasing of pulsation frequencies higher than the LC Nyquist frequency at 24.462 d^{-1} (*i.e.*, at half the sampling rate of ~ 49 photometric observations per day). The problem of identifying ‘super-Nyquist’ frequencies has been discussed by Murphy (2012), Murphy *et al.* (2013a), Chaplin *et al.* (2014) and others. For the three stars with SC photometry such aliasing was not a problem owing to the high Nyquist frequency of the SC data, 734 d^{-1} (= half the sam-

Figure 14 – continued



pling rate of 1468 points per day), and the fact that SX Phe and δ Sct stars have in the past been found to have maximum frequencies under 100 d^{-1} . The SC periodogram for KIC 9267042 clearly reveals a dominant *real* super-Nyquist frequency at 24.66 d^{-1} (responsible for the strong 24.26 d^{-1} *alias* peak seen in the LC periodogram).

For the majority of the stars only LC photometry is available. To identify the super-Nyquist frequencies, searches from 0 - 50 d^{-1} were conducted using both Lomb-Scargle periodograms and the Fourier methods implemented in the PERIOD04 program of Lenz & Breger (2005). The criterion used to discriminate between real and alias frequencies was based on the assumption that the alias (which, for real super-Nyquist frequencies occurs at twice the LC Nyquist frequency minus the real frequency) has a smaller peak amplitude than the corresponding real frequency. This

Figure 14 – continued

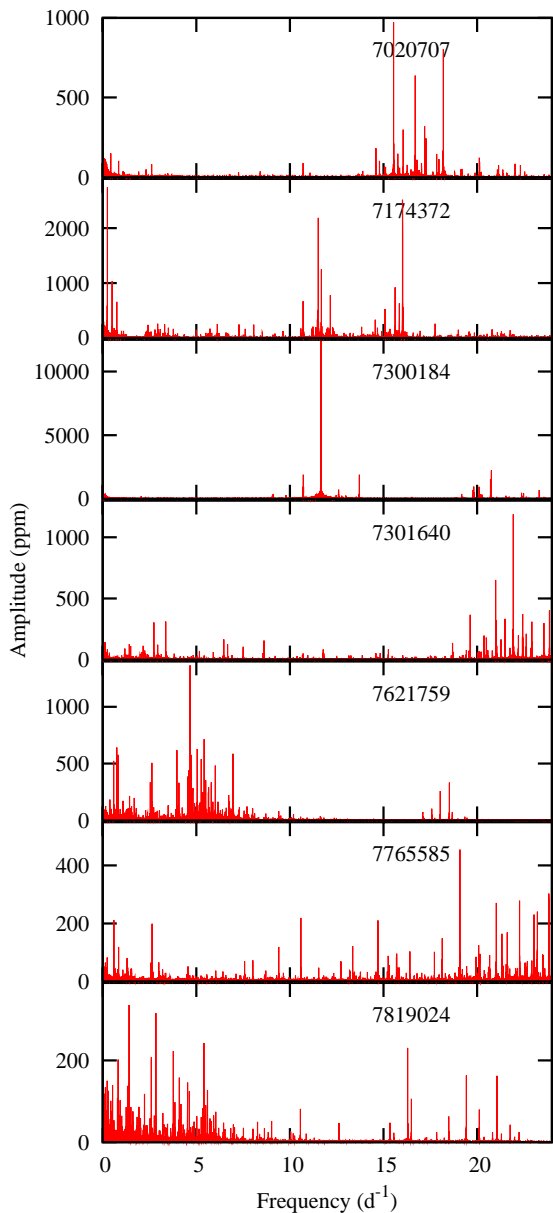
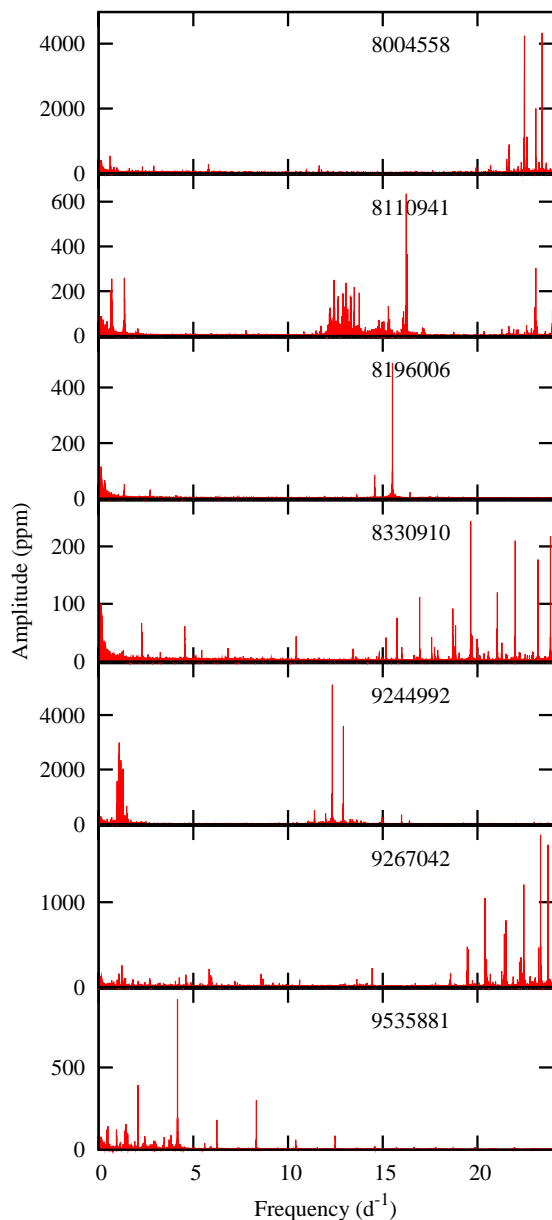


Figure 14 – continued



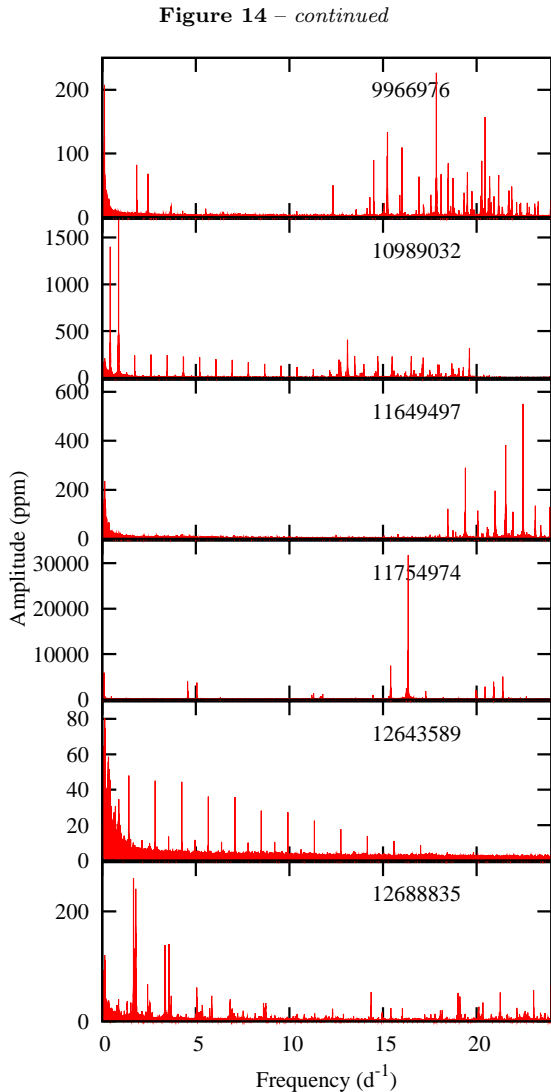
classification rule appears to be borne out by the detailed analyses discussed in the references given above. By applying this rule half of the program stars were found to have super-Nyquist frequencies, with the highest dominant real frequency occurring at 54.7 d^{-1} (for KIC 6520969).

In **Table 6** the pulsation frequencies, ν_n (d^{-1}), and amplitudes, A_n (μmag), for the periodogram peaks with the largest amplitude and greatest significance are given for the program stars. The numbers in the table are based on PERIOD04 analyses of the Q0-Q17 LC (and any available SC) photometry. In general, the uncertainties in the frequencies are smaller than 10^{-5} d^{-1} , while the amplitude uncertainties depend on the method used to construct the periodogram and may amount to as much as 10%.

CoRoT and *Kepler* observations have shown that most, if not all, δ Sct stars exhibit both low and high frequency

pulsations (Balona 2014a). All 32 of the *Kepler*-field SX Phe candidates show frequencies $>5 \text{ d}^{-1}$ (by definition), and ~ 25 of the stars also exhibit significant pulsation at low frequencies. Since most δ Sct stars are too hot to possess a significant outer convection zone expectation was that the low frequencies are unlikely to be due to the convective blocking mechanism that is thought to drive the γ Dor pulsations seen at frequencies $0.3 < \nu_{\text{puls}} < 3.3 \text{ d}^{-1}$ (Guzik *et al.* 2000). However, the asteroseismic analysis of KIC 9244992 by Saio *et al.* (2015) showed that at least one of the stars exhibits rotationally split core g -modes characteristic of γ Dor pulsators, as well as surface p -mode multiplets.

Detailed examination of the periodograms provides fundamental information about pulsation modes, a means for identifying binary systems (from time delays and phase modulations), and a framework for making inferences (which



involves identification of rotationally-split multiplets or light variations due to rotational modulation and the presence of possible starspots). A brief summary of the main findings for each star follows; many of the stars deserve more detailed study.

KIC 1162150 (*15) - The strongest frequencies are between 15 and 20 d^{-1} , all of which are below the LC Nyquist frequency. The three highest peaks occur at 16.407, 17.232 and 18.490 d^{-1} and give rise to a beat pattern of (variable) period $\sim 1.0 - 1.3$ d (best seen in the SC light curve).

KIC 3456605 (*24) - The two strongest peaks occur at 13.8771 and 14.2277 d^{-1} , with a third strong frequency at 10.6943 d^{-1} . Two of these, 10.6943 and 13.8771 d^{-1} , have a ratio 0.77 which might be the ratio of the fundamental to the first overtone radial mode (and therefore indicative of the star's mass). All the frequencies appear to be sub-Nyquist.

KIC 4168579 (*23) - The periodogram is dominated by low frequencies near 2.5, 5.0, 7.5 and 10 d^{-1} , and a distinct, but not very strong, p -mode frequency at 17.22 d^{-1} . Quite possi-

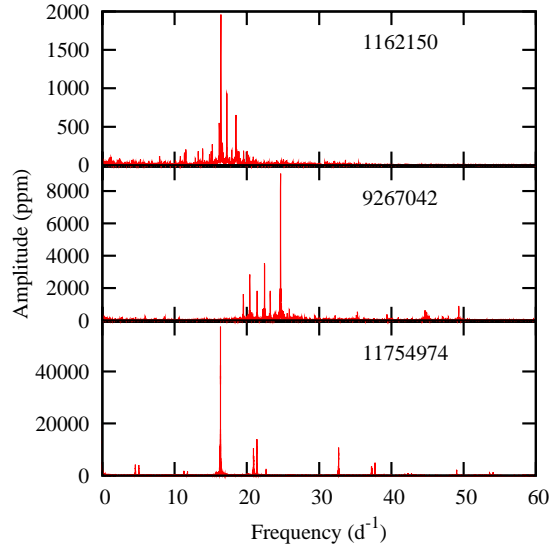


Figure 15. Periodograms derived from the short-cadence *Kepler* photometry for KIC 1162150 (*15, Q4.3, ~ 42000 points), KIC 9267042 (*12, Q3.3, ~ 42000 points) and KIC 11754974 (*13; Q3.1, Q6, Q7; ~ 300000 points). The maximum frequency of the graphs, 60 d^{-1} , is well below the 734 d^{-1} Nyquist frequency of the SC data.

bly the former are harmonics (retrograde modes?) caused by the pulsator's rapid rotation ($\langle v \sin i \rangle \sim 200$ km/s), in which case the rotation frequency is 2.49 d^{-1} . However other modes also are possible (for example, see Breger *et al.* 2013). Also present at low frequencies is an interesting group of peaks symmetric in spacing (and amplitude) at $\nu_1 = 5.87206$, $\nu_2 = 5.93402$, $\nu_3 = 5.96988$ and $\nu_4 = 6.03183$ d^{-1} . While $\nu_4 - \nu_3 = \nu_2 - \nu_1 = 0.06195$ d^{-1} , the meaning of this pattern is not clear. All the significant frequencies appear to be sub-Nyquist. Visual inspection of the periodogram gives the impression of equal spacing among some peaks, but closer study reveals that the spacings are not equal.

KIC 4243461 (*4) - Many peaks are present with frequencies higher than 13 d^{-1} and amplitudes in excess of 200 ppm. Frequency modulations also are seen. The peak of highest amplitude, at 21.458 d^{-1} , may be detectable from the ground. Also seen are a large number of frequencies below 4 d^{-1} , all with amplitudes less than 30 ppm; since the star is cool these are probably g modes. No evidence for spots is seen at low frequencies. The pulsator is in a time-delay binary system with a 460 d orbital period. In support of its binary nature, the observed RV range, $\Delta \text{RV} = 5.1$ km/s, agrees well with the predicted $K_1 = 5$ km/s.

KIC 4662336 (*14) - The frequencies of largest amplitude (above 500 μmag) are all sub-Nyquist and should be readily detectable from the ground. No obvious frequency modulation (FM) sidelobes are seen. A system of low-frequency peaks at around 1.7 d^{-1} (possibly g modes) is striking because of the almost equal spacing; the frequencies, periods and spacings are identified in **Table 7**. Although neither the frequencies nor the periods are equally spaced, the change in spacing forms a nice linear trend; similar such trends are seen in γ Dor stars (e.g. Bedding *et al.* 2014). Most of the

Table 7. KIC 4662336 (*14) - sequence of periodogram peaks around 1.7 d^{-1} , at frequencies $\nu_n \text{ (d}^{-1}\text{)}$ with amplitudes $A_n \text{ (}\mu\text{mag)}$, consecutive frequency spacings $\Delta\nu = \nu_{n+1} - \nu_n \text{ (d}^{-1}\text{)}$, periods $P_n \text{ (day)}$ and consecutive period spacings $\Delta P = P_n - P_{n+1} \text{ (d}^{-1}\text{)}$. Frequencies 1,2,4 appear to be aliases of 3, while 5,7,8 appear to be aliases of 6; and in general the frequency spacings are increasing.

| n | ν_n | A_n | $\Delta\nu$ | P_n | ΔP |
|-----|---------|-------|-------------|--------|------------|
| 1 | 1.5486 | 197 | 0.0236 | 0.6457 | 0.0096 |
| 2 | 1.5722 | 275 | 0.0251 | 0.6361 | 0.0100 |
| 3 | 1.5973 | 957 | 0.0269 | 0.6261 | 0.0104 |
| 4 | 1.6242 | 192 | – | 0.6157 | – |
| 5 | 1.6843 | 702 | 0.0339 | 0.5937 | 0.0117 |
| 6 | 1.7181 | 754 | 0.0368 | 0.5820 | 0.0122 |
| 7 | 1.7550 | 643 | 0.0400 | 0.5698 | 0.0127 |
| 8 | 1.7950 | 401 | 0.0435 | 0.5571 | 0.0132 |
| 9 | 1.8385 | 494 | 0.0477 | 0.5439 | 0.0137 |
| 10 | 1.8861 | 425 | – | 0.5302 | – |

peaks are concentrated in the range $10 < \nu < 22 \text{ d}^{-1}$, but there is no obvious pattern or common separation in this range.

KIC 4756040 (*20) - Shortward of the LC Nyquist frequency the four highest amplitude peaks occur at 19.808, 22.424, 20.410 and 21.960 d^{-1} ; the second of these is an alias of the higher-amplitude super-Nyquist frequency 26.515 d^{-1} . One also sees many low-amplitude peaks in the range $19\text{--}24 \text{ d}^{-1}$, and rich but low-amplitude peak systems in the frequency ranges $0.5\text{--}2.7 \text{ (}g\text{-modes?)}$ and $7.3\text{--}10.0 \text{ d}^{-1}$. There are no apparent equidistant spacings. About half of the peaks between 15 and 24.4 d^{-1} are alias peaks, and no frequencies of significant amplitude are seen above 35 d^{-1} .

KIC 5036493 (*26) - The $0\text{--}50 \text{ d}^{-1}$ LC periodogram is dominated by many peaks with frequencies between 18 and 31 d^{-1} and amplitudes in excess of 300 ppm; several of the super-Nyquist frequencies are real. The dominant real frequency is at 28.809 d^{-1} , with an alias at 20.130 d^{-1} . Low-amplitude peaks are seen in the range $12\text{--}15 \text{ d}^{-1}$, many of which have a spacing of 0.148 d^{-1} . There are very few peaks with $\nu < 5 \text{ d}^{-1}$, though there might be a long-term variation of $\nu = 0.135 \text{ d}^{-1}$ (similar to the frequency spacing just mentioned).

KIC 5390069 - The periodogram shows a clump of peaks between 7 and 9 d^{-1} , and four prominent frequencies between 1.5 and 2.5 d^{-1} (at 1.601, 1.663, 2.081 and 2.274 d^{-1}), all of which have amplitudes smaller than $200 \mu\text{mag}$. A series of equally-spaced peaks seen at 0.1593, 0.3187, 0.4710 and 0.6220 d^{-1} may correspond to the rotation frequency and its harmonics, but the amplitudes increase with frequency.

KIC 5705575 (*22) - In the $0\text{--}50 \text{ d}^{-1}$ LC periodogram nearly all the real peaks are located between 16 and 32 d^{-1} , some of which are super-Nyquist. Several low-amplitude peaks can be seen at low frequencies (5.3314, 1.1367, 1.3427, 2.5202 d^{-1}), but there is no evidence for the rotation frequency (*i.e.*, no harmonic peaks). Time-delays suggest an orbital period close to 538 days (see §3.3). The nine spectra taken at seven epochs clearly show RV variability

($\Delta\text{RV} \sim 17 \text{ km/s}$) consistent with the photometry and with the photometrically-derived RV curve.

KIC 6130500 (*9) - The pulsation is dominated by several p -mode frequencies between 15 and 20 d^{-1} , in addition to a rich spectrum of g -mode frequencies between 1 and 4 d^{-1} . There are no obvious super-Nyquist frequencies, no frequency modulation sidelobes, and no obvious spacings. Ground-based observations probably would classify this star as a hybrid as there are several peaks with amplitudes greater than 1 mmag .

KIC 6227118 (*27) - The dominant peaks, none of which have amplitudes exceeding $\sim 300 \mu\text{mag}$, are all above the LC Nyquist frequency, and amplitude modulation is visible in the light curve. All the major peaks exhibit a similar multiplet structure, caused mainly by aliasing with the 372.5 d orbital period of the *Kepler* telescope. The dominant peak, at $\nu_1 = 33.7160 \text{ d}^{-1}$, is flanked by the second highest peak at $\nu_2 = 33.7145 \text{ d}^{-1}$. This is the only system in which almost all the power is beyond the LC Nyquist frequency.

KIC 6445601 (*2) - The periodogram is relatively simple, with high p -mode peaks at 13.07, 14.33 and 13.42 d^{-1} , and several low-frequency equally-spaced peaks corresponding to the rotation frequency 0.5415 d^{-1} (Neilsen *et al.* 2013) and its harmonics at 1.083, 1.624, 2.166 d^{-1} . No FM sidelobes are seen, but there exists the possibility of amplitude variability.

KIC 6520969 (*21) - Two *real* super-Nyquist frequencies, at $\nu_1 = 39.195 \text{ d}^{-1}$ and $\nu_2 = 54.749 \text{ d}^{-1}$, both of which are single and well-defined, dominate the $0\text{--}60 \text{ d}^{-1}$ periodogram. The latter is greater than twice the LC Nyquist frequency (*i.e.*, $> 48.92 \text{ d}^{-1}$). The high peaks at 5.812 and 9.74 d^{-1} (and at 43.126 and 58.68 d^{-1}) are aliases of ν_1 and ν_2 , respectively. Near the ν_1 peak are less significant single peaks at 39.1520 and 39.0645 d^{-1} . Other significant super-Nyquist frequencies include 41.44, and 51.01 d^{-1} . In the vicinity of 43.13, 54.72, 58.68, 58.72, and 58.81 d^{-1} one sees frequency quintuplets with separations of $\sim 0.0027 \text{ d}^{-1}$; the splittings most likely are due to aliasing with the 372.5 d orbital period of the *Kepler* telescope. Below 4 d^{-1} the dominant frequencies are at 0.99, 1.53, 1.58, 2.07 and 3.73 d^{-1} and show no evidence of rotational harmonics.

KIC 6780873 (*5) - The periodogram shows only two prominent peaks in the δSct range, at 14.188 and 13.436 d^{-1} , and a very rich low-frequency spectrum with many dozens of peaks concentrated around 0.20–1.25, 2.25–3.33 and $3.33\text{--}4.45 \text{ d}^{-1}$, with amplitudes in the range 300–1625 ppm. No obvious frequency spacings can be detected. Except for the two p -mode peaks this star would be classified as a γ Dor star. In §2.1.2 the RV variations revealed that this star is a double-lined spectroscopic binary, consistent with a time-delay analysis of the Q0-Q17 LC photometry (§3.3) that reveals it to be a close binary system with an orbital period $P_{\text{orb}} = 9.16 \pm 0.03 \text{ d}$.

KIC 7020707 (*16) - The dominant frequencies are between 15 and 20 d^{-1} . The three highest peaks, at 15.54, 18.20 and 16.70 d^{-1} , are real (*i.e.*, not aliases) and show no evidence of multiplet structure. At low frequencies a few peaks are seen (all with amplitudes less than $150 \mu\text{mag}$), two

Table 6. Pulsation frequencies, ν_n (d^{-1}), and amplitudes, A_n ($\mu\text{mag} = \text{ppm}$), for the periodogram peaks of largest amplitude and greatest significance. The numbers are based on analysis of the SC data if available, otherwise of the Q0-Q17 LC data. When the amplitude of the super-Nyquist peak (at $\nu > 24.4615 d^{-1}$) was greater than that of the corresponding sub-Nyquist peak the former was assumed to be the real frequency and the latter an alias frequency. Binary systems are identified with **boldface** KIC numbers, and frequencies used in the time-delay analyses have been underlined, and rotation (and/or orbital) frequencies are in *red italics*.

| Star | $\nu_1(A_1)$ $\nu_7(A_7)$ | $\nu_2(A_2)$ $\nu_8(A_8)$ | $\nu_3(A_3)$ $\nu_9(A_9)$ | $\nu_4(A_4)$ $\nu_{10}(A_{10})$ | $\nu_5(A_5)$ $\nu_{11}(A_{11})$ | $\nu_6(A_6)$... etc. |
|-----------------------|---|---|---|--|--|--|
| 1162150 (*15) | 16.40793 (1601) | 17.23122 (816) | 18.49044 (648) | 16.40005 (563) | 16.18382 (523) | 15.22177 (285) |
| 3456605 (*24) | 13.87706 (4640) | 14.22773 (3559) | 10.69431 (1650) | 13.87217 (1167) | 12.94050 (789) | 13.25948 (721) |
| 4168579 (*23) | 5.10953 (234) | 4.74623 (199) | <i>2.49131</i> (165) | 17.21841 (75) | 2.38202 (79) | 7.60083 (73) |
| 4243461 (*4) | 21.45819 (1300) <u>16.67878</u> (209) | <u>13.36151</u> (817) <u>17.35007</u> (208) | <u>20.01540</u> (650) | <u>18.04597</u> (461) | <u>19.13558</u> (306) | <u>18.11525</u> (291) |
| 4662336 (*14) | 12.51132 (4037) | 13.55432 (3428) | 12.19013 (1854) | 13.90794 (1672) | 14.26849 (1277) | 20.84469 (1249) |
| 4756040 (*20) | 19.80761 (2566) | 26.51536 (1455) | 20.41056 (1183) | 21.96026 (1092) | 2.23450 (447) | 20.67829 (363) |
| 5036493 (*26) | 28.80941 (1439) | 23.89670 (1164) | 23.73328 (568) | 30.06947 (531) | 26.39105 (535) | 29.88074 (502) |
| 5390069 | 7.94464 (183) 2.27398 (116) | 8.65358 (181) 1.66293 (93) | 8.03156 (143) 0.1593 (40) | 7.83105 (130) 0.3187 (45) | 8.08036 (112) 0.4710 (48) | 1.60096 (186) 0.6220 (55) |
| 5705575 (*22) | <u>20.53586</u> (1387) 22.31121 (317) | 26.66737 (872) 21.35656 (276) | <u>20.27854</u> (751) 23.99475 (211) | 25.27748 (706) 24.78404 (211) | 25.36201 (469) | 22.39538 (317) |
| 6130500 (*9) | 16.96920 (4988) 20.02412 (1023) <i>1.15158</i> (1767) | 15.65390 (3785) 18.04089 (998) 1.02188 (1413) | 17.19123 (2164) 21.69512 (654) 1.44498 (1325) | 17.58345 (1700) 16.65137 (537) 1.11645 (901) | 17.19123 (1396) 11.39845 (537) 2.29761 (821) | 17.58005 (1371) 2.07024 (2005) 1.27516 (605) |
| 6227118 (*27) | 33.71604 (304) | 33.71445 (159) | 35.39488 (134) | 36.09299 (99) | 37.05546 (88) | 30.14356 (85) |
| 6445601 (*2) | 13.06792 (1696) 10.50716 (40) | 14.32617 (838) 8.12804 (36) | 13.41806 (487) 1.62431 (136) | 13.73040 (108) 1.08296 (107) | 13.70703 (93) <i>0.5416</i> (76) | 16.73954 (49) |
| 6520969 (*21) | 39.19536 (265) | 54.74894 (230) | 39.15203 (198) | 39.06451 (69) | | |
| 6780873 (*5) | <u>14.18757</u> (1635) 1.04091 (1077) | <u>13.43627</u> (912) 1.08573 (945) | 0.74535 (1507) 0.99881 (947) | 0.70228 (1360) 1.06323 (919) | 0.86415 (1358) | 0.67020 (1154) |
| 7020707 (*16) | 15.53514 (1428) 17.96163 (196) 14.78336 (141) | 18.20383 (1332) 16.78914 (169) 10.70760 (105) | 16.70110 (986) 22.02607 (182) 15.04419 (100) | 17.20074 (496) 22.31278 (170) 0.33502 (153) | 16.05242 (454) 21.15035 (151) 0.84609 (97) | 17.83731 (244) 17.03594 (145) 2.61767 (87) |
| 7174372 (*8) | 16.02162 (3692) 10.70399 (823) | 11.52111 (2560) <i>0.2500</i> (2700) | 11.68348 (1601) 0.5000 (1028) | 15.62332 (1419) 0.7501 (642) | 12.15787 (957) | 15.84335 (907) |
| 7300184 | <u>11.65981</u> (28895) 22.48131 (960) | 20.76654 (4324) 0.25325 (2081) | 20.72239 (2982) 0.29738 (1348) | 13.71237 (2524) | 20.11222 (1941) | 23.31961 (1637) |
| 7301640 (*10) | 21.93607 (2483) 20.36786 (373) | 26.50609 (977) 20.49722 (339) | 23.86695 (1007) 26.98485 (286) | 23.57156 (702) 27.18351 (250) | 19.63272 (652) 3.36753 (317) | 26.72637 (498) 2.73281 (311) |
| 7621759 (*6) | 4.66961 (1487) 18.51980 (564) | 5.41867 (741) 6.01497 (532) | 3.96393 (693) 2.62024 (531) | 5.05030 (685) 0.83635 (515) | 4.71298 (616) 0.74907 (486) | 5.25911 (572) 18.03528 (427) |
| 7765585 (*28) | 19.07862 (873) 14.70550 (317) | 24.16114 (765) 10.58127 (263) | 23.98715 (622) 23.53583 (197) | 22.27004 (609) 20.15150 (191) | 21.02492 (552) 2.64222 (188) | 21.61366 (353) 0.84329 (112) |
| 7819024 (*19) | <u>16.29036</u> (332) 2.83717 (322) | <u>21.06214</u> (315) 5.40761 (252) | <u>19.42795</u> (297) 3.76815 (228) | <u>16.49367</u> (158) 2.59583 (214) | <u>21.76567</u> (89) 0.8252 (206) | <i>1.4066</i> (339) |
| 8004558 (*1) | <u>25.52139</u> (11886) | <u>24.91583</u> (5381) | <u>26.32943</u> (2689) | <u>25.68562</u> (916) | <u>27.30128</u> (864) | 0.60555 (604) |
| 8110941 (*29) | 16.24003 (941) 13.34605 (285) | 24.91933 (788) 13.50247 (283) | 16.29438 (547) 1.36114 (265) | 12.41964 (320) <i>0.68793</i> (204) | 13.06036 (299) 1.37657 (173) | 23.95900 (289) 0.64287 (127) |
| 8196006 (*30) | 15.51033 (701) | <i>1.35986</i> (49) | 2.72124 (40) | 4.08092 (14) | 5.44320 (8) | |
| 8330910 (*3) | 24.14147 (547) <i>2.2724</i> (69) | 21.99215 (445) 4.5513 (64) | 19.63965 (464) 6.8246 (24) | 16.94367 (175) | 15.75556 (115) | 18.84284 (108) |
| 9244992 (*7) | 12.33937 (6515) 1.09100 (2987) | 12.92006 (4642) 1.07591 (2580) | 15.99298 (502) 1.15851 (2265) | 12.31246 (495) 1.17432 (2256) | 14.96647 (359) 1.21147 (2046) | 12.35230 (313) 1.29332 (2019) |
| 9267042 (*12) | <u>24.6637</u> (9099) | <u>22.4487</u> (3617) | <u>20.4008</u> (2872) | 23.2384 (1864) | <u>21.4236</u> (1800) | 19.5155 (1650) |
| 9535881 [*25] | 2.08152 (409) <i>0.48885</i> (172) | 4.16301 (972) 0.42386 (140) | 6.24452 (219) 0.94685 (133) | 8.32602 (347) 1.44971 (157) | 10.40754 (79) 1.38111 (125) | 12.48903 (106) 1.48714 (102) |
| 9966976 (*31) | <u>17.8582</u> (376) <i>0.1145</i> (197) | <u>20.4512</u> (302) 0.228 (50) | <u>33.7040</u> (218) 0.346 (40) | <u>30.4500</u> (165) 1.8407 (82) | 20.2785 (168) 2.4505 (71) | 16.0114 (165) |
| 10989032 (*32) | <i>0.43382</i> (1415) 34.21988 (449) | 0.86764 (1790) 31.79224 (466) | 29.31930 (768) 35.45244 (404) | 35.83161 (709) 36.28355 (334) | 32.42100 (494) 31.01511 (258) | 33.45078 (451) 36.20560 (249) |
| 11649497 (*11) | 22.48921 (1161) | 19.40347 (495) | 27.94219 (384) | 24.85830 (340) | 26.99322 (263) | 27.93027 (207) |
| 11754974 (*13) | <u>16.34477</u> (67903) | <u>21.39904</u> (14121) | <u>20.90745</u> (10566) | <u>20.94360</u> (7289) | <u>22.66036</u> (2263) | |
| 12643489 [*17] | 0.07080 (61) 1.41678 (48) 5.66722 (37) | 0.12817 (75) 2.12519 (10) 6.37565 (12) | 0.33354 (61) 2.83359 (46) 7.08401 (38) | 0.33868 (54) 3.54204 (13) 7.79239 (10) | 0.70823 (30) 4.25041 (46) 8.50086 (32) | 0.88463 (35) 4.95881 (12) 9.20922 (12) |
| 12688835 (*18) | <i>1.67430</i> (264) 5.0452 (40) | 1.78784 (239) 23.98174 (178) | 1.78263 (178) 27.66717 (111) | 3.5704 (100) 19.01177 (79) | 3.3798 (90) 29.83500 (78) | 3.3389 (85) 34.56846 (72) |

of which appear to be $\nu_{\text{rot}} = 0.43 \text{ d}^{-1}$ and its harmonic at 0.85 d^{-1} .

KIC 7174372 (*8) - The LC periodogram exhibits two sets of complex p -mode pulsations (near 12 d^{-1} and 16 d^{-1}), a distinct triplet of high-SNR peaks at 0.25 , 0.50 and 0.75 d^{-1} , and many low-amplitude peaks distributed over a wide range of frequencies. In the light curve the 0.25 d^{-1} peak shows up as broad dips every four days, which, if not fictitious, may correspond to the rotation period claimed by Nielsen *et al.* (2013), or may be due to 4-d orbital motion in a close ‘ellipsoidal’ binary (see §3). The multi-periodic pulsations all occur at amplitudes below 0.01 mag .

KIC 7300184 - The periodogram shows an extreme peak at 11.66 d^{-1} , the amplitude of which, $28900 \mu\text{mag}$, is exceeded only by the $57690 \mu\text{mag}$ dominant peak for KIC 11754974. Features with smaller amplitudes ($\sim 4300\text{-}2500 \mu\text{mag}$) are seen at 20.76 , 20.72 and 13.71 d^{-1} . Four other peaks are also seen at 20.11 , 20.19 , 20.27 and 20.35 d^{-1} , all of which are separated by $\sim 0.08 \text{ d}^{-1}$. A binarogram analysis shows the SX Phe star to be in a wide binary system with an orbital period of 640 ± 60 days.

KIC 7301640 (*10) - Most of the power is at frequencies between 19 and 28 d^{-1} , including super-Nyquist frequencies 26.51 , 26.73 , 27.18 and 27.89 d^{-1} . At low frequencies there are many scattered low-amplitude peaks ($< 400 \text{ ppm}$), the highest amplitude being at 3.37 and 2.73 d^{-1} . There are no obvious FM sidelobes, and there is no evidence for ν_{rot} harmonics.

KIC 7621759 (*6) - The highest peak is at 4.67 d^{-1} , and most of the peaks in the periodogram are of low frequency, with hundreds of peaks having $\nu < 8 \text{ d}^{-1}$ (g -modes?). The high frequencies at 18.52 and 18.04 d^{-1} are of intermediate amplitude. There are no obvious equal spacings and no obvious FM sidelobes.

KIC 7765585 (*28) - Many frequencies are present, with most of the power above 18 d^{-1} and no evidence for super-Nyquist frequencies. A few low-frequency peaks with moderate amplitudes are present (0.5992 , 2.6422 d^{-1}) along with many dozens of low-amplitude peaks. Although $v \sin i$ is large there is no evidence at short frequencies for rotational harmonics.

KIC 7819024 (*19) - The $0\text{-}25 \text{ d}^{-1}$ LC periodogram shows several high frequency peaks, almost all having amplitudes higher than their super-Nyquist counterparts. Much of the power is at frequencies below 6 d^{-1} , including significant peaks at 1.41 and 2.84 d^{-1} . Frequency modulations due to binary motion suggest $P_{\text{orb}} \sim 216$ days.

KIC 8004558 (*1) - All the highest peaks in the $0\text{-}50 \text{ d}^{-1}$ LC periodogram occur at super-Nyquist frequencies. A variable beat pattern is seen in the light curve, due mainly to the three strongest frequencies at 25.521 , 24.916 and 26.329 d^{-1} . At frequencies below 4 d^{-1} the greatest power occurs at 0.6056 d^{-1} . Several other g -mode peaks between 0.6 and 3.0 d^{-1} are seen, with no evidence for ν_{rot} harmonics. This high-velocity star is a time-delay binary system with an orbital period of ~ 262 days.

KIC 8110941 (*29) - The $0\text{-}50 \text{ d}^{-1}$ LC periodogram reveals two well-resolved triplets, at 16.2400 , 16.2943 and 16.1856 d^{-1} , and at 24.9193 , 24.9800 and 24.8578 d^{-1} . The latter triplet is located beyond the LC Nyquist frequency and so alias peaks appear at 24.0197 , 23.9590 and 24.0812 d^{-1} . One also sees a distinct set of many closely-spaced peaks between $12.1\text{-}13.9 \text{ d}^{-1}$ and some scattered peaks at high frequencies. Below 3 d^{-1} one sees two sets of peaks, at $\sim 0.66 \text{ d}^{-1}$ and near 1.36 d^{-1} , where each set contains many closely-spaced unresolved peaks within a band of about 0.06 d^{-1} . These correspond to the $\nu_{\text{rot}} = 0.6456 \text{ d}^{-1}$ (and its harmonic) given in the Nielsen *et al.* (2013) catalogue. A possible third harmonic at 2.07 d^{-1} is also weakly visible.

KIC 8196006 (*30) - Almost all the pulsation power is at 15.51 d^{-1} with no evidence for g -mode frequencies. At low frequencies four low-amplitude peaks dominate, three of which (at 2.72 , 4.08 and 5.44 d^{-1}) are harmonics of the rotation frequency 1.360 d^{-1} (Balona 2013).

KIC 8330910 (*3) - The six highest peaks in the $0\text{-}50 \text{ d}^{-1}$ LC periodogram all occur at frequencies below the LC Nyquist frequency. No obvious FM sidelobes are seen, and possibly the amplitudes are variable. The spacing and amplitudes of the peaks at 2.2725 , 4.551 and 6.825 d^{-1} suggest that the first of these is the rotation frequency and the other two are its harmonics. Such a high ν_{rot} is consistent with the high $\langle v \sin i \rangle = 224 \pm 3 \text{ km/s}$.

KIC 9244992 (*7) - The $0\text{-}50 \text{ d}^{-1}$ frequency spectrum is dominated by two p -mode peaks at 12.339 and 12.920 d^{-1} , which, after pre-whitening, reveal a ‘‘plethora’’ of p -mode peaks between 11 and 17 d^{-1} , and a complex high-amplitude group of g -mode peaks between 0.9 and 1.3 d^{-1} . A detailed asteroseismic analysis of the pulsations, and an asteroseismic application of their use for determining physical characteristics, including the rotation profile, was made by Saio *et al.* (2015). Their best-fit model was: $\mathcal{M} = 1.45 \mathcal{M}_{\odot}$; $T_{\text{eff}} = 6622 \text{ K}$; $L = 7.14 L_{\odot}$; $R = 2.03 R_{\odot}$; $\log g = 3.982$; $\text{age} = 1.9 \text{ Gyr}$; and $(X, Y, Z) = (0.724, 0.266, 0.010)$, corresponding to $[\text{Fe}/\text{H}] = -0.15 \text{ dex}$. No peak in the low-frequency periodogram at the well-established asteroseismic rotation frequency of 0.015 d^{-1} is seen, perhaps suggesting an absence of spots or other surface features.

KIC 9267042 (*12) - The SC periodogram (middle panel of Fig. 15) reveals that all of the significant real p -mode frequencies are higher than 19 d^{-1} and that the highest peak is super-Nyquist at $\nu_1 = 24.664 \text{ d}^{-1}$. Thus, in the LC periodogram the sub-Nyquist high-amplitude peak at 24.26 d^{-1} is an alias. The next highest real peaks occur at 22.449 and 20.401 d^{-1} and are mainly responsible for the complex beat pattern seen in the *Kepler* light curve. The peak amplitudes may be variable. Time-delay analyses suggest that the pulsator may be in a binary (triple?) system with P_{orb} longer than the four year duration of the *Kepler* photometry (see §3.3).

KIC 9535881 [*25, KOI 4228] - This W UMa-type interacting binary system is one of the two mistakenly classified SX Phe candidates. Initially it was flagged as a *Kepler* Object of Interest (KOI) but it is now considered

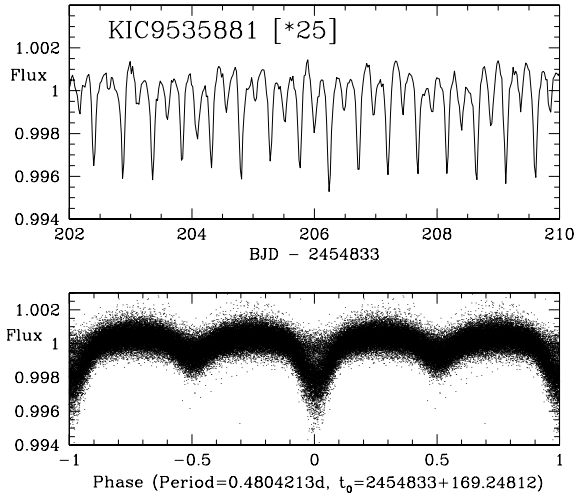


Figure 16. Light curves for the W UMa-type non-SXPhe binary KIC 9535881 [*25]. The top panel shows an eight-day portion of the light curve, and the bottom panel shows all 63416 LC data points phased with the 0.48 d orbital period given in the Villanova EB catalog.

to be a ‘false positive’. The Villanova EB catalog lists it as having an orbital period of 0.4804213 d and a mid-time for the primary eclipse of $\text{BJD}_0=2455002.248121$. In the periodogram this period corresponds to the peaks at 2.0815 d^{-1} and 4.1630 d^{-1} , with additional harmonics of these at 6.244, 8.326, 10.407, 12.489, 14.571 and 16.652 d^{-1} . The primary and secondary minima both exhibit variable depths, shown in **Figure 16**. At frequencies below 2 d^{-1} several low-amplitude peaks are seen, possibly indicating that at least one component is a γ Dor variable, or that $\nu_{\text{rot}} \sim 0.49 \text{ d}^{-1}$ (*i.e.*, $P_{\text{rot}} \sim 2.1 \text{ d}$).

KIC 9966976 (*31) - The pulsations are of very low amplitude ($< 400 \mu\text{mag}$), with most peaks occurring at frequencies higher than 12 d^{-1} , including real super-Nyquist frequencies at 33.704 and 30.450 d^{-1} , and a fairly sparse low-frequency spectrum. The strongest low- ν peak occurs at 0.1146 d^{-1} (with harmonics at 0.228 and 0.346 d^{-1}), identified as ν_{rot} by Balona (2013); all three peaks exhibit an underlying broad Gaussian feature somewhat similar to those seen in Figure 6 of Balona (2013). Additional low-frequency peaks are seen at 1.84 and 2.45 d^{-1} (*g*-modes?). Rømer time-delay analyses (see §3.3) suggest that the pulsator is in a binary system with an orbital period longer than four years.

KIC 10989032 (*32, KOI 7397) - The *Kepler* light curve shows both eclipses and pulsations. These appear as two distinct sets of frequencies in the 0-25 d^{-1} long cadence periodogram: (1) two high peaks associated with the 2.3 day orbital motion, one peak at $\nu_{\text{orb}}=0.43375 \text{ d}^{-1}$ and another at twice this, accompanied by a series of equally-spaced harmonic peaks between 1.73 and $\sim 12 \text{ d}^{-1}$ – the harmonics that are even multiples of ν_{orb} have much larger amplitudes than those at odd multiples of ν_{orb} ; and (2) a group of intermediate-amplitude pulsation peaks at frequencies between 12 and 20 d^{-1} , almost all of which are aliases of real *p*-mode pulsations at frequencies between 29 and 37 d^{-1} . As a KOI it is characterised as a “false positive with a signif-

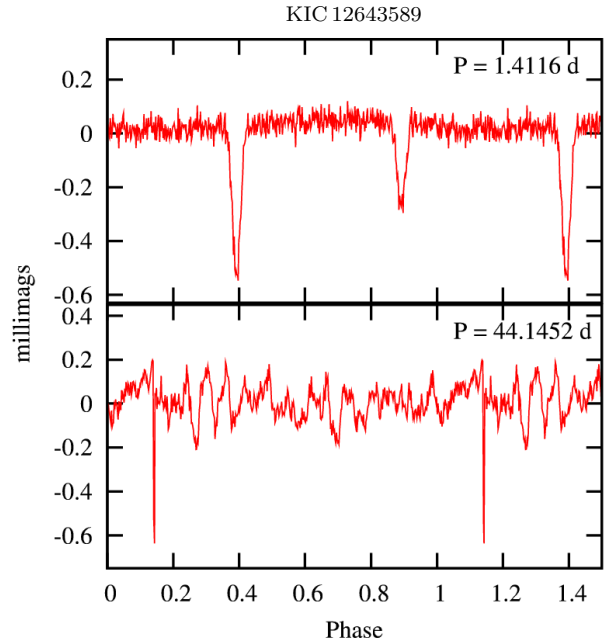


Figure 17. Light curves for the eclipsing binary KIC 12643589 [*17], based on the *Kepler* Q1-17 LC photometry, and phased with the orbital period 1.4116 d (upper panel) and with the 44.1452 d transit period (lower panel).

icant secondary event and a centroid offset”. The spectral type is based on an excellent match to the A5 V standard star HD 23194.

KIC 11649497 (*11) - Almost all of the significant real frequencies are above 15 d^{-1} , with many in the super-Nyquist region. All the major peaks show substructure due to aliasing caused by the orbital periods of *Kepler* and the Earth. ‘Low-amplitude eclipses’ were noted by BN12. The analysis is complicated by location on Module 3 and by amplitude modulation.

KIC 11754974 (*13) - Murphy *et al.* (2013b) discovered (from a careful asteroseismic investigation using the LC:Q0-Q13 and SC:Q6-Q7 data) that the SX Phe pulsator is in a 343-day non-eclipsing binary system. An independent pulsation and time-delay analysis using all the LC:Q0-17 data was later conducted by Balona (2014b). These studies identified five independent *p*-mode frequencies between 16 and 23 d^{-1} , the most powerful of which is at 16.34475 d^{-1} . Also seen were many combination frequencies, including some very distinctive low-amplitude quintuplets. The strong peak at 0.09524 d^{-1} seen in the binarogram of Balona (2014) is confirmed as fictitious; neither it nor the weaker peak at 16.24951 d^{-1} ($=16.34475-0.09524$) is seen in the SC periodogram (see Fig. 15). No peaks are seen in the low-frequency LC or SC periodograms at the asteroseismic rotation frequency of 0.383 d^{-1} , perhaps suggesting the absence of spots or other surface features.

KIC 12643589 [*17, KOI 376] - This close binary (along with KIC 9535881) was mistakenly classified as an SX Phe star. The *Kepler* light curve plotted in **Figure 17** shows eclipses and transits that agree with the Villanova EB cat-

alog orbital periods of 1.4116278 d and 44.1471769 d. As a KOI it was identified as having two ‘false positive’ planet identifications. The well-defined harmonic series seen in Fig. 14 is due to the binarity; the harmonics with higher peaks are seen at even multiples of the orbital frequency, $\nu_{\text{orb}}=0.70840 \text{ d}^{-1}$, and those with lower peaks are seen at odd multiples of ν_{orb} . A secondary series of low-amplitude harmonics, equally spaced by an amount 0.02265 d^{-1} and caused by the transits, is seen in the periodogram out to $\sim 6 \text{ d}^{-1}$. Two complex multi-peaked gaussians of unknown origin are seen centered on 0.13 and 0.33 d^{-1} . No evidence for pulsations is seen.

KIC 12688835 (*18) - The periodogram is dominated by two sets of complex, relatively low-amplitude (~ 150 - $250 \mu\text{mag}$) peaks, at 1.67 and 1.78 d^{-1} , with possible harmonics (also complex) at 3.35 and 3.56 d^{-1} , and at 5.05 and 5.35 d^{-1} . If the harmonics are real and due to rotation then $P_{\text{rot}} \sim 0.60 \text{ d}$ (Balona 2013). Differential rotation cannot be excluded. Concerning the pulsations, the low-frequency spectrum does not resemble that of a typical γ Dor star. Several of the strongest p -mode frequencies are in the super-Nyquist region.

3.2 Rotation

The *Kepler* data have proven to be useful for establishing surface and interior rotation periods for many stars across the HR diagram (see review by Aerts 2015), including the two stars in our sample that were subjected to detailed asteroseismic investigations. For KIC 11754974 (*13), the inclination angle of the rotation axis ($= 47_{-15}^{+7}$ deg), the equatorial rotation velocity ($= 34.18 \text{ km/s}$), and the radius ($= 1.764 R_{\odot}$) were determined by Murphy *et al.* (2013b). These values imply $\nu_{\text{rot}} = 0.383 \text{ d}^{-1}$ and $v \sin i = 25.0_{-6.9}^{+2.7} \text{ km/s}$, the latter being in close agreement with the mean projected rotation velocity measured from the spectra, $28.8 \pm 1.7 \text{ km/s}$. For KIC 9244992 (*7), the core and envelope rotation rates (both assumed to be constant) are available from Saio *et al.* (2015), who deduced from rotational splitting of its pulsation frequencies, a rotation period of $66.2 \pm 0.6 \text{ d}$ (*i.e.*, $\nu_{\text{rot}} = 0.015 \text{ d}^{-1}$) at its surface and $63.9 \pm 0.2 \text{ d}$ at its core; such slow rotation corresponds to an equatorial rotation velocity of only 1.5 km/s , which is consistent with the measured $v \sin i < 7 \text{ km/s}$. Owing to the importance of rotation further such detailed investigations ought to be carried out.

Surface rotation frequencies have also been derived by examining low frequency periodograms. If a star exhibits light variation due to the presence of a surface spot or other co-rotating surface feature, estimation of the rotation period may be possible. Light variations due to surface features are unlikely to be sinusoidal and therefore harmonics might be expected in the low-frequency periodogram. Thus, detection of a low-frequency peak and its harmonic(s) might reasonably be attributed to a revolving surface feature, in which case the rotation period of the star can be deduced (see Balona 2011, and Balona & Dziembowski 2011). By identifying low-frequency peaks and their associated harmonics in *Kepler* periodograms, Balona (2013) derived rotation periods for 875 *Kepler* A-type stars, six of which are among the stars being considered here. Rotation periods for four other BN12 stars were similarly derived by Nielsen *et al.* (2013) as

Table 8. Rotation rates for the program SX Phe stars. Columns (2)-(4) contain the rotational frequency, ν_{rot} , the rotational period, P_{rot} , and a reference label, where B13, N13, M13 and S15 represent Balona (2013), Nielsen *et al.* (2013), Murphy *et al.* (2013) and Saio *et al.* (2015), respectively. The last column contains the spectroscopically-measured mean projected rotational velocity from Table 3. **Boldface** numbers identify binaries (see §3.3), and values followed by colons are considered uncertain.

| KIC (CFHT) (1) | ν_{rot} [d^{-1}] (2) | P_{rot} [d] (3) | Ref. (4) | $\langle v \sin i \rangle$ [km s^{-1}] (5) |
|-----------------------|--|---|-------------|---|
| 9244992 (*7) | 0.015 | 66.2 | S15 | $< 6.7 \pm 0.3$ |
| 9966976 (*31) | 0.114 | 8.77 | B13 | 123 ± 1 |
| 7174372 (*8) | 0.2501 | 3.998 | N13 | 41.6 ± 1.0 |
| 11754974 (*13) | 0.383 | 2.61 | M13 | 28.8 ± 1.7 |
| 7020707 (*16) | 0.431 | 2.32 | new | 105 ± 2 |
| 10989032 (*32) | 0.434 | 2.30 | B13 | 45.0 ± 0.9 |
| 6445601 (*2) | 0.5415 | 1.847 | N13 | 71.3 ± 0.4 |
| 8110941 (*29) | 0.6456 | 1.549 | N13 | $< 7.5 \pm 0.2$ |
| 7819024 (*19) | 0.825: | 1.21: | N13 | 95.1 ± 1.3 |
| | 1.407 | 0.711 | new | 95.1 ± 1.3 |
| 6130500 (*9) | 1.152 | 0.87 | B13 | 49.3 ± 1.1 |
| 8196006 (*30) | 1.360 | 0.74 | B13 | 92.6 ± 1.3 |
| 9267042 (*12) | 1.360: | 0.74: | B13 | 106 ± 3 |
| 12688835 (*18) | 1.674 | 0.60 | B13 | 230 ± 5 |
| 8330910 (*3) | 2.273 | 0.44 | new | 224 ± 3 |
| 4168579 (*23) | 2.491 | 0.40 | new | 197 ± 4 |

part of their program to measure rotation periods for 12000 *Kepler*-field main-sequence stars⁸. Because the ν_{rot} range investigated by Nielsen *et al.* was limited to frequencies between 0.03 and 1.0 d^{-1} none of the stars in their catalog has a rotation period longer than 33 days or shorter than one day. Of course other non-rotational interpretations of low-frequency peaks are possible, including that some or all of the low-frequency peaks have a pulsation origin and are combination frequencies (e.g., Kurtz *et al.* 2015), an interpretation favoured by SJM.

In **Table 8** rotation rates from the papers by Balona, by Nielsen *et al.*, and from the two abovementioned asteroseismic investigations, have been summarized. Note that all of the rotation periods, except that for KIC 9244992, are shorter than 10 days, as might be expected for stars with spectral types earlier than $\sim \text{F5}$ (see Fig. 2 of Nielsen *et al.*).

A systematic search of the low-frequency periodograms of all the BN12 stars was conducted to identify low-frequency ‘peaks and harmonics’. For most of the stars, including KIC 11754974 and KIC 9244992, no obvious ν_{rot} harmonics were detected. However, possible rotation frequencies were identified for three previously unmeasured stars, KIC 7020707, KIC 8330910 and KIC 4168579, and for KIC 7819024, all fast rotators with $v \sin i$ values greater than 90 km s^{-1} ; these too are given in Table 8.

Low-frequency periodograms for 12 of the surveyed stars are plotted in **Figure 18**. The locations of the highest peaks, all with high S/N ratios, usually correspond to

⁸ Nielsen *et al.* (2013) assume that their sample stars are Sun-like with convective envelopes and spots due to dynamo-driven magnetic fields, a situation which may not apply to the radiative envelopes of SX Phe stars.

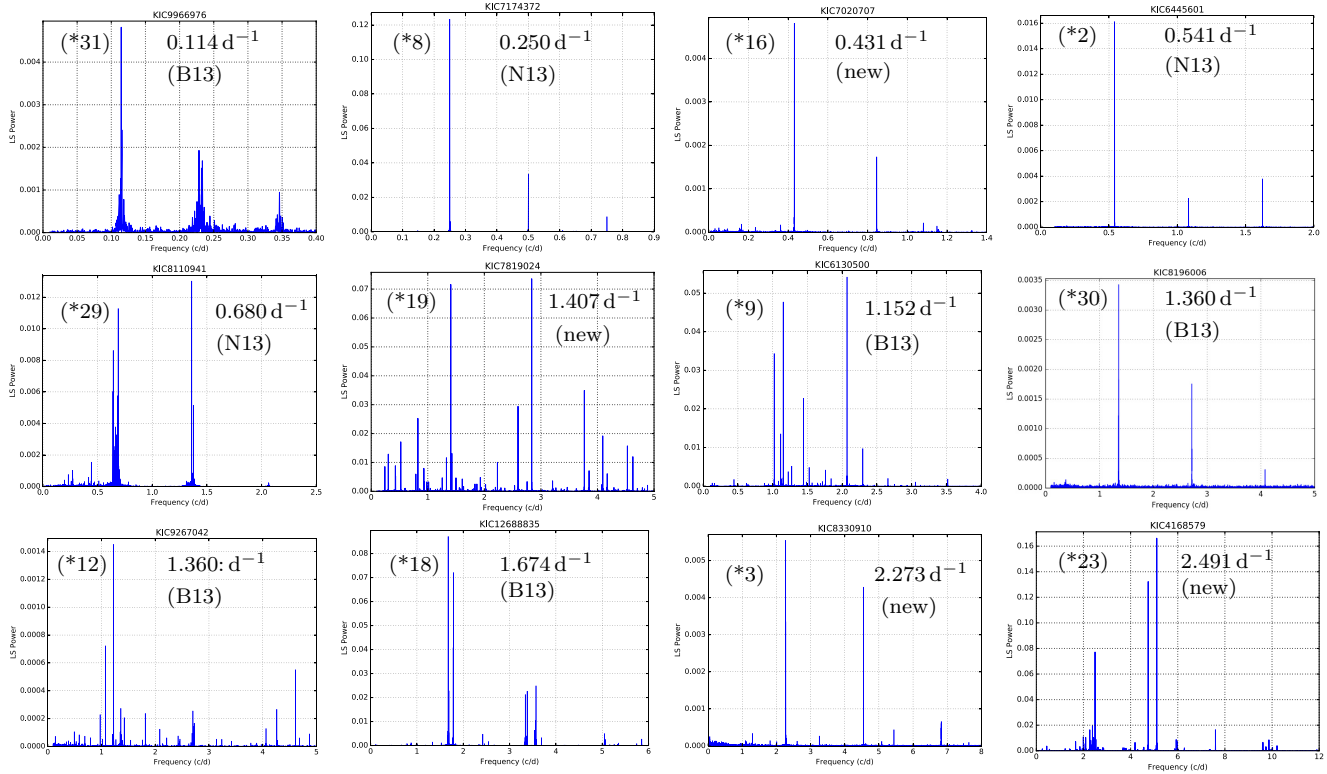


Figure 18. Peaks and possible harmonics seen at low frequencies in *Kepler* Q0-Q17 LC periodograms. KIC number (on top), CFHT star number (in parentheses), rotation frequency, ν_{rot} (rotations per day), and source of the rotation frequency (see Table 8), are noted in each panel.

the rotation frequency (or its harmonic) given by Balona or Nielsen *et al.* An exception is KIC 7819024 (*19). For the moderate-amplitude peak at the Nielsen *et al.* rotation frequency, 0.825 d^{-1} , shows no harmonic at 1.65 d^{-1} and thus 0.825 d^{-1} is probably spurious; on the other hand, large peaks at 1.41 d^{-1} and 2.84 d^{-1} suggest ν_{rot} is 1.41 d^{-1} .

Another discrepancy was found for KIC 9267042 (*12). Below 3 d^{-1} several significant, but low amplitude, peaks are seen, the strongest of which occur at 1.226 , 1.0737 , 1.3604 and 2.701 d^{-1} , where the last two correspond to the value $\nu_{\text{rot}} = 1.360 \text{ d}^{-1}$ suggested by Balona (2013), and its harmonic. Since the first two frequencies have significantly higher amplitudes $\nu_{\text{rot}} = 1.360 \text{ d}^{-1}$ must be considered questionable.

Further inspection of the periodograms shows that only five stars (CFHT nos. 8, 16, 2, 30 and 3) exhibit single, well-defined peaks at the presumptive ν_{rot} , with lower-amplitude harmonics at two (and sometimes three) times ν_{rot} . KIC 9966976 (*31) has a dominant peak at 0.114 d^{-1} , the ν_{rot} value given by Balona (2013), with apparent harmonics of lower amplitude at two and three times ν_{rot} , but the peaks are broad and made up of several distinct frequencies, possibly due to differential rotation in a spotted star, or due to combination frequencies. Such groupings of two, three or more frequencies at the peaks and harmonics, rather than single frequencies, also are seen for CFHT nos. 29, 9, 12, 18 and 23 (Fig. 18).

Since $v \sin i = 2\pi R \sin i \nu_{\text{rot}}$ one might expect to observe a positive correlation between ν_{rot} and $v \sin i$, where the degree of correlation depends on the distributions of

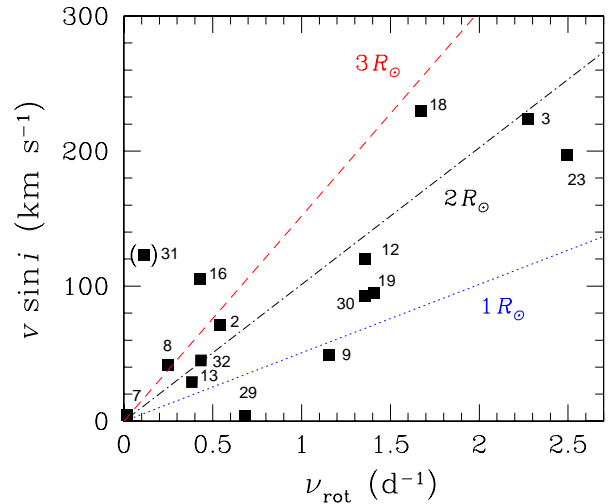


Figure 19. Projected rotational velocity as a function of the SX Phe stars in the *Kepler* field (see Table 8). The three lines show the equatorial velocities (*i.e.*, $v \sin i$ when $i = 90^\circ$) as a function of ν_{rot} for typical A-type stars having radii of $1 R_\odot$ (blue dotted line), $2 R_\odot$ (black dash-dot line) and $3 R_\odot$ (red dashed line). The labels are the CFHT star numbers.

the unknown radii and unknown inclination angles of the stars. **Figure 19** is a plot of $v \sin i$ versus ν_{rot} for the stars in Table 8, where the location of any given point below, say, the $R=2 R_\odot$ line, can be understood as arising from either a smaller radius or an inclination angle less than

90° , or some combination of the two possibilities. For instance, the location of KIC 8110941 (*29), a narrow-lined star with $v \sin i < 7 \pm 1$ km/s, is readily explained if its inclination angle is near 0° (*i.e.*, it is observed pole-on). On the other hand, the estimated rotation frequency of KIC 9966976 (*31), $\nu_{\text{rot}} = 0.114 \text{ d}^{-1}$, is too low to account for a $v \sin i$ as large as the measured value, which suggests that the features seen in its low frequency periodogram may not be attributable to a spot or other co-rotating feature, but could be an artifact attributable to the long-term trends and jumps in *Kepler* photometry, or due to combination frequencies (see Kurtz *et al.* 2015).

3.3 Binary Systems

SX Phe stars are Pop.II blue stragglers (BSs) in the lower instability strip, and BSs are believed to be binary (or triple) systems that have experienced mass transfer or possibly coalescence (Hoyle 1964; McCrea 1964; Iben & Tutukov 1984; Iben 1986; Nemeč & Mateo 1990b; Mateo *et al.* 1990; Bailyn 1995; Ferraro *et al.* 2006, 2014; Perets & Fabrycky 2009), from which it follows that SX Phe stars likewise have a binary (or triple star) nature. Of course, if coalescence has occurred then the original binary nature may no longer be visible. In any case, since only a few SX Phe stars in binary systems are known (see §3.3.3) determination of the fraction of binaries among the BN12 stars and their properties is of considerable interest.

During the course of this investigation 11 SX Phe binaries have been identified. Three of these stars are close binaries with orbital periods less than 10 days, and the other eight stars were discovered, from Rømer time-delay analyses, to be in wider binaries with orbital periods ~ 200 -1800 days. Orbital periods and other significant characteristics for the eleven SX Phe binaries are summarized in **Table 9**. The quantities recorded are: the orbital period, P_{orb} ; the half-range of the primary star's RV variation, K_1 ; the orbital eccentricity, e ; the argument of periastron, ω ; the time of periastron passage, T_{per} ; the projected semi-major axis of the primary, $a_1 \sin i$; and the mass function for the secondary star, $f_2(\mathcal{M}_1, \mathcal{M}_2, \sin i)$. Table 9 also gives the orbital characteristics for the two misclassified non-pulsating binaries: KIC 9535881 [*25] is a WUMa system with $P_{\text{orb}} = 0.4804$ d (and possible γ Dor pulsations); and KIC 12643589 [*17] is a triple system consisting of a 1.41 d eclipsing binary with additional transits every $P_{\text{orb}}=44$ d (see bottom panel of Fig.17). Both systems are of interest in their own right because they are binaries belonging to the galactic halo stellar population; however, we are concerned in this paper primarily with the SX Phe stars so little more will be said about these two stars.

3.3.1 Close Binaries

Based on the appearance of their light curves, their observed RV variations, and their broad CCFs, it is clear that KIC 10989032 (*32), KIC 7174372(*8) and KIC 6780873 (*5) have orbital periods less than 10 days and small separations. Their orbital and other properties are discussed next.

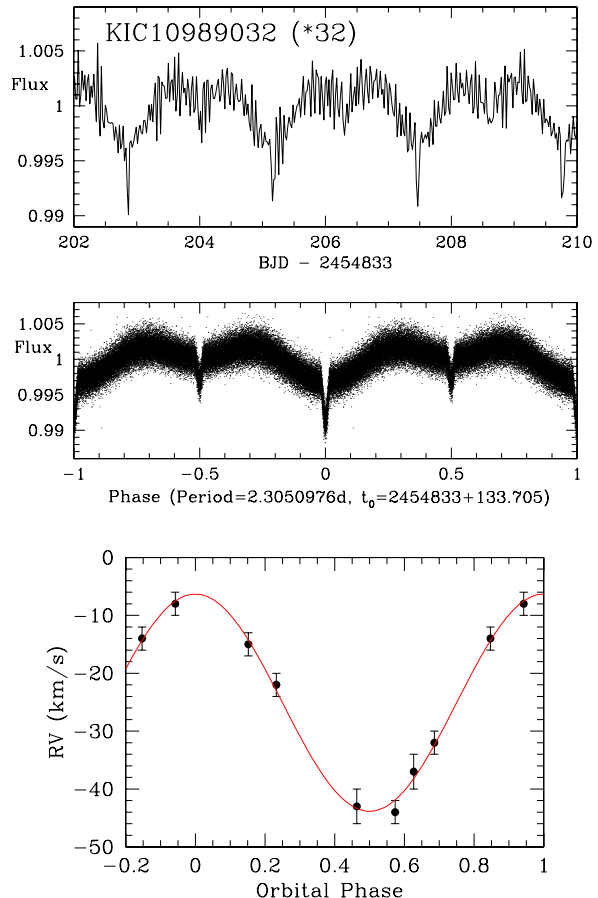


Figure 20. *Kepler* light curves (top, normalized LC fluxes) and radial velocity curve (bottom) for KIC 10989032 (*32), phased with the 2.3-day orbital period and mid-eclipse time of the primary eclipse given in the Villanova EB catalog. The fitted cosine curve is shown in red.

KIC 10989032 (*32) – This eclipsing system is listed in the Villanova EB catalog as having $P_{\text{orb}} = 2.3050976(35)$ d, and a ‘morphology classification parameter’, 0.53, indicating that it is probably semi-detached (morph ~ 0.5 -0.7) but is close to being detached (morph $\lesssim 0.5$). Other basic characteristics include: mid-eclipse time for the primary eclipse, $\text{BJD}_0 = 2454966.705 \pm 0.013$; primary and secondary eclipse depths of 0.0095 and 0.0043 (*i.e.*, very low amplitude grazing eclipses); primary and secondary phase widths of 0.025 and 0.034; and a separation in phase between the primary and secondary eclipses of 0.499, suggesting a near-circular orbit (unless the major axis of the orbital ellipse is orientated towards us, *i.e.* $\omega = \pm 90^\circ$). Additional parameters of the system include (see Table 1 in Prša *et al.* 2011): temperature ratio, $T_2/T_1 = 0.454$; sum of the fractional radii, $(R_1 + R_2)/a = 0.208$ (where a is the semi-major axis of the orbit, equal to the separation of the two stars, $a_1 + a_2$); orbital inclination angle, $\sin i = 0.9947$ (*i.e.*, nearly edge-on, $i = 84.10^\circ$); and radial and tangential components of the orbital eccentricity, $e \sin \omega = -0.241$ and $e \cos \omega = 0.459$.

Figure 20 shows an eight-day portion of the *Kepler* light curve (top panel), the long cadence fluxes phased with the Villanova P_{orb} and BJD_0 (middle panel), and the RV curve (bottom panel). The radial velocities are well fit with

Table 9. Orbital elements for the *Kepler*-field SX Phe stars in binary systems, ordered by orbital period. The columns contain: (1) KIC and CFHT star numbers; (2) orbital period; (3) half-range of the RV variation of the primary star (*i.e.*, the more-massive SX Phe star); (4) projected semi-major axis of the orbit of the primary star; (5) orbital eccentricity; (6) argument of periastron; (7) time of periastron passage; and (8) mass function of the (less-massive) secondary star, f_2 . The last column indicates the source of the information in that row, where ‘TD’ stands for the time-delay (binarogram) method of Balona (2014b), ‘FM’ and ‘PM’ refer to the frequency and phase modulation methods described by Shibahashi & Kurtz (2012) and Murphy *et al.* (2014), ‘EB’ refers to the Villanova EB catalog, and ‘RV’ refers to a ‘Spectroscopic Binary Solver’ (Johnson 2004) solution using the RVs in Table 1. Also given in the table are the previously published orbital elements for KIC 11754974 from Murphy *et al.* (2013b, ‘M13’) and from Balona (2014b, ‘B14’), and the results of simultaneously solving for the phase modulations given the observed radial velocities (‘PM+RV’).

| KIC (CFHT) (1) | P_{orb} [days] (2) | K_1 [km s ⁻¹] (3) | $a_1 \sin i$ [AU] (4) | e (5) | ω [deg] (6) | T_{per} 2450000+ (7) | $f_2(\mathcal{M}_1, \mathcal{M}_2, i)$ [\mathcal{M}_{\odot}] (8) | Method (9) |
|---|---|---|---|------------------------------|--------------------------|-------------------------------------|--|------------------------------|
| (a) Close binaries (orbital periods < 10 days) | | | | | | | | |
| 10989032 (*32) | (2.3050976) 2.3050976 | 18.3 ± 0.5 | 3.86×10^{-3} | 0.08 ± 0.03 | 211 ± 15 | 6547.6 ± 0.1 | $(1.45 \pm 0.18) \times 10^{-3}$ | RV EB |
| 7174372 (*8) | 4.0 ± 0.1 | 1.3 ± 0.5 | 4.9×10^{-4} | 0.0 | undef. | undef. | $(9.5 \pm 0.1) \times 10^{-7}$ | FM,RV |
| 6780873 (*5) | 9.1547±.0003 9.156 ± 0.046 9.16 ± 0.03 9.161 ± 0.001 | 38.73±.12 44.4 ± 6.0 | 0.0325±.0001 0.037 ± 0.005 | $(5 \pm 5) \times 10^{-4}$ | undef. | undef. 6531 ± 1 6518.7 ± 0.3 | $(5.51 \pm 0.05) \times 10^{-2}$ $(8.0 \pm 3.0) \times 10^{-2}$ $(7.2 \pm 12.8) \times 10^{-2}$ $(5.5 \pm 0.2) \times 10^{-2}$ | PM+RV TD FM RV |
| (b) Rømer time-delay (wide) binaries | | | | | | | | |
| 7819024 (*19) | 216.6 ± 0.7 216.2 ± 3.9 216.2 ± 3.1 | 7.27 ± 0.43 7.37 ± 0.95 | 0.144 ± 0.007 0.147 ± 0.019 | 0.09 ± 0.08 | 299 ± 82 | 5050 ± 50 | $(8.48 \pm 1.24) \times 10^{-3}$ $(8.96 \pm 3.42) \times 10^{-3}$ $(9.2 \pm 3.2) \times 10^{-3}$ | PM+RV TD FM |
| 8004558 (*1) | 259.8 ± 0.2 262.1 ± 0.2 261.2 ± 0.9 | 9.70 ± 0.08 10.57 ± 0.08 | 0.231 ± 0.002 0.255 ± 0.002 | 0.020 ± 0.012 | 287 ± 11 | 4993 ± 8 | $(2.45 \pm 0.06) \times 10^{-2}$ $(3.21 \pm 0.07) \times 10^{-2}$ $(2.83 \pm 0.04) \times 10^{-2}$ | PM+RV TD FM |
| 11754974 (*13) | 342.6 ± 0.5 344.8 ± 0.2 343.3 ± 0.3 343.1 ± 0.8 | 8.39 ± 0.08 8.19 ± 0.06 8.35 ± 0.04 | 0.264 ± 0.003 0.259 ± 0.002 0.263 ± 0.002 | 0.013 ± 0.012 0.01 ± 0.01 | 37 ± 8 102 ± 38 | 5110 ± 6 4999 ± 37 | $(2.09 \pm 0.06) \times 10^{-2}$ $(1.96 \pm 0.04) \times 10^{-2}$ $(2.07 \pm 0.03) \times 10^{-2}$ $(2.06 \pm 0.07) \times 10^{-2}$ | PM+RV TD,B14 M13 FM |
| 4243461 (*4) | 481.6 ± 1.8 488.8 ± 2.9 475.5 ± 6.2 | 5.29 ± 0.12 5.34 ± 0.28 | 0.233 ± 0.005 0.240 ± 0.013 | 0.045 ± 0.031 | 163 ± 36 | 5296 ± 48 | $(7.35 \pm 0.41) \times 10^{-3}$ $(7.69 \pm 0.12) \times 10^{-3}$ $(8.17 \pm 1.09) \times 10^{-3}$ | PM+RV TD FM |
| 5705575 (*22) | 537.7 ± 0.9 537.2 ± 1.5 539.5 ± 4.1 (537.5) | 6.70 ± 0.04 6.60 ± 0.18 6.55 ± 0.83 | 0.331 ± 0.003 0.326 ± 0.009 0.324 ± 0.040 | 0.018 ± 0.014 (0.0) | 52 ± 10 undef. | 5367 ± 16 undef. | $(1.68 \pm 0.04) \times 10^{-2}$ $(1.60 \pm 0.13) \times 10^{-2}$ $(1.57 \pm 0.09) \times 10^{-2}$ $(1.57 \pm 0.59) \times 10^{-2}$ | PM+RV TD FM RV |
| 7300184 | 635 ± 20 640 ± 60 | 0.02 ± 0.02 0.07 ± 0.04 | 0.001 ± 0.001 0.004 ± 0.002 | | | | $(3.2 \pm 3.2) \times 10^{-11}$ $(1.8 \pm 1.8) \times 10^{-8}$ | PM TD |
| 9966976 (*31) | >1500 1750 ± 100 | 0.62 ± 0.05 0.66 ± 0.08 | 0.088 ± 0.006 0.106 ± 0.011 | | | | $(3.8 \pm 1.0) \times 10^{-5}$ $(5.2 \pm 1.7) \times 10^{-5}$ | PM TD |
| 9267042 (*12) | (>1500?) 1760 ± 70? | 0.72 ± 0.02 0.70 ± 0.03 | 0.091 ± 0.003 0.113 ± 0.004 | | | | $(5.4 \pm 0.5) \times 10^{-5}$ $(6.3 \pm 0.6) \times 10^{-5}$ | PM TD |
| (c) Close eclipsing binaries (Pop.II) that do not contain an SX Phe star | | | | | | | | |
| 9535881 [*25] | 0.4804213 | 2.1 ± 0.2 | 9.2×10^{-5} | 0.0 | undef. | undef. | $(4.4 \pm 0.9) \times 10^{-7}$ | EB,RV |
| 12643589 [*17] | 1.4116278 44.147177 | 1.7 ± 0.1 | 2.2×10^{-4} | 0.0 | undef. | undef. | $(7.0 \pm 1.0) \times 10^{-7}$ | EB,RV EB |

a cosine function. From the optimum RV fit the eccentricity $e=0.08 \pm 0.03$, with systemic velocity $\gamma = -24.96 \pm 0.31$ km/s, RV amplitude $K_1 = 18.28 \pm 0.45$ km/s, argument of periastron $\omega = 211 \pm 16^\circ$ and time of periastron passage 2456547.61 ± 0.09 . With these values the mass function for the secondary, $f_2 = (\mathcal{M}_2 \sin i)^3 / (\mathcal{M}_1 + \mathcal{M}_2)^2$, which can also be expressed as $P_{\text{orb}} K_1^3 (1 - e^2)^{3/2} / 2\pi G$, has the value $0.00145 \pm 0.00018 \mathcal{M}_{\odot}$; also, the projected semi-major axes,

$a \sin i = 8.60 R_{\odot}$, and $a_1 \sin i = 0.83 R_{\odot}$. Since $\sin i$ is so close to 1.0 this mass function is practically identical to the de-projected mass function, $f'_2 = 0.00149$, and the observed RV curve is practically identical to the curve that would be seen if the system were viewed edge-on. Combining the separation, $a = 8.65 R_{\odot}$, with the sum of the fractional radii given above, implies $R_1 + R_2 = 1.8 R_{\odot}$. From the cosine fit to the observed RVs the time of maximum RV

occurs at $\text{BJD} = 2456548.563 \pm 0.011$, from which one can infer that eclipses occurred $\frac{1}{4}P_{\text{orb}}$ earlier and later, *i.e.*, at $\text{BJD} 2456547.986$ and 2456549.139 , respectively. These ‘observed’ eclipse times are to be compared with the primary eclipse time predicted from the Villanova EB catalog: $\text{BJD}_0 + 686P_{\text{orb}} = 2456548.002$, the time difference amounting to only 0.016 day or 23 min. This difference is much smaller than the error expected from the propagated uncertainties and is consistent with the observed lack of eclipse timing variations (see Conroy *et al.* 2014, and the online EB catalog). Finally, with no RV information for the secondary, the mass ratio, q , and the individual masses are unknown. However, if the primary of KIC 10989032 were a typical A5 V star (see Table 3) it might be expected to have a mass $\sim 2.0 M_{\odot}$ and a radius near $1.7 R_{\odot}$ (Gray 2005). Models of Pop. II blue stragglers that have undergone mass transfer suggest lower total masses, possibly in the range 1.1 to $1.5 M_{\odot}$ (see Fiorentino *et al.* 2014, 2015). Assuming $1.5 M_{\odot}$ for the mass of the primary, the observed $K_1 = 18.28$ km/s suggests $q = 0.11$ and a mass for the secondary of $0.16 M_{\odot}$. The mass-radius relation of Demory *et al.* (2009) suggests that such a low-mass star might be expected to have a radius $R_2 \sim 0.15\text{--}0.20 R_{\odot}$, consistent with the above discussion of sizes.

KIC 7174372 (*8) – As noted earlier, the *Kepler* light curve shows low-amplitude, high-frequency oscillations superimposed on periodic low-amplitude dips. It is possible that the four day period of the dips is due to rotation (Nielsen *et al.* 2013); however, the dips may also be due to orbital motion in an ellipsoidal binary system, *i.e.*, a system comprising “non-eclipsing close binaries whose components are distorted by their mutual gravitation” where “the light variations are due to the changing cross-sectional areas and surface luminosities that the distorted stars present to the observer at different phases” (Morris 1985). The star is not listed in the Villanova EB catalog. Owing to large uncertainties in the measured RVs (caused by the broad spectral lines), it is difficult to tell if the RVs are varying ($\Delta RV = 4.9 \pm 4.8$ km/s); however, considerable broadening is seen in the CCFs (Fig. 5). If both P_{orb} and P_{rot} are near 4.0 d then the system is tidally synchronized; such synchronization is common in binary systems with short orbital periods (Duquenooy & Mayor 1991).

KIC 6780873 (*5) - This double-lined spectroscopic binary (see §2.1) exhibits the largest RV range of all the program stars, $\Delta RV = 69.9 \pm 0.3$ km/s. Six of the nine CCFs resolve into two components, with heights that clearly identify the primary and secondary components (see Fig. 3). From an FM analysis the orbital period was initially estimated to be 9.16 ± 0.03 d. Similar periods were derived from a time-delay binarogram analysis, from a PM analysis (where a sampling window of 3 d instead of the usual 10 d was needed), and from an analysis based only on the 18 RVs (using the ‘Spectroscopic Binary Solver’ [SBS] program of Johnson 2004). The current best estimate of the orbital period, $P_{\text{orb}} = 9.1547 \pm 0.0003$ d, combines the results of the PM method with RV information (see Murphy *et al.* 2016). With this period the symmetric RV curves were well fit with eccentricity, $e=0.0$, and gamma velocity (*i.e.*, median RV),

Table 10. Example orbital properties for the non-eclipsing SB2 system KIC 6780873 (*5), for four possible primary-star masses. The quantities were calculated assuming the following observational constraints: $P_{\text{orb}}=9.161 \pm 0.001$ d; $e=0.04 \pm 0.02$; $a \sin i = 16.48 R_{\odot}$; $\gamma=10.07 \pm 0.26$ km/s; $K_1=38.8 \pm 0.9$ km/s; $K_2=52.4 \pm 1.0$ km/s; $q = 0.74 \pm 0.03$; time of periastron passage, $T_{\text{per}}=2455518.73 \pm 0.33$; argument of periastron for the primary and the secondary, $\omega_1=311 \pm 14^\circ$ and $\omega_2=131 \pm 14^\circ$. The velocities in the last two rows were calculated assuming circular orbits.

| $\mathcal{M}_1 =$ | $0.9 M_{\odot}$ | $1.2 M_{\odot}$ | $1.5 M_{\odot}$ | $1.8 M_{\odot}$ |
|-----------------------------|-----------------|-----------------|-----------------|-----------------|
| $\mathcal{M}_2 [M_{\odot}]$ | 0.67 | 0.89 | 1.11 | 1.33 |
| i [deg] | 50.40 | 44.43 | 40.53 | 37.70 |
| $a [R_{\odot}]$ | 21.39 | 23.56 | 25.38 | 26.97 |
| $a_1 [R_{\odot}]$ | 9.10 | 10.02 | 10.79 | 11.47 |
| $a_2 [R_{\odot}]$ | 12.29 | 13.54 | 14.59 | 15.50 |
| v_1 [km/s] | 50.3 | 55.4 | 59.6 | 63.4 |
| v_2 [km/s] | 67.9 | 74.8 | 80.6 | 85.7 |

$\gamma = 10.07 \pm 0.26$ km/s (see Figure 4). The observed amplitudes of the two RV curves, $K_1 = 38.8 \pm 0.9$ km/s and $K_2 = 52.4 \pm 1.0$ km/s, give a mass ratio, $q = 0.74 \pm 0.03$, which is independent of the orbital inclination angle. The projected semi-major axis, $a \sin i = 16.48 R_{\odot}$ ($=0.077$ AU), follows from $K_1(P_{\text{orb}}/2\pi)((1+q)/q)$. Assuming the parameters given in the caption for Fig. 4 the predicted RV curves fit well the measured individual RVs, with standard deviations of the O-C residuals ~ 0.62 km/s for both components. Since the photometry shows no evidence of eclipses, the individual masses and the orbital inclination angle, i , could not be determined; only the mass functions for the individual components, $f_1 = 0.136 M_{\odot}$ and $f_2 = 0.055 M_{\odot}$ could be estimated.

To resolve the degeneracy between mass and inclination angle four different masses were assumed for the SX Phe (primary) star, $\mathcal{M}_1 = 0.9, 1.2, 1.5$ and $1.8 M_{\odot}$, and inclination angles were calculated by constraining the predicted RV curves to have the observed K_1 and K_2 values. Some properties of the binary system for the assumed masses are summarized in **Table 10**, where: \mathcal{M}_2 follows from the observed mass ratio $q (=K_1/K_2)$; the semi-major axis, a , follows from Kepler’s third law, $a^3 = G(\mathcal{M}_1 + \mathcal{M}_2)P^2/(4\pi^2)$; and the individual distances from the centre of mass, a_1 and a_2 , were computed from the a and K values. RV curves were computed for each mass, from which the best-fit inclination angles, i , were found. Since e is near zero, the individual velocities, v_1 and v_2 , which follow from the a_1 , a_2 and P_{orb} values, are very nearly constant. Note that for a doubling of \mathcal{M}_1 , from 0.9 to $1.8 M_{\odot}$, the inclination angle changed little, from 50.4 to 37.7 degrees.

3.3.2 Rømer Time-Delay (Wide) Binaries

Shibahashi *et al.* (2012, 2015), Telting *et al.* (2012), Murphy *et al.* (2013b, 2014, 2015a,b), Balona (2014b), Balona *et al.* (2015), Kurtz *et al.* (2015), Koen (2014) and others have shown that it is possible, using only *Kepler* time-series photometry, to derive RV curves and orbital elements for binary systems in which one or more of the stars is pulsating. As the pulsating star orbits the barycentre of the binary system its distance changes, resulting in Rømer time delays of the pulsation frequencies (also seen as phase modulations),

which are equivalent to frequency modulations. When working in the time domain these methods have been variously referred to as the ‘time-delay’ (TD) method (Telting *et al.* 2012, Balona 2014b), the ‘phase modulation’ (PM) method (Murphy *et al.* 2014, 2015b, 2016), and the ‘O-C (and light travel time)’ method (Koen 2014); and in the frequency domain the ‘frequency modulation’ (FM) method (Shibahashi *et al.* 2012, 2015). Successful application of these methods requires: (1) high precision photometry (in order to derive accurate pulsation frequencies and to detect contamination by nearby frequencies); (2) photometry with a time baseline sufficiently long to resolve long orbital periods, and of sufficiently short cadence to resolve close binaries with short orbital periods; and (3) one or more members of the binary system pulsating with one or more high-amplitude frequencies that are uncontaminated by close frequencies (*i.e.*, no significant neighbouring peaks in the periodogram) and which exhibit *steady* pulsation (*i.e.*, no amplitude or intrinsic variations). The 32 SX Phe candidates and associated *Kepler* photometry meet all these requirements in the case of binary systems that have orbital periods in the range ~ 10 to ~ 1700 days.

One prior application of the time-delay method was the detailed asteroseismic analysis of KIC 11754974 (*13) by Murphy *et al.* (2013b). Time delays of up to ~ 180 s revealed the SX Phe star to be the primary in a non-eclipsing 343 d binary system that has an almost circular orbit; assuming $1.5 M_{\odot}$ for the mass of the primary and orbital inclination angle $i = 90^{\circ}$, gives a secondary mass of $0.6 \pm 0.2 M_{\odot}$, which is characteristic of a K- or early-M main-sequence star. More recent analyses of KIC 11754974 using the complete *Kepler* Q0-17 data set have been made by Balona (2014b) and Murphy *et al.* (2014).

For the present paper both time- and frequency-domain methods were used to search the BN12 stars for SX Phe pulsators residing in binary systems. The analyses were carried out using the TD (binarogram) method described by Balona (2014b), and the FM and PM methods described by Shibahashi *et al.* (2012, 2015) and Murphy *et al.* (2014, 2015b, 2016). All the available Q0-Q17 *Kepler* photometry was utilized, and for the time-domain analyses, a sampling interval of 10 d was adopted, which corresponds to a Nyquist frequency of 0.05 d^{-1} and precludes measurement of orbital periods shorter than ~ 20 d. Care was taken to select only real frequencies with amplitudes high enough to allow detection of binary motion (use of an incorrect alias frequency often results in an apparent ‘orbital period’ close to that of the *Kepler* satellite, *i.e.*, 372 d). For the FM analyses the short-period limit was reduced to ~ 4 d, and led to the initial discovery of the 9.16 d orbital period for KIC 6780873 and the 4.0 d orbital period for KIC 7174372. Sensitivity to short periods is the biggest advantage that the frequency domain has over the time domain. Orbital elements derived from the current analysis are summarized in Table 9.

Observed phase shifts from the time-delay analyses are shown in **Figure 21** for six of the stars. The graphs for each star give, for the frequencies noted on the right side of each graph, the phase variation as a function of orbital phase. The points in each graph represent the measured pulsation phase (10 d segments) of the photometry. The six stars have orbital periods between 208 and 670 days and therefore can be classified as ‘wide’ binaries. The high signal-to-noise ratios of the

phase variations leave little doubt about the binary nature for five of the six stars. In the case of KIC 7300184 only one pulsation frequency was employed in the analysis, therefore the orbital parameters e , ω and T_{per} could not be calculated.

In **Figure 22** time-delay diagrams and Fourier transforms of the weighted average time delays from PM analyses are plotted for seven of the wide binaries. The panels are ordered by orbital period, shortest at the top and longest at the bottom. For each time-delay graph (left side) individual extracted frequencies that were used for the analysis are plotted with different symbols (see legend on right). For all but the two longest period binaries the null hypothesis that there is no time delay can be ruled out with considerable confidence. The panel for KIC 11754974 (third row from the top) shows that dominant pulsation frequencies do not always lead to the same time-delay (or phase modulation) curve. In some cases the chosen pulsation frequencies may have been contaminated by other close frequency peaks, which would have had the effect of perturbing the phases at the sampling times and obscuring the frequency variation due to binarity; by analyzing multiple frequencies this problem was largely overcome.

The derived orbital periods for KIC 9267042 (*12) and KIC 9966976 (*31), if real, are longer than the ~ 4 -year duration of the *Kepler* data set and are too long to be resolved by the FM method. However, phase variations indicative of binarity were found using both the PM and TD methods (see Table 9). The strongest argument that can be made for the reality of the measured time delays is that in Fig. 22 similar curvatures can be seen for all of the pulsation frequencies employed for the analyses, a finding that is consistent with variation caused by binary motion. When KIC 9966976 was analyzed using the binarogram method the same P_{orb} was found for the four frequencies that were considered, and similar values of $a \sin i$ were derived for all four frequencies, which lends considerable support to the conclusion of its binary nature. The evidence was less convincing for KIC 92670423; while the same dominant peak (*i.e.*, P_{orb}) was found for the four test frequencies, a range was seen in the amplitudes of the associated peaks (*i.e.*, $a \sin i$) thereby reducing the likelihood of the binary conclusion.

Figure 23 shows the results of PM+RV analyses for six time-delay binaries where both the phase modulations *and* the RVs were included in the orbit solutions. The graphs were created using the method outlined in Murphy *et al.* (2016). Inclusion of the RVs extended the time baselines by almost two years, and added weight to several of the orbital solutions. The biggest improvement compared to the single-method results was for KIC 6780873 (*5), the 9.1 day double-lined spectroscopic binary; in this case, the precision of the orbital period improved to a few tens of seconds for a light travel time (across the orbit) of only a few tens of milli-seconds, and the uncertainty of its orbital eccentricity improved to within 0.0005 of zero (signifying circular orbits). For the binaries with large $v \sin i$ values the addition of the RVs to the solutions resulted in minimal improvement over the PM-only solutions; and for KIC 11754974 (*13) the maximum time delay is now seen to be ~ 140 sec, down from the ~ 180 s noted earlier.

Masses and radii for the program stars, taken from Huber *et al.* (2014), are given in **Table 11**. The average mass, $1.70 M_{\odot}$, and average radius, $2.25 R_{\odot}$ (exclud-

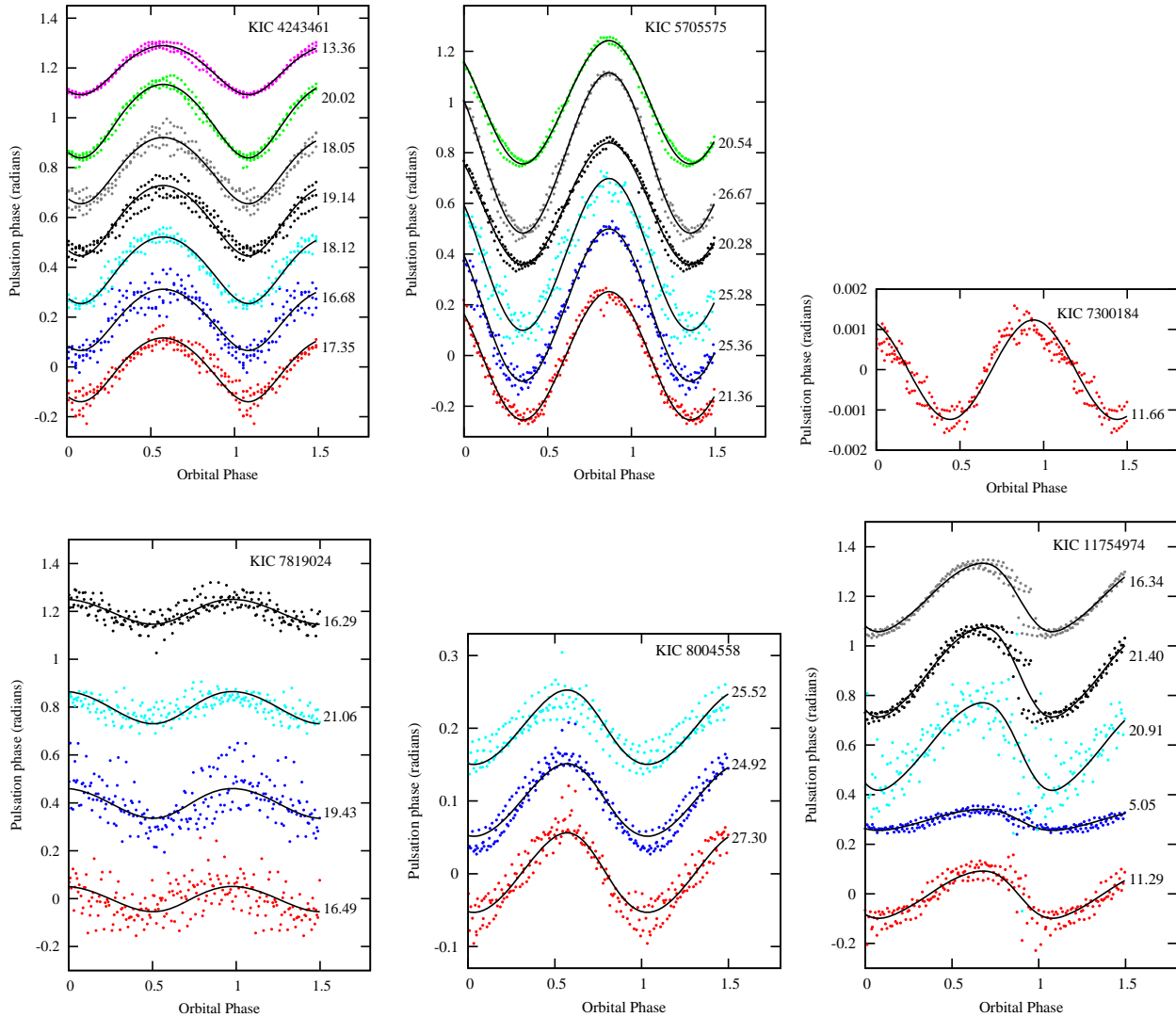


Figure 21. Time delay (TD) results for six binary stars: phase variation of the pulsation modes as a function of the orbital phase. For clarity an arbitrary vertical displacement has been made (and different colour used) for each pulsation frequency, and the particular frequency (units of d^{-1}) is given on the right. For KIC 7300184 the periodogram shows only one pulsation frequency of sufficiently high amplitude to reveal possible pulsation phase variations. The solid (black) curves are the fitted phase variations assuming the orbital parameters given in Table 10.

ing the extreme outlier KIC 6227118), were adopted for the two stars that are missing from the Huber *et al.* sample, KIC 5390069 and KIC 7300184. For the binary systems, lower limits for the masses of the secondary stars are also in the table. These were derived by assuming an orbital inclination angle, $i = 90^\circ$ (*i.e.*, edge-on), adopting the Huber *et al.* mass for the primary star, and using the mass function $f_2(\mathcal{M}_1, \mathcal{M}_2, \sin i)$ given in Table 9 to solve for the minimum mass of the secondary. Assuming $1.5 \mathcal{M}_\odot$ for the KIC 11754974 primary star mass, instead of the H14 value of $1.73 \mathcal{M}_\odot$, gives a slightly lower minimum mass for the secondary, $0.43 \pm 0.15 \mathcal{M}_\odot$, still characteristic of a K- or early-M main-sequence star. The secondaries for KIC 7174372 (*8), KIC 9267042 (*12) and KIC 9966976 (*31) are seen to have \mathcal{M}_2 lower limits below $0.08 \mathcal{M}_\odot$, which offers the possibility that the companions are brown dwarfs.

Based on our findings, eight of the SX Phe stars appear

to have companions with orbital periods between 200 and 1800 days, seven of which are new discoveries (the binarity of KIC 11754974 having already been discovered by Murphy *et al.* 2013b). The orbits for these stars are probably too large for there to have been the mass transfer necessary to create the SX Phe primary (*i.e.*, a pulsating blue straggler). Of course, if one star already entered the red giant phase it could now exist as an extreme horizontal branch star with an exposed core, *i.e.*, an sdB or WD star. It seems most likely that the primary of these ‘wide’ binaries is a coalesced star while the secondary is the third star in a triple system. Indirect evidence for the coalescence hypothesis comes from the presence in HR diagrams of various types of binary systems seen among the BSs found in globular clusters and dwarf galaxies (Mateo *et al.* 1990; Kaluzny *et al.* 2007, 2013; Thompson *et al.* 2010; Rozyczka *et al.* 2010). It would be interesting to know if any of the program stars contain white

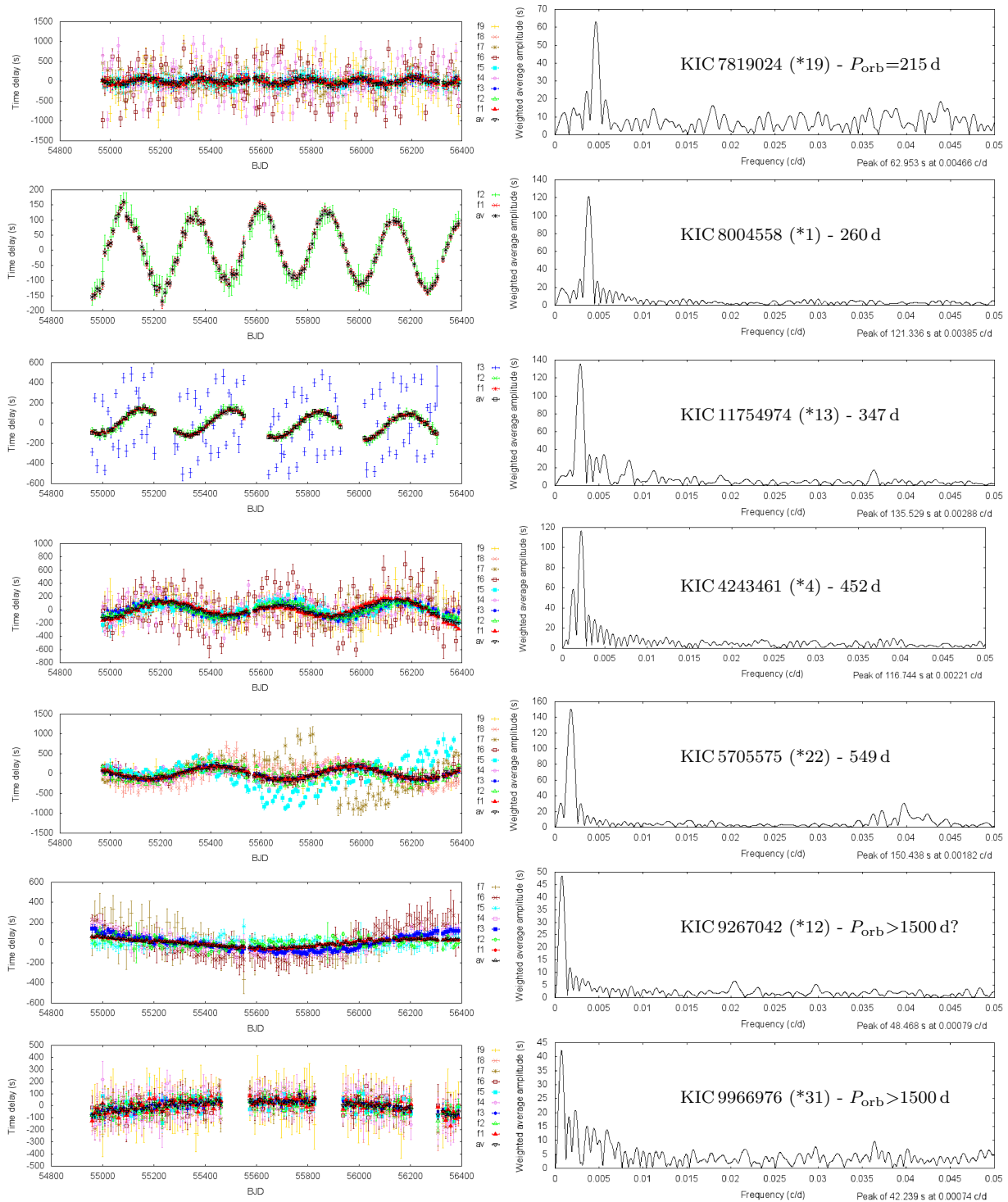


Figure 22. Phase modulation (PM) analysis results: time-delay diagrams (left) and Fourier transforms of the weighted average time delays (right) for six of the photometric binary systems, including the two long-period stars. The ordering (top to bottom) is by increasing orbital period. For each star the weighted-average time delays are shown with black symbols (inverted open triangles).

dwarf companions of the sort recently observed in three BSs in the 7 Gyr old open cluster NGC 188 (Gosnell *et al.* 2014).

3.3.3 Other SX Phe Binaries

Approximately one third of the BN12 sample of *Kepler*-field SX Phe stars (eleven of 30 stars) have been found to be in binary systems with orbital periods ranging from a few days to several years. While these are not the first SX Phe stars in binary systems to be identified, the long baseline (four

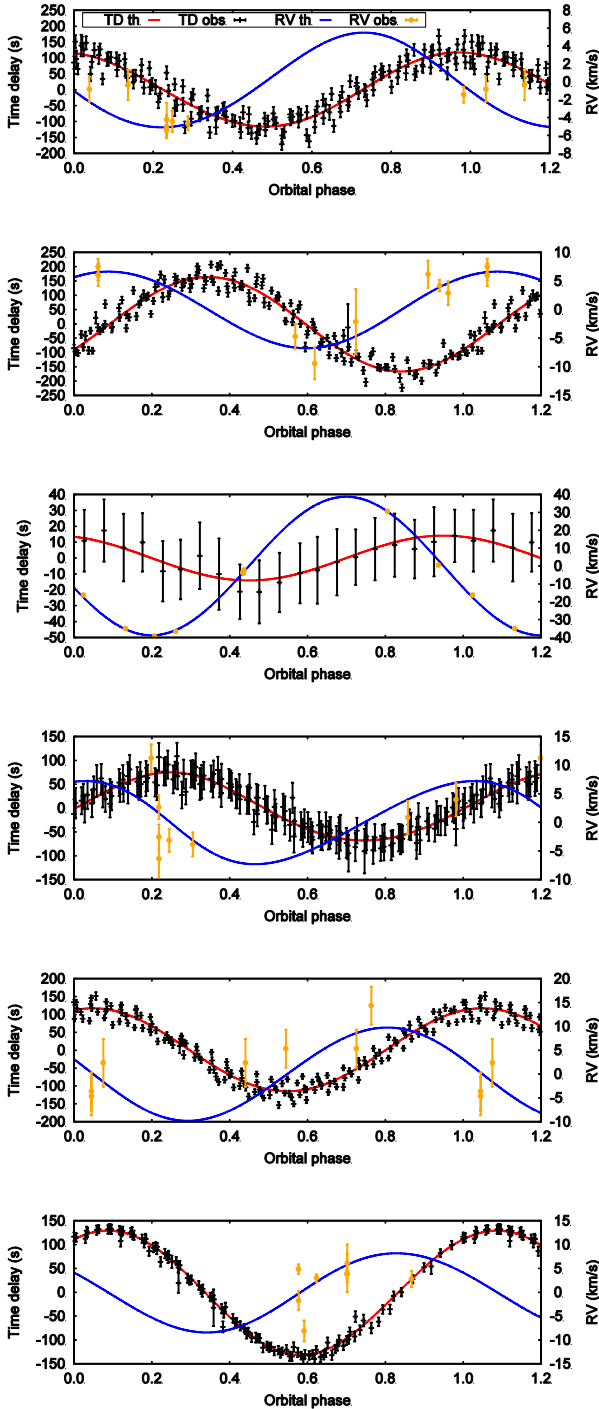


Figure 23. Phase modulation plus radial velocity (PM+RV) analysis results for six wide binaries. From top to bottom the curves shown are for the stars KIC 4243461 (*4), KIC 5705575 (*22), KIC 6780873 (*5), KIC 7819024 (*19), KIC 8004558 (*1) and KIC 11754974 (*13). For each star time-delay and radial-velocity curves are plotted, phased with the orbital periods given in Table 9. The RVs have been offset by the systemic RVs. Both measured and fitted time-delays (black points and red curves), and measured and fitted RVs (ochre points and blue curves), are plotted.

Table 11. Radii and masses for the 34 program stars. The radius and mass of the primary, R_1 and \mathcal{M}_1 , are from Table 5 of Huber *et al.* (2014). The mass of the secondary, \mathcal{M}_2 , was calculated by combining the mass function, $f_2(\mathcal{M}_1, \mathcal{M}_2, \sin i)$, from Table 9, with the H14 primary mass from column (4), and assuming $i = 90^\circ$; thus the \mathcal{M}_2 are lower limits. The KIC numbers of the binary systems are in **boldface**.

| KIC no. (1) | CFHT no. (2) | R_1/R_\odot (H14) (3) | $\mathcal{M}_1/\mathcal{M}_\odot$ (H14) (4) | $\mathcal{M}_2/\mathcal{M}_\odot$ (this paper) (5) |
|-----------------|-----------------|-------------------------------|---|--|
| 1162150 | 15 | 4.31 | 2.09 | |
| 3456605 | 24 | 2.27 | 1.64 | |
| 4168579 | 23 | 2.78 | 1.94 | |
| 4243461 | 4 | 1.55 | 1.39 | > 0.27 |
| 4662336 | 14 | 2.54 | 1.77 | |
| 4756040 | 20 | 1.97 | 1.74 | |
| 5036493 | 26 | 2.42 | 2.00 | |
| 5390069 | – | [2.25] | [1.70] | |
| 5705575 | 22 | 2.08 | 1.68 | > 0.42 |
| 6130500 | 9 | 1.90 | 1.71 | |
| 6227118 | 27 | 11.32: | 3.24: | |
| 6445601 | 2 | 1.80 | 1.52 | |
| 6520969 | 21 | 3.03 | 2.01 | |
| 6780873 | 5 | 1.11 | 1.01 | > 0.50 |
| 7020707 | 16 | 2.32 | 1.73 | |
| 7174372 | 8 | 1.77 | 1.46 | > 0.01 |
| 7300184 | – | [2.25] | [1.70] | |
| 7301640 | 10 | 1.78 | 1.56 | |
| 7621759 | 6 | 1.99 | 1.52 | |
| 7765585 | 28 | 1.37 | 1.40 | |
| 7819024 | 19 | 1.83 | 1.53 | > 0.31 |
| 8004558 | 1 | 2.45 | 1.71 | > 0.49 |
| 8110941 | 29 | 1.74 | 1.50 | |
| 8196006 | 30 | 1.35 | 1.27 | |
| 8330910 | 3 | 1.90 | 1.55 | |
| 9244992 | 7 | 3.93 | 1.87 | |
| 9267042 | 12 | 3.12 | 2.03 | > 0.06 |
| 9535881 | [25] | 1.65 | 1.46 | > 0.01 |
| 9966976 | 31 | 2.54 | 1.97 | > 0.05 |
| 10989032 | 32 | 2.18 | 2.11 | > 0.20 |
| 11649497 | 11 | 2.16 | 1.81 | |
| 11754974 | 13 | 2.23 | 1.73 | > 0.46 |
| 12643589 | [17] | 1.12 | 1.15 | > 0.01 |
| 12688835 | 18 | 2.88 | 1.97 | |

years) and high-precision of the photometry has allowed us to define with great precision the orbits of several of the stars and their oscillations.

Other presently known SX Phe binaries (which exhibit a similarly large range of separations and types) include: (1) four “blue metal poor” (BMP) halo stars found by George Preston and his collaborators – CS 22966-043 (see Preston & Landolt 1998, 1999), which has an orbital period of ~ 319 days and pulsations closely resembling those of the SX Phe stars in the very metal-poor globular cluster NGC 5053 (Nemec *et al.* 1995), and CS 22871-040, CS 22896-103 and CS 29499-057 (Preston & Sneden 2000). Curiously CS 22896-103 is not metal-poor but has a metallicity similar to the Sun, $[\text{Fe}/\text{H}] = -0.10$ dex, and is one of ~ 17 metal-rich BSs found among the sample of BMP stars studied by Preston & Sneden (see their Tables 1 and 5).

(2) BL Cam, which from an analysis of its O-C diagram, is a multi-periodic low-metallicity high-amplitude SX Phe

star, and was found to be in a 144.2 d close binary system, possibly orbited by a brown dwarf having an orbital period ~ 9.3 years (Fauvaud *et al.* 2006, 2010);

(3) QU Sge in M71 is the first SX Phe binary found in a globular cluster (Jeon *et al.* 2006; see McCormac *et al.* 2014). It is a semi-detached Algol-type eclipsing binary (orbital period 3.8 days) with “the secondary component fully filling its Roche lobe and the primary filling its Roche lobe by about 33%”. After subtracting the eclipses the primary star was seen to be an SX Phe star with two close frequencies, 35.883 d^{-1} and 39.867 d^{-1} (corresponding to periods of 40.2 and 36.1 min, respectively) indicative of non-radial pulsations. Given that the mean $[\text{Fe}/\text{H}]$ of M71 is near -0.80 dex, with a small (0.03 dex) standard deviation that suggests considerable homogeneity (Cordero *et al.* 2015, and references therein), it is reasonable to assume that QU Sge too has a similar metal abundance.

Relaxing the distinction between SX Phe and δ Sct stars, δ Sct binary systems were first identified over 40 years ago. The first such identification was AB Cas, a δ Sct star in a 1.37 d Algol-type system (Tempesti 1971; Rodríguez *et al.* 1994, 1998), where the δ Sct star has a small amplitude range, $\Delta V \sim 0.05$ mag, and appears to be monophasic with $f = 17.16 \text{ d}^{-1}$. Another early identification was Y Cam (Broglia 1973; Broglia & Conconi 1984; Rodríguez *et al.* 2010), which shows several significant frequencies between 15 and 18 d^{-1} (Kim *et al.* 2002). More recently, numerous low-amplitude δ Sct stars in eclipsing binary systems have been identified by Rodríguez & Breger (2001), Mkrtichian *et al.* (2005) and Soydugan *et al.* (2006). The last of these papers identified 25 EBs containing low-amplitude (0.007 to 0.02 mag) δ Sct stars. Derekas *et al.* (2009) have investigated the question of binarity and multiplicity in 10 δ Sct (HADS) stars. Other recent studies include those by Southworth *et al.* (2011), Lampens *et al.* (2011), Hambleton *et al.* (2013), Debosscher *et al.* (2013), and Lee *et al.* (2016).

4 SUMMARY

Our goal was to characterize better the sample of 34 *Kepler*-field SX Phe stars identified by BN12. High-resolution spectra for 32 of the 34 stars were acquired and analyzed, and all the available Q0-Q17 long- and short-cadence *Kepler* photometry for the 34 stars were re-analyzed.

Radial velocities were derived from 184 program star spectra (calibrated with 24 spectra of IAU standard stars). Approximately half of the stars show some evidence for RV variability. By combining the measured mean RVs with the tangential motions, U, V, W space motions were derived. Five of the stars were found to have large negative V -velocities, and 29 of the 32 stars have a total space motion $T > 300 \text{ km/s}$. All of the stars lie in the ‘galactic halo’ region of the Toomre diagram (except possibly KIC 6227118 which appears to lie in the ‘thick disk’ region).

Also derived from the spectra were projected rotation velocities and macroturbulent velocities. Two thirds of the stars are fast rotators with $v \sin i > 50 \text{ km/s}$, including four stars with $v \sin i \geq 200 \text{ km/s}$. Several stars were found to have macroturbulent velocities in the range 10-30 km/s; such turbulence may be an even larger contributor to observed broadening of spectral lines than rotation.

Other atmospheric parameters that were measured include T_{eff} , $\log g$, v_{mic} and $[\text{Fe}/\text{H}]$; these spectroscopic estimates improve upon previous values, such as those that rely only on calibrations involving photometry (KIC, H14). The spectral types range from A2-F2, corresponding to surface temperatures in the range 8600-6900 K. The mean metallicity of the sample is near solar, with only a few of the stars having a marked metal weakness; in this sense the stars resemble the metal-rich A-stars (Perry 1969, Preston 2015). By analogy with metal-rich RR Lyrae stars, such as those found in metal-rich globular clusters the BN12 sample can be characterized as ‘metal-rich SX Phe stars’. In fact, the existence of metal-rich SX Phe stars complements the recent finding by Torrealba *et al.* 2015) that suggests a higher concentration of more metal-rich stars near the galactic disk (see their Figs.12-13).

SX Phe stars have, until now, been thought of as “metal-poor Population II variables that have high space velocities and fall in the blue straggler domain of the color-magnitude diagrams of globular clusters” (McNamara 1995). The identification in this paper of *bona fide* metal-rich SX Phe stars suggests that the definition of such stars should not be limited to “metal-poor” pulsators.

ACKNOWLEDGMENTS

This paper is based on spectra acquired with the Canada-France-Hawaii 3.6-m telescope (CFHT) and the 3.5-m telescope at the Apache Point Observatory (APO), and on photometry from NASA’s *Kepler* mission and the Korean 1.8-m Bohyunsan Observatory. CFHT is operated by the National Research Council of Canada, the Institut National des Sciences de l’Univers of the Centre National de la Recherche Scientifique of France, and the University of Hawaii. The CFHT pipeline, Upena, uses J.-F. Donati’s software LibRESprIT (Donati *et al.* 1997). We wish to thank the CFHT time allocation committee for its generous awards of observing time, and Nadine Manset and her team of service observers for making the ESPaDOnS observations. We also wish to thank Dr. Suzanne Hawley, the director of the APO 3.5-m telescope which is owned and operated by the Astrophysical Research Consortium, for observing time, and the telescope operators for their assistance. Funding for the *Kepler* mission is provided by the NASA Science Mission directorate. The authors thank the *Kepler* team for their generosity in allowing the data to be released and for their outstanding efforts which have made these results possible. JMN thanks Federico González for his ‘rcros’ software (see Díaz *et al.* 2011) that was used for deriving the $v \sin i$ values, Dr. Karen Kinemuchi for her hospitality at the Apache Point Observatory and at New Mexico State University, Dr. Simón-Díaz for making public his IACOB software, and the referee for useful comments. A special thanks is owed to Dr. Amanda Linnell Nemec for helpful suggestions and for making critical readings of the paper. We also thank Drs. Don Kurtz, Andrzej Pągowski, Conny Aerts and Patricia Lampens for useful discussions. JMN is grateful to the Camosun College Faculty Association for financial assistance. LAB wishes to thank the National Research Foundation and the South African Astronomical Observatory for financial support. SJM is supported by the Australian Re-

search Council, and by the Danish National Research Foundation and ASTERISK project (grant agreement numbers: DNR106 and 267864, respectively). Some of the data presented in this paper were obtained from the Multimission Archive at the Space Telescope Science Institute (MAST). STScI is operated by the Association of Universities for Research in Astronomy, Inc., under NASA contract NAS5-26555. Support for MAST for non-HST data is provided by the NASA Office of Space Science via grant NNX09AF08G and by other grants and contracts. This research has also made use of the SIMBAD database, operated at CDS, Strasbourg, France, of the Aladin Sky Atlas, and of the VALD3 database (operated at Uppsala University, the Institute of Astronomy RAS in Moscow, and the University of Vienna).

REFERENCES

- Adelman, S. 2004, Proc. IAU Symp. 224, 1, ed. Zverko *et al.*
Aerts, C. 2015, *Astr. Nachr.* 336, 477
Aerts, C., Puls, J. *et al.* 2009, *A&A*, 508, 409
Aerts, C., Simón-Díaz, S. *et al.* 2014, *A&A*, 569, A118
Asplund, M. *et al.* 2009, *Ann. Rev. Astron. Ap.*, 47, 481
Bailyn, C.D. 1995, *Ann. Rev. Astron. Ap.*, 33, 133
Balona, L.A. 2011, *MNRAS*, 415, 1691
Balona, L.A. 2013, *MNRAS*, 431, 2240
Balona, L.A. 2014a, *MNRAS*, 437, 1476
Balona, L.A. 2014b, *MNRAS*, 443, 1946
Balona, L.A. 2015, *MNRAS*, 448, 1378
Balona, L.A. *et al.* 2011, *MNRAS* 413, 2403
Balona, L.A. & Dziembowski, W., 2011, *MNRAS*, 417, 591
Balona, L.A. & Nemeč, J.M. 2012, *MNRAS*, 426, 2413
Balona, L.A. *et al.* 2015, *MNRAS*, 448, 1378
Bedding, T. *et al.* 2014, EPJ Web Conf., 101, 01005
Bensby, T., Oey, M.S. *et al.* 2007, *ApJ*, 655, L89
Böhm-Vitense, E. 1958, *Zs.f.Ap.*, 46, 108
Böhm-Vitense, E. 1989, *Introduction to Stellar Astrophysics*, Vol.2, Cambridge University Press
Böhm-Vitense, E. & Canterna, R. 1974, *ApJ* 194, 629
Böhm-Vitense, E. & Nelson, G.D. 1976, *ApJ* 210, 741
Böhm-Vitense, E. & Dettmann, T. 1980, *ApJ* 236, 560
Breger, M. 1975, *ApJ*, 201, 653
Breger, M. 1977a, *PASP*, 89, 55
Breger, M. 1977b, *PASP*, 89, 339
Breger, M. 1980, *ApJ*, 235, 153
Breger, M. *et al.* 2013, *ApJ*, 773:56
Broglia, P. 1973, *Inf. Bull. Var. Stars*, No.823
Broglia, P. & Conconi, P. 1984, *A&A*, 138, 443
Brown, T.M., Latham, D.W. *et al.* 2011, *AJ*, 142:112
Bruntt, H., Catala, C. *et al.* 2002, *A&A*, 389, 345
Bruntt, H., Frandsen, S. *et al.* 2001, *A&A*, 371, 614
Bruntt, H., Deleuil, M. *et al.* 2010a, *A&A*, 519, A51
Bruntt, H., Bedding, T.R. *et al.* 2010b, *MNRAS*, 405, 1907
Cantiello, M. *et al.* 2009 *A&A*, 499, 279
Carney, B.W., Latham, D.W. *et al.* 2001 *AJ*, 122, 3419
Carney, B.W., Latham, D.W. *et al.* 2005, *AJ*, 129, 466
Carollo, D., Beers, T.C. *et al.* 2007, *Nature*, 450, 1020
Carollo, D., Beers, T.C. *et al.* 2010, *ApJ*, 712, 692
Carollo, D., Beers, T.C. *et al.* 2016, *Nature*, doi:10.1038
Carroll, J.A. 1928, *MNRAS*, 553, 1928
Carroll, J.A. 1933, *MNRAS*, 93, 478
Castelli, F. & Kurucz, R.L. 2004, arXiv:astro-ph/0405087
Catanzaro, G., Ripepi, V. *et al.* 2011, *MNRAS* 411, 1167
Chaplin, W.J. *et al.* 2014, *MNRAS*, 445, 946
Coşkunoğlu, B. *et al.*, 2011, *MNRAS*, 412, 1237
Cohen, R.E. & Sarajedini, A. 2012, *MNRAS*, 419, 342
Conroy, K.E. *et al.* 2014, *AJ*, 147:45
Coppola, G., Marconi, M. *et al.* 2015, *ApJ*, 814:71
Cordero, M.J., Pilachowski, C.A. *et al.* 2015, *ApJ*, 800:3
Dall, T.H. *et al.* 2010, *A&A*, 514, A25
Debosscher, J. *et al.* 2013, *A&A*, 556, A56
de Jager, C. 1990, *Solar Physics* 126, 201
Demory, B.-O. *et al.* 2009 *A&A*, 505, 205
Derekas, A., Kiss, L.L. *et al.* 2009, *MNRAS*, 394, 995
Díaz, C.G., González, F. *et al.*, 2011, *AA*, 531, A143
Donati, J.-F. *et al.* 1997, *MNRAS*, 291, 658
Donati, J.-F. & Landstreet, J. 2009, *ARA&A*, 47, 333
Doyle, A.P., Davies, G.R. *et al.* 2014, *MNRAS*, 444, 3592
Dravins, D. 1982, *ARA&A*, 20, 61
Dupret, M.-A. *et al.* 2004, *A&A*, 414, L17
Duquenois, A. & Mayor, M. 1991, *A&A*, 248, 485
Eggen, O.J. 1970, *PASP*, 82, 274
Eggen, O.J. 1979, *ApJS*, 41, 413
Eggen, O.J. & Iben, I. 1989, *AJ*, 97, 431
Everett, M.E. *et al.* 2012, *PASP*, 316
Ferraro, F.R. *et al.* 2006, *ApJ*, 647, L53
Ferraro, F.R. *et al.* 2015, *Ap.Sp.Sc.Lib.*, 413, 99
Fauvaud, S. *et al.* 2006, *A&A*, 451, 999
Fauvaud, S. *et al.* 2010, *A&A*, 515, A39
Fiorentino, G., Lanzoni, B. *et al.* 2014, *ApJ*, 783:34
Fiorentino, G., Marconi, M. *et al.* 2015, *ApJ*, 810:15
Fusi Pecci, F. 1992, *AJ*, 104, 1831
Gilliland, R. L., Bono, G. *et al.* 1998, *ApJ*, 507, 818
Gosnell, N. *et al.* 2014, *ApJ*, 783:L8
Grassitelli, L., Fossati, L., *et al.* 2015, *A&A*, 584, L2
Gray, D.F. 1973, *ApJ*, 184, 461
Gray, D.F. 1975, *ApJ*, 202, 148
Gray, D.F. 1978, *Solar Physics*, 59, 193
Gray, D.F. 1988, “Lectures on Spectral Line Analysis: F, G and K Stars” (The Publisher, Arva, Ontario).
Gray, D.F. 2005, “The Observation and Analysis of Stellar Photospheres” (3rd ed., Cambridge Univ. Press).
Gray, D.F. 2009, *ApJ*, 697, 1032
Gray, D.F. 2014, *AJ*, 147:81
Gray, D.F. & Nagle, T. 1989, *ApJ*, 341, 421
Gray, D.F. & Toner, C.G. 1986, *ApJ*, 310, 277
Gray, R.O. & Garrison, R.F. 1989, *ApJS*, 70, 623
Gray, R.O. & Corbally, C.J., 1994, *AJ*, 107, 742
Gray, R.O. & Corbally, J.C., 2009, *Stellar Spectral Classification*. Princeton University Press
Gray, R.O., Graham, P.W. & Hoyt, S.R. 2001, *AJ* 121, 2159
Green, G.M. *et al.* 2014, *ApJ*, 783:114
Green, G.M. *et al.* 2015, *ApJ*, 810:25
Greiss, S. *et al.* 2012, *AJ*, 144:24 (KIS)
Guzik, J.A., Kaye, A.B. *et al.* 2000, *ApJ*, 542, L57
Hambleton, K.M. *et al.* 2013 *MNRAS*, 434, 925
Helt, B.E., Jørgensen, H.E. *et al.* 1993, *A&A*, 270, 297
Hobbs, L.M. & Mathieu, R.D. 1991, *PASP*, 103, 431
Hodder, P.J.C., Nemeč, J.M. *et al.* 1992 *AJ*, 103, 460
Hoyle, F. 1964, *R.O.B.* 82, 90
Huber, D. *et al.* 2014, *ApJS*, 211, 2
Iben, I. Jr. & Tutukov, A.V. 1984, *ApJ*, 284, 719
Iben, I. Jr. 1986, *Mem.S.A.It.*, 57, 453
Jensen, K.S. & Jørgensen, H.L. 1985, *A&AS* 60, 229

- Jeon, Y.-B. *et al.* 2004, *AJ*, 128, 287
Jeon, Y.-B. *et al.* 2006, *ApJ*, 636, L129
Johnson, D.O. 2004, *J.Astron.Data* 10, 3
Johnson, D.R.H. & Soderblom, D.R. 1987, *AJ*, 93, 864
Jørgensen, H.E. 1982, *A&A*, 108, 99
Jørgensen, H.E. & Hansen, L. 1984, *A&A*, 133, 165
Kallrath, J., Milone, E.F. *et al.* 1992, *ApJ*, 389, 590
Kaluzny, J. 2000, *ASP Conf.Ser.*, 203, 19
Kaluzny, J. *et al.* 1996, *A&AS*, 120, 139
Kaluzny, J. *et al.* 2007, *AJ*, 133, 2457
Kaluzny, J. *et al.* 2013, *Acta Astron.*, 63, 309
Kim, S.-L., Lee, J.W. *et al.* 2002, *A&A*, 391, 213
Koen, C. 2014, *MNRAS*, 444, 1486
Kupka, F., Piskunov, N. *et al.* 1999, *A&AS*, 138, 119
Kurtz, M.J. & Mink, D.J. 1998, *PASP*, 110, 934
Kurtz, D., Shibahashi, H. *et al.* 2015, *MNRAS*, 450, 3015
Lampens, P. *et al.* 2011, *A&A*, 534, A111
Landstreet, J.D. 1998, *Å338*, 1041
Landstreet, J.D. *et al.* 2009, *Å*, 503, 973
Lee, J.W. *et al.* 2016, *MNRAS*, 460, 4220
Leigh, N., Sills, A. & Knigge, C. 2011, *MNRAS*, 416, 1410
Lenz, P. & Breger, M. 2005, *Comm. Asteroseis.*, 146, 53
Leonard, P.J.T., 1989, *AJ*, 98, 217
Lucy, L.B. 1976, *ApJ*, 206, 499
McCormac, J. *et al.* 2014, *MNRAS*, 438, 3383
McCrea, W.H. 1964, *MNRAS*, 128, 147
McNamara, D.H. 1995, *AJ*, 109, 1751
McNamara, D.H. 1997, *PASP*, 109, 1221
McNamara, D.H. 2011, *AJ*, 142, 110
McNamara, D.H. & Feltz, F.A.Jr. 1978, *PASP*, 90, 275
McNamara, D.H. *et al.* 2007, *AJ*, 133, 2752
Margon, B. & Cannon, R.D. 1989, *Observatory*, 109, 82
Markova, N., Puls, J. *et al.* 2014, *A&A*, 562, A37
Martínez-Vázquez, C.E. *et al.* 2016 *MNRAS*, 462, 4349
Massarotti, A., Latham, D.W. *et al.* 2008, *AJ*, 135, 209
Matijević, G., Prša, A. *et al.* 2012, *AJ*, 143:123
Mateo, M. *et al.* 1990, *AJ*, 100, 469
Mateo, M. *et al.* 1998, *AJ*, 115, 1856
Mazur, B., Krzemiński, W. *et al.* 2003, *MNRAS*, 340, 1205
Michaud, G., Charland, Y. *et al.* 1976, *ApJ*, 210, 447
Mkrtychian, D.E. *et al.* 2005, *ASP Conf. Ser.*, 333, 197
Momany, Y. 2014, *Ap.Sp.Sci.Lib.*, 413, 129
Morris, S.L. 1985, *ApJ*, 295, 143
Murphy, S.J. 2012, *MNRAS*, 422, 665
Murphy, S.J. *et al.* 2013a, *MNRAS*, 430, 2986
Murphy, S.J. *et al.* 2013b, *MNRAS*, 432, 2284
Murphy, S.J. *et al.* 2014, *MNRAS*, 441, 2515
Murphy, S.J. *et al.* 2015a, *MNRAS*, 447, 3948
Murphy, S.J. *et al.* 2015b, *MNRAS*, 450, 4475
Murphy, S.J. *et al.* 2016, *MNRAS* (arXiv:1607.07879)
Nemec, J.M. 1989, in *The Use of Pulsating Stars in Fundamental Programs in Astronomy*, ed. E.G. Schmidt (Cambridge, Cambridge University Press), p.215
Nemec, J.M. & Harris, H.C. 1987, *ApJ*, 316, 172
Nemec, J.M. & Cohen, J.G. 1989, *ApJ*, 336, 780
Nemec, J.M., Cohen, J.G. *et al.* 2013, *ApJ*, 773, 181
Nemec, J.M. & Linnell Nemec, A.F. 1991, *PASP*, 103, 95
Nemec, J.M. & Linnell Nemec, A.F. 1993, *AJ*, 105, 1455
Nemec, J.M. *et al.* 1994, *AJ*, 108, 222
Nemec, J.M. & Mateo, M. 1990a, *ASP Conf.Ser.* 10, 134
Nemec, J.M. & Mateo, M. 1990b, *ASP Conf.Ser.* 11, 64
Nemec, J.M., Mateo, M. *et al.* 1995, *AJ*, 110, 1186
Nemec, J.M. *et al.* 2015, *EPJ Web Conf.*, 101, 06049
Nielsen, M.B. *et al.* 2013, *A&A*, 557, L10
Nidever, D.L., Marcy, G.W. *et al.* 2002, *ApJS*, 141, 503
Niss, B. *et al.* 1978 *A&AS*, 32, 387
Niss, B. 1981, *A&A*, 98, 415
Olech, A. *et al.* 2005, *MNRAS*, 363, 40
Palaversa, L. *et al.* 2013, *AJ*, 146:101
Park, N.-K. & Nemec, J.M. 2000, *AJ*, 119, 1803
Paxton, B. *et al.* 2011, *ApJSS*, 192:3
Paxton, B. *et al.* 2013, *ApJSS*, 208:4
Paxton, B. *et al.* 2015, *ApJSS*, 220:15
Perets, H.B. & Fabrycky, D.C. 2009, *ApJ*, 697, 1048
Perry, C.L. 1969, *AJ*, 74, 139
Petersen, J.O. & Hog, E. 1998, *Mem.S.A.It.*, 69, 59
Pinsonneault, M.H. *et al.* 2012, *ApJS*, 199:30
Piskunov, N.E. *et al.* 1995, *A&AS*, 112, 525
Poretti, E., Clementini, G. *et al.* 2008, *ApJ*, 685, 947
Poznanski, D. *et al.* 2012, *MNRAS*, 426, 1465
Press, W.H. & Rybicki, G.B. 1989, *ApJ*, 338, 277
Preston, G.W. 1974, *ARA&A*, 12, 257
Preston, G.W. 2015, *Ap.Sp.Sci.Lib.* 413, 65
Preston, G.W., Beers, T.C. *et al.* 1994, *AJ*, 108, 538
Preston, G.W. & Landolt, A.U. 1998, *AJ*, 115, 2515
Preston, G.W. & Landolt, A.U. 1999, *AJ*, 118, 3006
Preston, G.W. & Sneden, C. 2000, *AJ*, 120, 1014
Prša, A., Batalha, N. *et al.* 2011, *AJ*, 141:83
Pych, W., Kaluzny, J. *et al.* 2001, *A&A*, 367, 148
Ramírez, I. *et al.* 2013, *ApJ*, 764:78
Ramsay, G., Napiwotzki, R. *et al.* 2011, *MNRAS*, 417, 400
Reiners, A. & Royer, F. 2004, *A&A*, 415, 325
Reiners, A. & Schmitt, J.H.M.M. 2002, *A&A*, 384, 155
Rodríguez, E. *et al.* 1994, *A&A*, 106, 21
Rodríguez, E. *et al.* 1998, *A&A*, 340, 196
Rodríguez, E. & López-González, M.J. 2000, *A&A*, 359, 597
Rodríguez, E. & Breger, M. 2001, *A&A*, 366, 178
Rodríguez, E. *et al.* 2010, *MNRAS*, 408, 2149
Royer, F., Zorec, J. & Gómez, A.E. 2007, *A&A*, 463, 671
Rozycka, M., Kaluzny, J. *et al.* 2010, *A&A*, 524, A78
Rucinski, S. 1999, *ASP Conf. Ser.*, 185, 82-90
Ryans, R.S.I., Dufton, P.L. *et al.* 2002, *MNRAS*, 336, 577
Saar, S.H. & Osten, R.A. 1997, *MNRAS*, 284, 803
Saio, H., Kurtz, D.W. *et al.* 2015, *MNRAS*, 443, 1946
Sandage, A.R. & Fouts, G. 1987, *AJ*, 93, 74
Sandage, A.R. & Tammann, G. 2006, *Ann.Rev.AA*, 44, 93
Sarajedini, A. 1993, Ph.D. thesis, Yale University
Schiodde, J.H. *et al.* 2013, *MNRAS*, 430, 1736
Schlafly, E.F. & Finkbeiner, D.P. 2011, *ApJ*, 737:103
Schlegel, D.J. *et al.* 1998, *ApJ*, 500, 525
Schuster, W.J., Moreno, E. *et al.* 2012, *A&A*, 538, A21
Shibahashi, H. & Kurtz, D.W. 2012, *MNRAS*, 422, 738
Shibahashi, H. *et al.* 2015, *MNRAS*, 450, 3999
Simón-Díaz, S. & Herrero, A. 2007, *A&A*, 468, 1063
Simón-Díaz, S., Herrero, A. *et al.* 2010, *ApJL*, 720, L174
Simón-Díaz, S. & Herrero, A. 2014, *A&A*, 562, A135
Slawson, R.W., Prša, A. *et al.* 2011, *AJ*, 142:160
Smalley, B. 2004, *Proc. IAU Symp.* 224, p.131
Smith, M.A. & Gray, D.F. 1976, *PASP*, 88, 809
Sneden, C. 1973, *ApJ*, 184, 839
Soszynski, I. *et al.* 2002, *Acta Astron.*, 52, 369
Soszynski, I. *et al.* 2003, *Acta Astron.*, 53, 93
Sousa, S.G., Santos, N.C. *et al.* 2007, *A&A*, 469, 783
Sousa, S.G., Santos, N.C. *et al.* 2015, *A&A*, 577, A67

- Southworth, J. *et al.* 2011, MNRAS, 414, 2413
Soydugan, E. *et al.* MNRAS, 370, 2013
Struve, O. & Elvey, C.T. 1934, ApJ, 79, 409
Telting, J.H. *et al.* 2012, A&A, 544, A1
Tempesti, P. 1971, Inf. Bull. Var. Stars, No.596
Thompson, I. *et al.* 2010, AJ 139, 329
Tillich, A., Przybilla, N. *et al.* 2010, A&A, 517, A36
Tonry, J.L. & Davis, M. 1979, AJ, 84, 1511
Torrealba, G., Catelan, M. *et al.* 2015, MNRAS, 2251
Torres, G., Fischer, D.A. *et al.* 2012, ApJ 757:161
Udry, S., Mayor, M. *et al.* 1999, ASP Conf. Ser. 185, 383
Valenti, J.A. & Piskunov, N. 1996, A&A Suppl. 118, 595
Valenti, J.A. & Fisher, D.A. 2005, ApJ Suppl. 159, 141
Venn, K., Irwin, M. *et al.* 2004, AJ, 128, 1177
Vivas, A.K. & Mateo, M. 2013, AJ, 146:141
Yan, L. & Mateo, M. 1994, AJ, 108, 1810
Zacharias, N. *et al.* 2010, AJ, 139, 2184